UNIVERSITY OF TURKU

The effects of roof-integrated reflectors on solar panels in Finland

Master of Science in Technology Thesis

University of Turku
Department of Mechanical and Materials Engineering
Materials Engineering
Modern Industrial Materials

Author:
Viljami Kukkola

15.12.2025
Turku

Master of Science in Technology Thesis
University of Turku

Subject: Materials Engineering
Author(s): Viljami Kukkola
Title: The Effects of Roof-Integrated Reflectors on Solar Panels in Finland
Supervisor(s): M.Sc. Timo Huuhtanen and Dr. Aapo Poskela
Number of pages: 120 pages
Date: 15.12.2025

Global energy demand is rising as urbanization and electrification expand. Fossil fuels, which dominate most countries' energy systems, are finite and expected to become more costly and decline in use over time. In contrast, solar energy offers an environmentally friendly alternative that has experienced rapid growth in the past decade. Improvements in solar panel technology have enhanced manufacturing, boosted production, and lowered costs, leading to widespread adoption worldwide. Several factors, such as the solar panel's location, orientation, temperature, and radiation levels, influence their output. A simple way to improve their efficiency is by using reflectors to direct more sunlight onto the panels.

This thesis is written as a commission for FF-Future Oy. The goal of the study is to evaluate the overall usability of reflectors as solar power enhancers through a literature review and to optimize the reflector's geometry to maximize the electricity output of solar panels in Finland. The optimization parameters include the reflector size, the reflectivity coefficient of the reflector material, and the tilt angle of both the reflector and the solar panel. The literature examines the impact of reflectors on solar panel output and radiation received, using either empirical outdoor experiments or computational analyses of the solar panel system geometry and radiation data. Both methods are used in the thesis to achieve more accurate results.

Reflectors increase the incident radiation on solar panels by an average of 15–40% annually, depending on location and optimization settings. Aluminum is the most effective reflector material, often coated to enhance durability. Other system parameters, such as tilt angles, are adjusted to achieve maximum solar energy output. A review of the literature shows that most studies focus on regions with high solar energy potential, like the Mediterranean, the Middle East, India, and Southeast Asia. Solar radiation varies greatly by location and weather conditions, so the most accurate yield estimates for each area are usually approximations.

According to the simulations in the thesis, under optimal installation angle and lighting conditions in Finland, the reflector's annual increase in radiation is approximately 35–38%. The highest yield improvement occurs in summer due to Finland's northern latitude. In outdoor tests, incident radiation increased by about 25% on the test day with standardized parameters using an aluminum reflector. The measurement and simulation results in the thesis confirm the overall assessment from the literature review regarding the significant additional yield of reflectors combined with solar panels, even in northern latitudes.

Key words: photovoltaic (PV) panels, reflectors, solar energy.

Diplomityö
Turun yliopisto

Oppiaine: Materiaalitekniikka
Tekijä(t): Viljami Kukkola
Otsikko: The Effects of Roof-Integrated Reflectors on Solar Panels in Finland
Ohjaaja(t): DI Timo Huuhtanen and TkT Aapo Poskela
Sivumäärä: 120 pages
Päivämäärä: 5.12.2025

Maailman energiantarve kasvaa kaupungistumisen ja sähköistymisen myötä. Fossiiliset polttoaineet, jotka hallitsevat useimpien maiden energiajärjestelmiä, ovat rajallisia ja niiden ennustetaan vähenevän ja kallistuvan tulevaisuudessa. Aurinkoenergia on ympäristöystävällinen vaihtoehto, jonka käyttö on kasvanut räjähdysmäisesti viimeisten kymmenen vuoden aikana. Aurinkopaneelien teknologinen kehitys on edennyt hyvin nopeasti ja valmistusprosessien vakiintuessa ja tuotantomäärien kasvaessa paneelin hinnat ovat myös laskeneet nopeasti. Tämä on osaltaan kiihdyttänyt niiden käyttöä maailmalla. Aurinkopaneelien sähkön tuottavuuteen vaikuttavat useat tekijät kuten paneelien sijainti, suunta, lämpötila ja säteilyn määrä. Yksinkertainen keino parantaa aurinkopaneelien tuotttavuutta on suunnata niihin auringon säteilyä heijastimien avulla.

Tämä diplomityö on kirjoitettu FF-Future Oy:n toimeksiannosta. Työn tarkoituksena on arvioida heijastimen käyttökelpoisuutta aurinkovoiman tehostimena kirjallisuuskatsauksen avulla ja optimoida heijastimena käytettävän eristeen geometria aurinkopaneelien sähkön tuotannon maksimoimiseksi Suomessa. Optimointiparametreina ovat heijastimen koko, heijastin materiaalin heijastuvuuskerroin sekä heijastimen ja aurinkopaneelin kaltevuuskulma. Kirjallisuudessa heijastimen vaikutusta aurinkopaneelin tuottoon ja siihen kohdistuvaan säteilyyn testataan empiirisesti eli ulkotesteillä tai laskennallisesti aurinkopaneelijärjestelmän geometrian ja säteilytilastojen avulla. Diplomityössä käytetään molempia tapoja tarkemman tuloksen saamiseksi.

Heijastimet lisäävät aurinkopaneeleihin kohdistuvaa säteilyä keskimäärin 15–40 % vuodessa sijainnista ja optimointiparametreistä riippuen. Paras heijastinmateriaali on ylivoimaisesti alumiini, joka yleensä pinnoitetaan kestävyyden parantamiseksi. Muita järjestelmän parametreja, kuten kaltevuukulmia, muutetaan kunnes saavutetaan paras energiantuotto. Kirjallisuuskatsauksen mukaan useimmat tutkimukset kohdistuvat korkean aurinkoenergianpotentiaalin alueille kuten Välimerelle, Lähi-Itään, Intiaan ja Kaakkois-Aasiaan. Auringon säteily vaihtelee merkittävästi sijainnin ja sään mukaan, joten tarkimmat tuottolaskelmat kunkin alueen osalta ovat arvioita.

Diplomityön simulaatiolaskujen mukaan Suomessa optimaalisissa olosuhteissa heijastimen aiheuttama säteilymäärän kasvu on noin 35–38 % vuodessa. Suurin tuoton kasvu kohdistuu kesään Suomen pohjoisen sijainnin takia. Ulkona suoritetuissa testeissä säteily kasvoi alumiiniheijastimella noin 25 % testauspäivänä vakioiduilla parametreilla. Diplomityön mittaus- ja simulaatiotulokset ovat siis vahvistavat kirjallisuuskatsauksen kokonaisarvion heijastimen huomattavasta lisätuotosta aurinkopaneelien kanssa myös pohjoisilla leveyspiireillä.

Avainsanat: aurinkopaneelit, heijastimet, aurinkoenergia.

Table of contents

1 Introduction

Almost every country embraced the Paris Agreement in 2015 in response to the environmental crisis caused by climate change. This treaty mandates that all signatory nations reduce their emissions. Fossil fuels, widely used across industries for energy production and as raw materials, are the primary source of emissions. To address these emissions, fossil fuels are increasingly replaced by renewable energy sources such as solar, wind, and hydropower. (Ministry of the Environment (FI), n.d.-a) The transition from fossil fuels to clean energy sources is part of the green transition, which aims to reduce the overconsumption of the Earth's limited resources (Ministry of the Environment (FI), n.d.-b).

In addition to the zero emissions from energy sources, the green transition also considers the energy consumption of manufacturing and usage, for which various standards have been established in different industries like construction and consumer electronics. In northern countries like Finland, heating can account for as much as a quarter of total energy consumption, which can be reduced through insulating walls and roofs. (Ilmasto-opas 2022; Ministry of the Environment (FI), n.d.-b) Additional insulation of older buildings can further decrease energy consumption. The purpose of this master's thesis, written for Finnish insulation manufacturer FinnFoam, is to study and evaluate an idea developed by FinnFoam to combine additional roof insulation with renewable energy production in the form of solar panels.

A roof insulator made by FinnFoam will be used as a reflector to increase irradiance on the solar panel and boost its energy yield. The thesis’s theoretical section covers the operating mechanisms, measurable quantities, and applications of solar panels. The section focuses on the characteristics of reflectors and their advantages and disadvantages. In the experimental section, the electricity production of solar panels in five Finnish cities and the additional yield from reflectors will be calculated. In addition to the calculations, reflection tests will be conducted using five different reflector materials and a solar panel.

The final thesis topic was developed at the University of Turku during a capstone course. This course aimed to create a calculation program that addresses the issue raised by Finnfoam regarding the optimization of roof insulation element dimensions to maximize solar energy yield. Finnfoam’s objective is to integrate roof insulation elements, reflectors, and solar panels to enhance the energy output of the solar panels. The side profile of the insulation

elements is triangular, allowing for the optimization of reflector angles to maximize energy yield. The thesis will build upon the coursework and provide a foundation for developing insulating elements for Finnfoam.

2 Theoretical Section

2.1 An Overview of Solar Panels

Solar cells are made from various semiconductor materials, with silicon being the most common, comprising about 90% of manufactured cells. Chapters 2.1.1 and 2.1.2 focus on silicon cells, examining their different types and functions. The chapter begins with a brief overview of the history and current status of solar panels, as well as a general introduction to the manufacturing process of silicon cells.

Chapter 2.1.3 examines how solar panels operate, the principles of photovoltaics, and the factors that influence electricity production. Higher temperatures directly impact the efficiency and output of solar panels; therefore, this factor should be considered when using a reflector with a solar panel.

2.1.1 History and current state of solar panels

The history of solar panels can be traced back to the discovery of the photoelectric effect by the French scientist, Alexander Edmond Becquerel, in 1839. The modern silicon-based solar cell was developed in Bell's laboratory in 1954 and attributed to Daryl Chap, Clavin Culler, and Gerald Pearson. The solar cell's first applications were in spacecraft and satellites, where the atmosphere does not affect the amount of radiation. (Gautam et al. 2024; Wirth et al. 2016) Modern solar panels have an electricity generation efficiency of about 15%-22%, representing a significant improvement over Bell's original panel, which had a 5% efficiency (Gautam et al. 2024).

In the 1960s, solar panels were primarily used in off-grid locations, such as lighthouses and rural regions, where accessing the electric grid was challenging. Following the oil crisis of the 1970s, interest in renewable energy, particularly solar panels, surged, prompting several companies to enter the industry. During the 1970s and 1980s, solar panel enclosures were developed, which, for the first time, offered protective glass and a plastic base for the panels. As the price of solar panels began to drop, they became more popular among consumers for powering small electrical appliances off-grid. (Wirth et al. 2016) Various government initiatives promoted the increase in the number and use of solar panels in households. A notable example is the German campaign of 1,000 Roofs in the 1990s, which later expanded to 100,000 (IEA, n.d.).

As solar panel production processes and technologies continued to improve, the volume of panels produced and efficiency have increased, and their price has fallen rapidly. Modern solar panels have an electricity generation efficiency of about 15-22%, representing a significant improvement over Bell's original panel, which had a 5% efficiency (Gautam et al. 2024). China surpassed the US and Japan in solar panel production in the late 2010s, becoming the largest producer (Woodhouse et al. 2011). Simultaneously, due to the high production volume, the price of solar panels, as shown in Figure 1, reached a record low of only 0.26 $/W in 2022 (OurWorld in Data 2024).

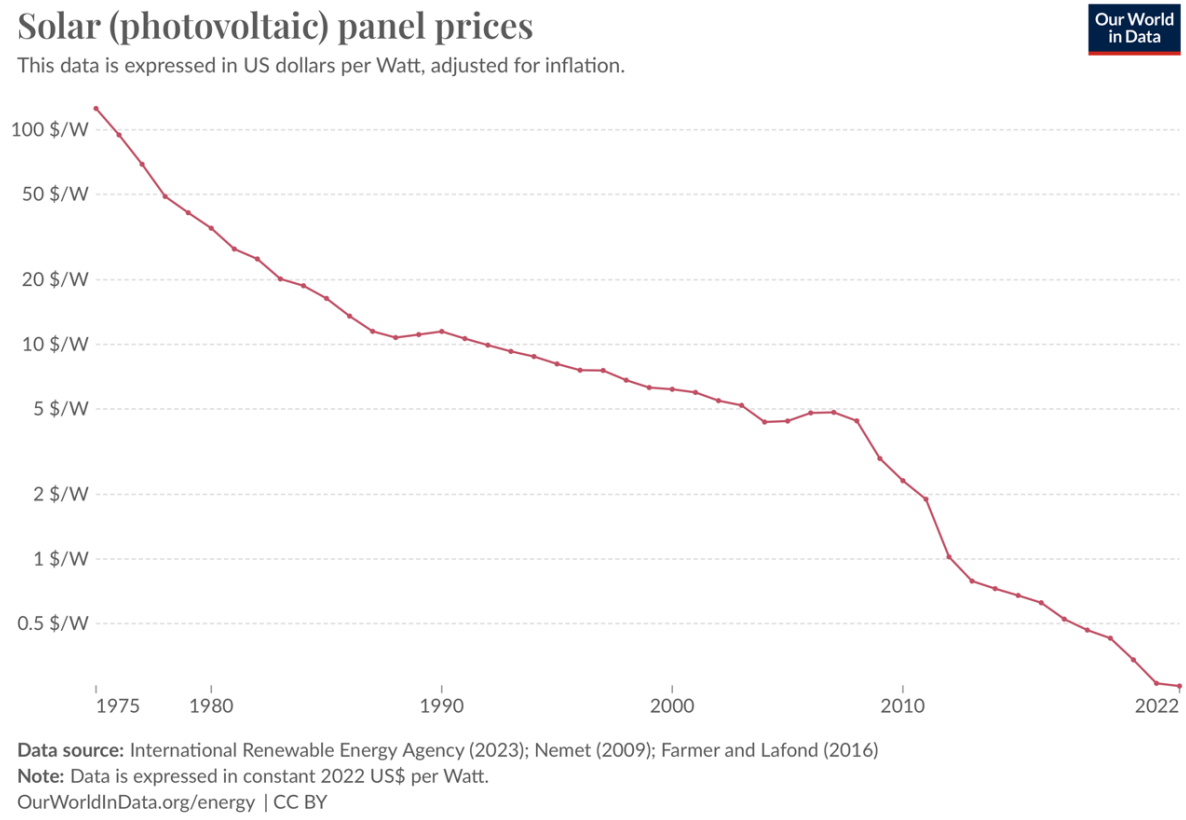

Figure 1. Price of solar panels ($/Watt) from 1975 to 2022 (OurWorld in Data 2024).

Today, the rapid growth of renewable energy sources, such as solar power, is fueled by shared concerns about depleting natural resources and the extreme weather events worsened by climate change. The green transition, which entails moving away from fossil fuels, has also increased demand for solar power. As the largest producer of solar panels, China has invested billions in solar energy, and the European Union and the United States have followed suit by investing in renewables and facilitating business investment through regulations, subsidies, and tax credits. (IEA 2023)

Haegel et al. (2023) estimate that solar energy demand will reach 75 TW in 2050 as society becomes more electrified. To achieve this, the PV industry must grow by at least 25% per year over the next decade, in line with recent years. To sustain this growth, cooperation among major producing countries such as China, Germany, Japan, and the United States, as well as manufacturers, is critical. Achieving such a significant increase in production will also necessitate more efficient recycling and strengthening supply chains to ensure the availability of raw materials. Additionally, using diverse materials in manufacturing reduces the demand for critical raw materials. (Haegel et al. 2023)

2.1.2 Manufacturing of photovoltaic panels

Modern silicon cells can be made from three different types of silicon: single crystal or monocrystal, polycrystalline, or amorphous silicon. The main differences between these materials are the size of the crystal structure and the manufacturing method. Crystal type also affects cells' efficiency. (Gautam et al. 2024; Wirth et al. 2016) Figure 2. shows a simplified production chain for solar cells. The manufacturing process begins with the extraction of silicon-containing quartz and the resulting silica sand, which is then processed into metallurgical-grade silicon. This material can be refined into solar and electronic-grade silicon, suitable for creating silicon crystal ingots for solar cells. (Liang and You 2023; Woodhouse et al. 2011)

Figure 2. The manufacturing process of a silicon-based solar panel, from quarts to module (U. S. Department of Energy, n.d.).

The most common way to make wafers is by cutting pieces of the desired thickness from the finished ingot. These ingots are usually pre-doped with boron, which makes silicon electrically conductive (SinoVoltaics 2015). A wafer can also be produced without casting and sawing, referred to as ribbon silicon. The monocrystalline wafer is one of the oldest solar cell technologies, where silicon atoms are arranged in a uniformly structured crystal. Polycrystalline consists of several crystals of varying sizes, and amorphous is a non-crystalline form of silicon used mainly in thin-film solar panels. (Kang 2021; Liang and You 2023; U. S. Department of Energy, n.d.)

After cutting, the silicon wafer is cleaned and processed into uniform cells. The manufacturing processes of a cell largely depend on its architecture. Cell fabrication commonly starts with the wafer's surface texturing, which removes any damage the saw makes and reduces reflection losses. After texturing, any remaining particles are removed with acid cleaning. Using a diffusion process, cells are doped with an electrically active dopant, usually phosphorus. Cell efficiency is increased by coating wafers with anti-reflective deposition. Finally, electrical contact is made possible by printing metal inlines to the wafer, which can now be called solar cells. (SinoVoltaics 2015; U. S. Department of Energy, n.d.)

The complete cells are laminated with a protective plastic layer, resting on a polymer base, and covered with protective glass. As shown in Figure 3, the panel edges are reinforced by an aluminum frame. (Isherwood 2022).

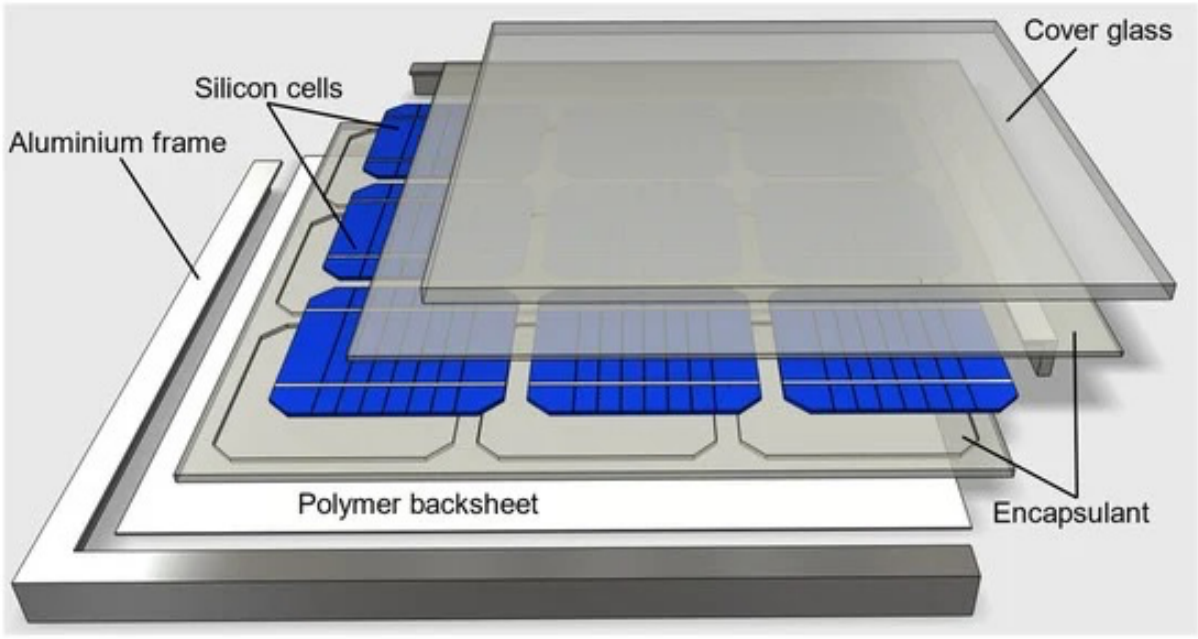

Figure 3. Layers of a typical solar panel, including the frame, backsheet, cells, encapsulant and cover glass (Isherwood 2022).

2.1.3 Basics of solar cells

Solar panels consist of multiple solar cells, each generating a small electric current, connected in both series and parallel (Gautam et al. 2024). Figure 4 shows the structure and electron orientation of a silicon solar cell.

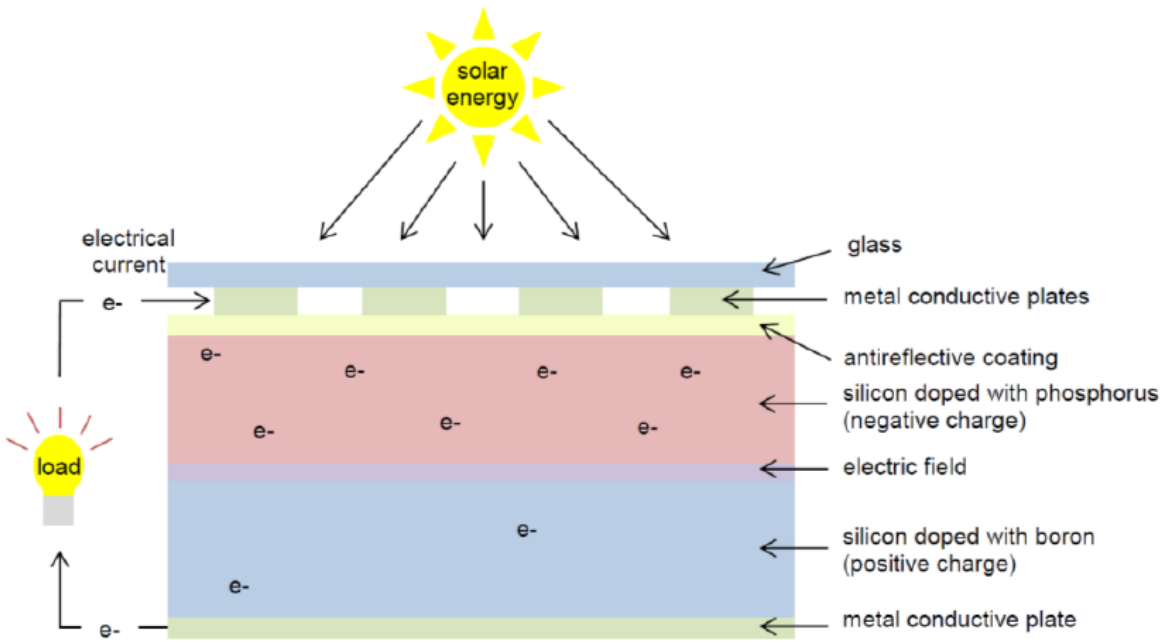

Figure 4. Silicon solar cell structure and mechanics (Fulcher 2019).

The operation of a solar panel is based on the photoelectric effect, where a photon's energy is converted into electrical energy through electron-hole pairs. In this process, when the photon's energy exceeds the semiconductor's band gap, it excites an electron from the valence band to the conduction band. The band gap is the minimum energy required to free an electron from its bound state. This process creates carriers: electrons and holes. A continuous electric field exists at the n-p junction, where two materials meet due to the ongoing exchange of electrons and holes. The electric field at the p-n junction prevents electrons from recombining with holes and releasing energy as heat or light. The carriers flow through an external circuit when the emitter and base are connected through an electric circuit, creating an electric current, as shown in Figure 4. (Honsbern and Bowden 2019)

A silicon solar cell consists of two layers of silicon, doped with phosphorus and boron atoms. The silicon layers are divided into two layers: the n-layer, which is about half a micrometre thick, and the p-layer, which is a thicker layer of about 0.25 millimeters. The silicon-phosphorus (p-type) layer donates free electrons, while the silicon-boron (n-type) layer accepts electrons into its vacant sites. (Kalogirou 2014; Wirth et al. 2016) Silicon cells harness the energy of photons that exceed the silicon energy gap of 1.12 eV, corresponding to a wavelength of approximately 1100 nm (Hossain et al. 2024). Light transmission through silicon depends on its wavelength: short-wavelength photons are absorbed within the first few

micrometers, while red light, with its longer wavelength, penetrates deeper into the layers (Honsberg and Bowden 2019a).

Solar cells do not use the entire spectrum of the sun's radiation; they only utilize a portion based on the material's energy gap (Honsberg Cristiana and Bowden Stuart 2019). Semiconductor materials function in different spectral regions depending on their energy gap, and even distinct silicon crystals exhibit slightly different characteristic ranges. Unused radiation increases the temperature of solar cells, leading to degradation, including aging, corrosion, and encapsulant degradation. (Fernández-Solas et al. 2021; Hossain et al. 2024)

2.2 The Electrical Characteristics of Solar Panels

The electrical characteristics of solar panels are crucial in their design and development. These characteristics are represented through various diode models and I-V diagrams. Chapter 2.2.1 addresses the single diode model, recognized as a simple yet sufficiently accurate model for solar panel. Chapter 2.2.2 highlights the key measurement points of the I-V diagram and their application in analyzing solar panel performance. Chapter 2.2.3 discusses the effect of temperature on solar panel performance, and Chapter 2.2.4 mentions the effect of shading. Chapter 2.2.5 summarizes the impact of irradiance on solar panel output and explains how it can be calculated.

The electrical performance of commercial solar panels is tested under Standard Test Conditions (STC) with an irradiance of 1000 W/m², a temperature of 25 °C, and an irradiance spectrum of AM 1.5. The solar panel manufacturer is required to report the results of these standard measurements, which have been conducted in specialized laboratories.

2.2.1 Single diode model

The simplest way to represent a solar cell circuit is using a single-diode model, which comprises a photosensitive power supply, a diode, and resistors, including series resistance R_S and parallel resistance R_P, as illustrated in Figure 5. (Wirth et al. 2016)

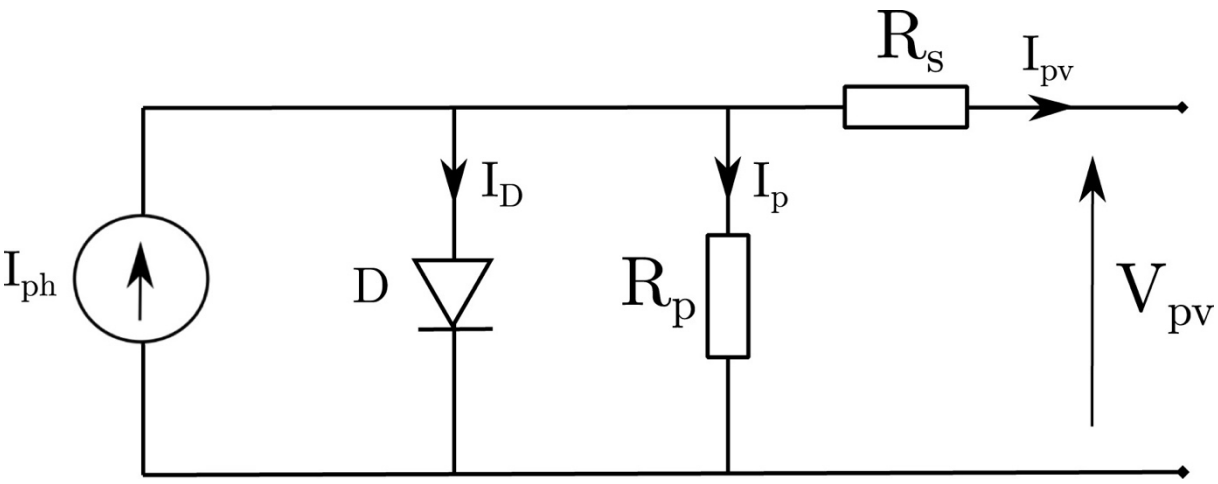

Figure 5. The electric circuit of the single-diode model (Azaioud et al. 2024).

The literature also uses two or three diode models to produce more accurate results. The drawback of multi-diode models is their complexity, which involves more variables and calculations. The accuracy of single-diode modeling is sufficient for most applications. The Shockley diode formula is often used to describe a single diode model as formula 1. (Wirth et al. 2016)

$$I = I_0 \times \left[exp\left(\frac{V_D}{nV_t}\right) - 1\right],\ V_t = \frac{kT}{q} \quad (1)$$

Where

- I_D diode current (A),
- I_0 is the diode saturation current (A),
- q is the charge on an electron (e = 1.602 × 10−19 C),
- n is the ideal factor of a diode,
- k is Boltzmann constant (8.617 × 10^{-5} eV/K),
- T is the absolute temperature (K)
- V_T is the thermal voltage (V) and
- V_D is the diode voltage (V).

The ideal coefficient n typically ranges from 1 to 2, depending on the type of recombination. The currents I_D and I_0 are influenced by the number of cells installed in parallel. The resistances R_S and R_P, shown in Figure 6, represent the actual current losses in the device and

cannot be precisely determined. R_S describes the contact and volume resistance, while R_P accounts for manufacturing defects in the cell. Generally, R_S is assumed to be small at the cell level, while R_P is considered quite large. Both resistances can be viewed as arising from different effects in the cell. The described single-diode model is also known as a five-parameter model, which includes I_{pv}, I_0, n, R_S, and R_P. (Wirth et al. 2016)

These five parameters can be calculated and estimated using various methods, which are categorized into analytical and algorithmic approaches. The accuracy and reliability of these methods have been tested in field experiments under different conditions. Bader et al. (2019) evaluate and compare several analytical approaches, applying these methods to indoor thin-film solar panels.

2.2.2 Solar panel I-V curve and parameters

There are several ways to measure solar panel performance, the most common and simplest of which is the IV curve and its associated parameters. The IV curve represents the ratio of current to voltage flowing through a device or material. Important parameters related to power generation include short-circuit current (Isc), open-circuit voltage (V_{oc}), and maximum power current and voltage (V_{mp} and I_{mp}). These parameters can be used to plot the IV and power curves. Additionally, they can help locate faulty cells. The main variables affecting these parameters are the amount of radiation and the panel temperature. (Wirth et al. 2016) Increasing the solar cell's temperature significantly raises the diode saturation current and slightly increases the overall current. These current changes adversely affect the open circuit voltage, degrading the cell's power output and efficiency. (Ahmed and Amer 2021; Wirth et al. 2016)

Figure 6 shows the IV curve, which is marked with a red line and includes the parameters mentioned earlier. The figure also shows the solar cell's power curve, PV curve, which is blue, with maximum P_{mp} at the points V_{mp} and I_{mp} of the IV curve. (Honsberg and Bowden 2019b)

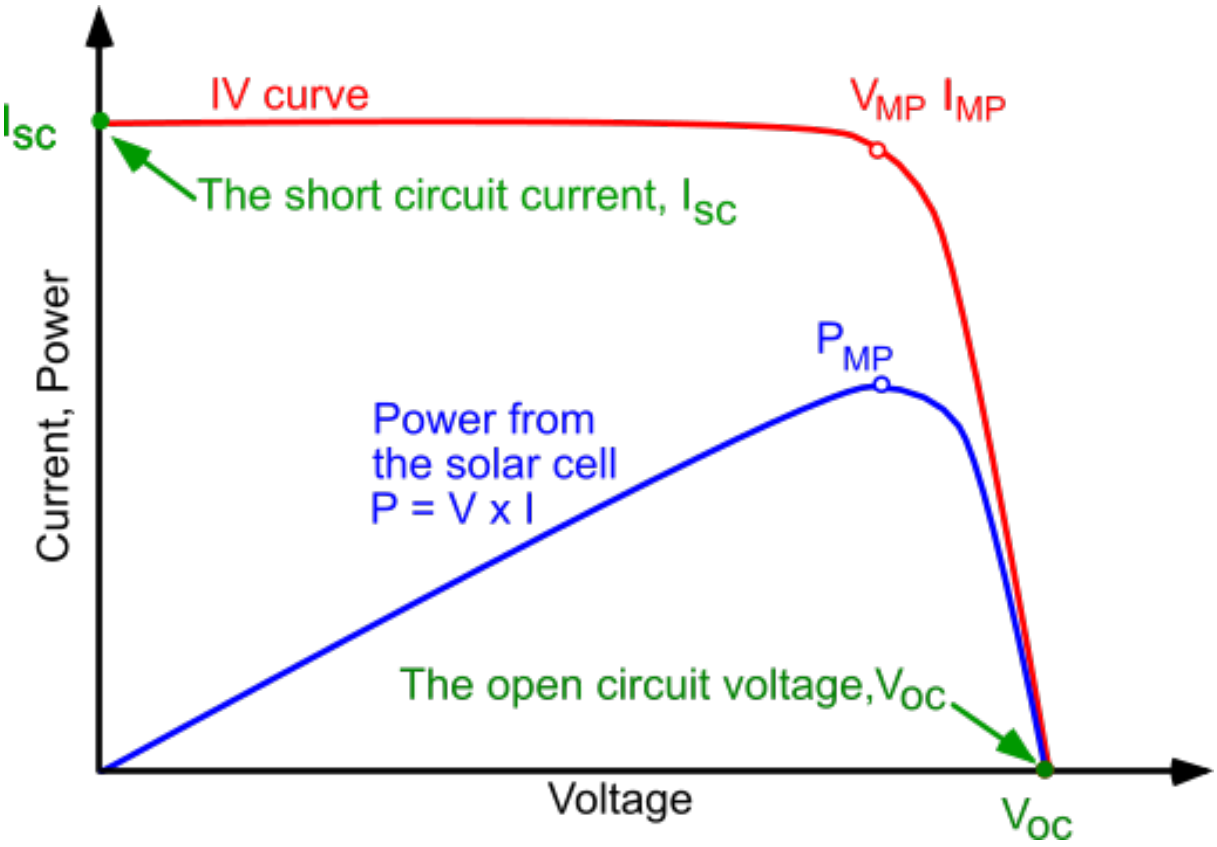

Figure 6. Solar cell IV curve and power curve with I_{sc}, V_{oc}, P_{mp}, V_{mp}. and I_{mp} locations (Honsberg and Bowden 2019b).

Solar panels operate based on the Sun's consistent radiation on Earth's surface. For more details on different types of radiation and its distribution across Earth, see Chapter 1.3.. Figure 7 shows a silicon cell's IV curve at various total irradiance levels ranging from 400 to 1000 W/m². A decrease in irradiance greatly impacts the cell's current and, to a lesser extent, its voltage. As the current drops, the power of the cell also declines. (Verma et al. 2021)

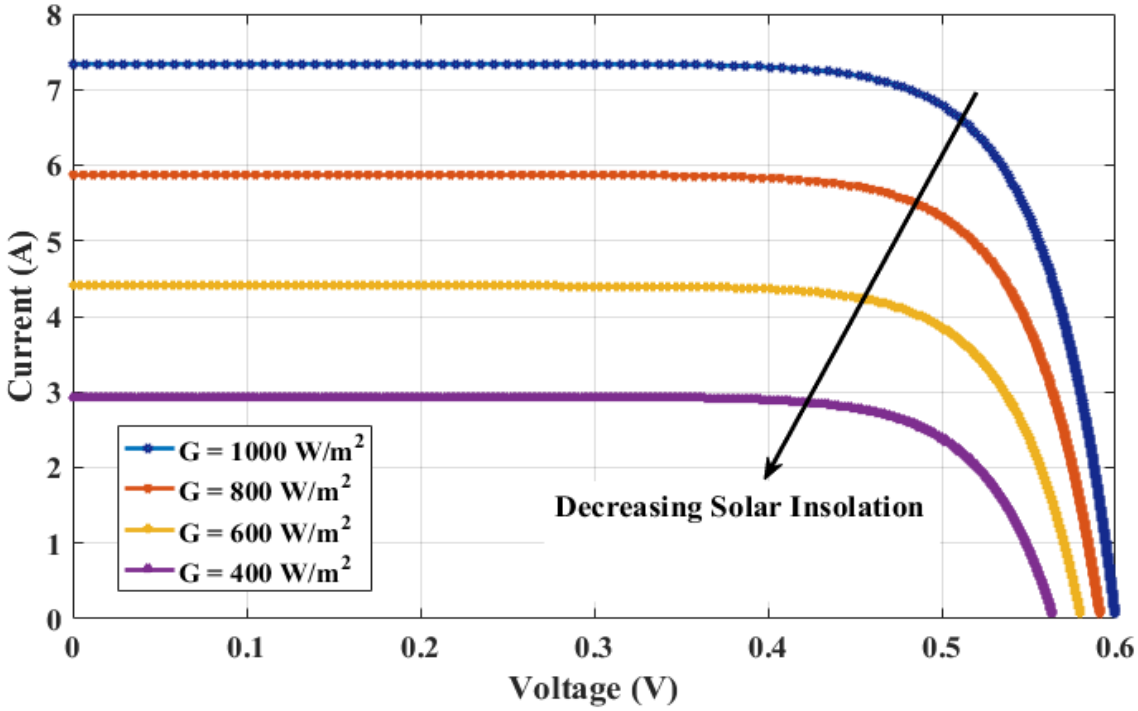

Figure 7. I-V curve of a silicon cell at different radiation levels (Verma et al. 2021).

These parameters of the IV curve can be used to calculate the fill factor (FF), a method for comparing the cell's maximum power to its short-circuit current and open-circuit voltage. Cells typically have a fill factor ranging from 76% to 83%, depending on the model. Fill factor can be used to identify faulty panels on a string by comparing the fill factors of different panels. It is calculated using formula 2. (Wirth et al. 2016)

$$FF = \frac{V_{mpp} \times I_{mpp}}{V_{OC} \times I_{SC}} = \frac{P_{mpp}}{V_{OC} \times I_{sc}} \quad (2)$$

Where

- V_{OC} represents the open circuit voltage [V],
- I_{SC} represents the short-circuit current [A],
- V_{mpp} represents the voltage at maximum power [V],
- I_{mpp} is the maximum current [A] and
- P_{mpp} represents the maximum power measured in watts (W).

Another valuable metric is solar panel efficiency. Manufacturers report the nominal efficiency of solar panels, which is calculated using formula 3. under Standardized Test Conditions (STC). (Wirth et al. 2016)

$$\eta = \frac{P_{mpp}}{\Phi_e} = \frac{P_{mpp}}{E \times A_{cell}} \quad (3)$$

Where

- P_{mpp} is the maximum power [W],
- Φ_e radiant flux [W],
- A_{cell} is the solar cell area [m2] and
- *E is* the amount of radiation [W/m2].

The theoretical maximum efficiency of a silicon solar cell is called the Shockley-Queisser limit, which is about 29% for single-junction cells (Wirth et al. 2016). This maximum depends on the method of measurement and calculation (Zanatta 2022). The efficiency limit can be increased by adding more junctions to the solar cell; in principle, this means installing more layers on top of one another. The theoretical maximum for a double-junction solar cell is up to 42.5%. Multi-junction cells are the most efficient among the solar cells developed, but they are also the most expensive, complex, and challenging to manufacture. Therefore, these cells are mainly used in high-tech applications like satellites and spacecraft. (Wirth et al. 2016)

Multilayer cells utilize the bandwidth of various semiconductor materials, enhancing the capture of solar radiation, as illustrated in Figure 8. In example (a) of the figure, the cell consists of a silicon bottom layer, a 1.5 eV middle layer (GaInAsP), and a 2.0 eV top layer (AlGaInP). The top layer absorbs high-energy photons, while the lower layers capture lower-energy photons. This configuration also helps reduce heat losses as layers capture energy from photons, which otherwise would increase the temperature. The diagram on the right (b) demonstrates the cell efficiency concerning the number of junctions. The efficiency gains from junctions diminish as the number of layers increases. Consequently, the practical maximum number of layers is four. (Heydarian et al. 2024)

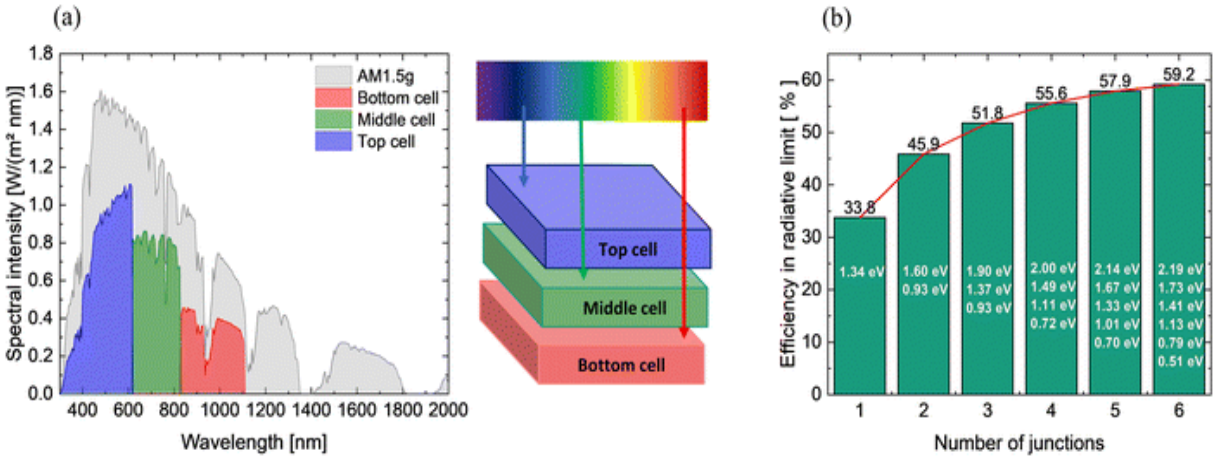

Figure 8. Solar spectrum of a triple-layer solar cell (a) and cell efficiency versus number of junctions (b) (Heydarian et al. 2024).

2.2.3 Effect of temperature on the solar panel

Temperature significantly influences the processes within a solar cell. An increase in temperature negatively affects the open-circuit voltage, efficiency of solar cells, and power output. The efficiency of silicon solar cells decreases by 0.3-0.6% for each 1°C increase. (Wirth et al. 2016) Given the sensitivity of solar cells, extensive research has focused on measuring, monitoring, and modeling temperature, as elevated temperatures can adversely impact the profitability of a solar power plant. However, measuring the internal temperature of a solar cell empirically presents challenges, leading to the development of various estimation models, which were compared in a review by Santiago et al. (2018) and tested at a power plant in southern Spain.

In the field, solar panel temperatures are measured from the back of the panel. The internal temperature of the solar cell is typically estimated to be about 1-3 °C higher than the measurement taken from the backside. Several factors must be considered when estimating the heat loss that affects the temperature of the solar cell. These factors include wind speed and direction, air temperature, and the amount of radiation. (Agrawal et al. 2021; Gan 2009; Santiago et al. 2018)

Figure 9 illustrates the effect of temperature on the I-V curve of a silicon cell, demonstrating that an increase in temperature decreases the cell voltage. Concurrently, the cell current experiences a slight increase. Consequently, the decrease in voltage also causes a reduction in the power output of the solar cell. In the study, the test temperature varied from 25 to 125 °C. (Verma et al. 2021) In practical applications, the temperature of a solar panel seldom exceeds 100 °C, and even then, only in exceptionally hot areas such as deserts.

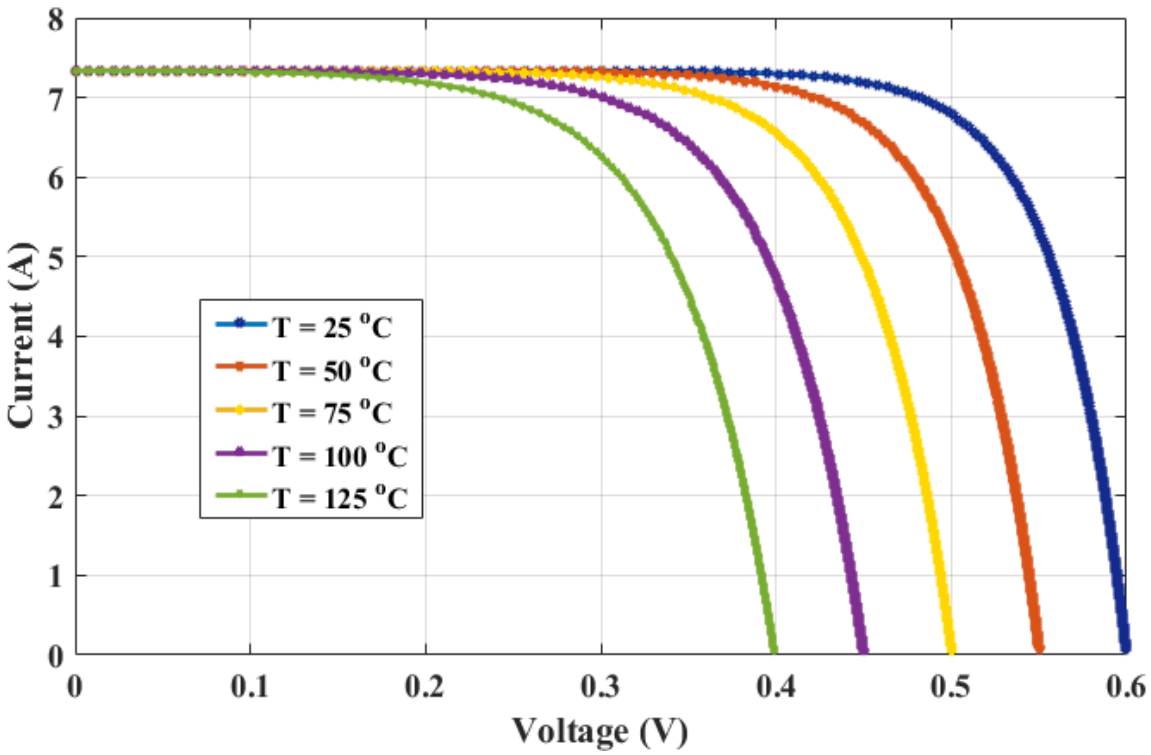

Figure 9. Effect of temperature on the IV curve of a silicon cell (Verma et al. 2021).

The increase in panel temperature also reduces its service life and increases deterioration. The deterioration of the panel is mainly affected by its operating temperature, relative humidity, and radiation intensity. High temperatures and humidity can cause problems in the panel, including corrosion and delamination. (Agrawal et al. 2021) Various cooling systems have been developed to prevent high operating temperatures.

Solar panel cooling methods can be categorized into active and passive approaches that lower temperatures. Active methods typically use power to cool panels, such as fans or water pumps. In contrast, passive methods do not require any power and rely on material properties for cooling, such as heat sinks and phase change materials. (Agyekum et al. 2021) Dwivedi et al. (2020) explore various cooling methods and their effects on solar panel efficiency in depth. Additionally, the operating temperature of a solar panel can be influenced by various installation options, such as the air gap between the panel and the roof and the roof pitch.

The use of air gaps as a cooling method is based on natural convection, which causes air to move behind the solar panel, thereby cooling the rear side of the panel. There is no optimal size for air gaps, but several studies have tested and recommended a gap of 10–20 centimeters. (Gan 2009; Naghavi et al. 2021) According to Naghavi et al. (2021), a 20-centimeter air gap has a temperature reduction of 12 ± 5 °C compared to no air gap, making air gaps an effective and inexpensive method for passive cooling, especially on rooftops.

The reflector reflects additional radiation onto the surface of the solar panel, thus increasing its power output and temperature. The choice of reflector material impacts the panel's temperature, as the material's reflectivity varies with wavelength. For example, an aluminium reflector will increase the panel temperature more than a steel reflector, as aluminium reflects more infrared radiation. (Agrawal et al. 2021; Sultan et al. 2024). The literature on solar reflectors generally considers the additional increase in solar panel temperature caused by the reflector and its effect on yield.

2.2.4 Impact of shading on the solar panel system

Power losses in a solar panel system can be classified into panel-specific and system losses. For individual panels, the primary output losses arise from various shading and soiling losses, panel fouling, and reflection losses due to the angle of incidence. Inherent power losses exist within a solar panel system, including conduction and wiring losses, modeling inverter losses, and panel mismatch losses. This occurs when PV panels with slightly different currents and voltages are connected as an array and equalized. (Bamisile et al. 2025; Sandia National Laboratories, n.d.)

The primary external factor influencing the performance of solar panels, aside from temperature, is shading, which can impact solar panels differently at various times of the day and year. Shadows causing the shading can be categorized into several types, including hard shadows, soft shadows, and self-shadowing. Hard shadows are primarily caused by soiling, such as sand, pollen, pollutants, snow, and leaves. In urban areas, buildings and trees also cast shadows during the day. Soft shadows result from fog, mist, and smoke, reducing the radiation from the ground surface. (Maghami et al. 2016) Reflectors can create hard shadows that can be minimized through proper design. Reflectors cast shadows, especially in the morning and evening, depending on their angle to the sun. (Baccoli et al. 2018)

When designing ground-mounted or flat-roofed solar panel systems, it is crucial to consider self-shadowing, which occurs when the shadows cast by rows of solar panels overlap. Due to these inter-row shadows, the angles of solar panel rows on limited flat roofs are usually set at a lower tilt angle compared to those on the ground and the optimum tilt angle. This arrangement maximizes the number of installed panels and minimizes shading. On the ground, the spacing between rows of solar panels is primarily determined by the sun's position, the size, tilt angle, and location of the panels. (Iskandar et al. 2023; Shekar et al. 2023)

Partial shading affects only some of the cells but negatively impacts the output of the entire panel. When the currents the cells produce do not align, shading can create hot spots that damage the panel. Additionally, a mismatch between the current in the cells and the voltage across the panels will impact the overall production of the entire system. To prevent power spikes, bypass diodes are installed in the panels to enhance safety by preventing uneven power flows and hot spots. Figure 10 illustrates the P-V curve for the partial shadow scenario. Uneven radiation across different panels leads to power losses for the entire system. (Verma et al. 2021)

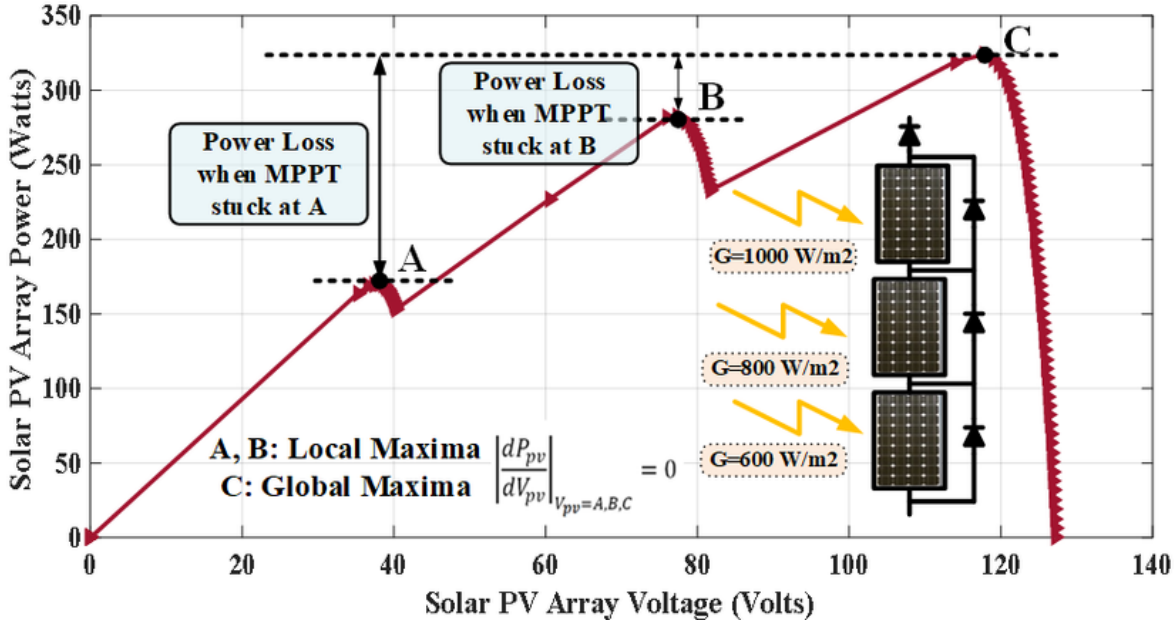

Figure 10. Power curve of a solar panel array under different radiation conditions and its impact (Verma et al. 2021).

2.2.5 Solar panels' energy yield

The variations in the solar panel's energy output and the measurement background are outlined in Chapter 2.3. Increases in the radiation received by a solar panel enhance its energy output; however, this increase is not proportional due to temperature and external factors, such as wind speed, impacting its temperature.

Skoplaki & Palyvos (2009) provided a detailed discussion of calculating solar panel energy production, efficiency, and their various functions. They presented numerous functions and studies related to solar panel energy output. The commonly used formula for calculating solar panel energy output is as follows:

$$P = P^* \times \frac{G}{G^*} \times (1 - \beta(T_c - T_c^*) \quad (4)$$

where P^*, G^*, and T^*_c are the STC parameters, namely the panel standard yield (P*), 1000 W/m² (G*), and the test temperature of 25 °C (T^*_c). Other parameters include the radiation incident on the panel G, the temperature coefficient β, which is generally -0.0035, and T_c representing the cell temperature. This formula enables the estimation of the energy yield of an individual panel under varying radiation conditions. The simplest formulas are linear functions, while more complex ones are non-linear, which are more accurate but require more computing power. (Skoplaki and Palyvos 2009)

Rönnelid et al. (2000) aimed to generalize the effects of energy production and temperature in solar panels and reflectors. The additional radiation is assumed to compensate for the yield loss caused by higher temperatures, and Formula 5 can estimate the annual solar panel yield.

$$Q_{out} = \eta H_{year} \tag{5}$$

where η is the solar panel's efficiency and H_{year} is the annual irradiance. This function provides a rough estimate of the panel's electricity output, as it is typically calculated based on the panel's theoretical efficiency, which is often higher than its actual efficiency. (Rönnelid et al. 2000)

The energy output of a solar panel system is also influenced by the AC-DC current conversion using inverters, various wiring, and power losses, which total about 14%, depending on the system. In addition to temperature, energy output is affected by panel type, airflow, and environmental effects. (Bamisile et al. 2025; PVGIS, n.d.) In practice, the power output of a solar power plant is estimated and calculated using various programs, such as the SAM software.

2.3 Solar Radiation on Surfaces

To estimate PV panel’s output, the amount of radiant energy coming from the sun must be calculated. The location of solar panels significantly impacts the amount of solar radiation, and this factor must also be considered when installing solar panels. The orientation of the Earth and the weather conditions in Chapter 2.3.1 explain how solar irradiance is calculated and distributed globally.

Chapters 2.3.2 and 2.3.3 define the time constants and the Sun, enabling calculations based on them. Quantities representing the Sun's position are essential because they affect irradiation on an inclined surface. The databases for horizontal radiation are detailed in Chapter 2.3.4.

These statistics are frequently used to calculate the radiation received by angled surfaces, which is addressed in Chapter 2.3.5.

2.3.1 Solar energy potential on Earth

The Sun is a crucial energy source for humanity and makes using solar and wind energy feasible. Harnessing the sun's radiant energy through solar and wind power will enable us to reduce our dependence on fossil fuels, as the amount of energy reaching Earth continuously is an astonishing 173,000 TWh (Chandler 2011).

The solar constant G represents the amount of energy from the Sun's radiation at the Earth's distance from the Sun, measured outside the atmosphere. It is approximately 1367 W/m². (Duffie and Beckman 2013, 5) The Sun emits radiation across all wavelengths, from gamma rays to radio waves. In addition to visible light, only a small portion of infrared and ultraviolet radiation reaches the Earth's surface, largely due to the reflective properties of the atmosphere. This also protects against radiation that is harmful to humans.

According to a 2020 Energy Sector Management Assistance Program (ESMAP) report, the highest energy concentrations are found in Africa, the Middle East, Australia, the west coast of the United States, and Chile and Peru in South America, as illustrated in Figure 11. It highlights the practical potential for solar energy (PVOUT) and provides a clear picture of solar energy potential across various countries.

This potential is influenced by factors such as deserts, which receive high levels of radiation, although building solar power plants is challenging due to limited infrastructure and electricity transmission. This map does not account for weather variations that can significantly impact solar energy availability in certain locations. The report also discusses the economic benefits and opportunities related to solar energy. (ESMAP 2020) Unfortunately, this study does not extend as far north as Finland; however, it still provides a solid overview of the solar energy potential across different countries and continents.

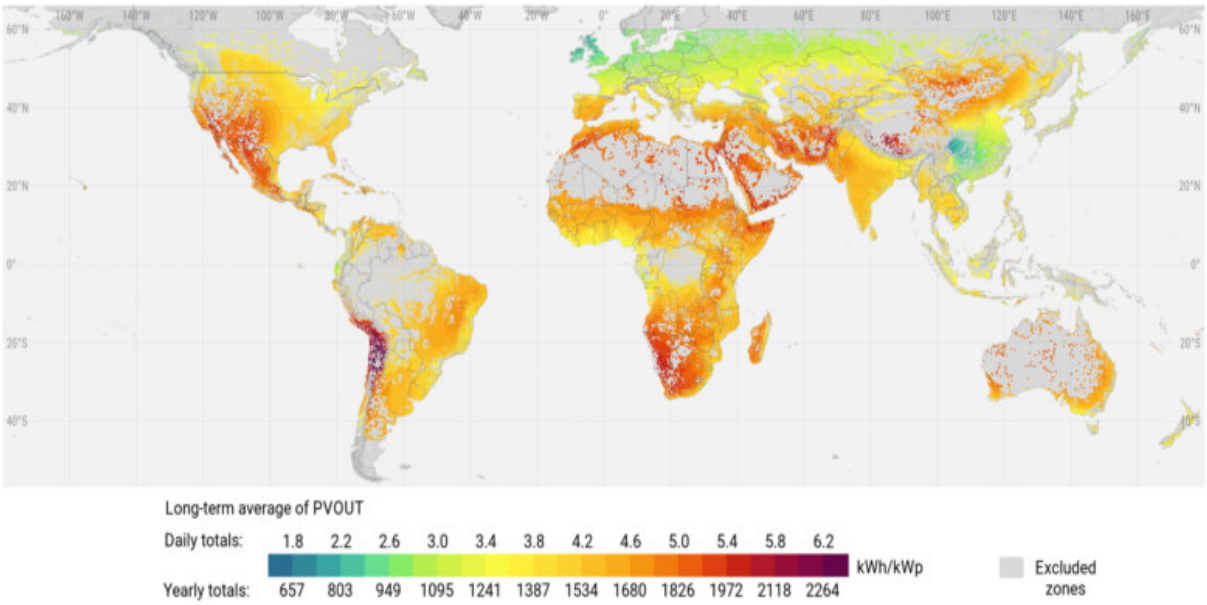

Figure 11. Long-term solar energy potential of the world (ESMAP 2020).

Figure 12 illustrates solar irradiance and solar panel production in Europe at the optimal angle. Only southern Finland and the coastal areas experience irradiance levels exceeding 1000 W/m² during the summer, similar to those found in central Europe (Mäki et al. 2015). Given Finland's overall irradiance and temperate climate, reflectors can effectively increase the amount of radiation reaching solar panels.

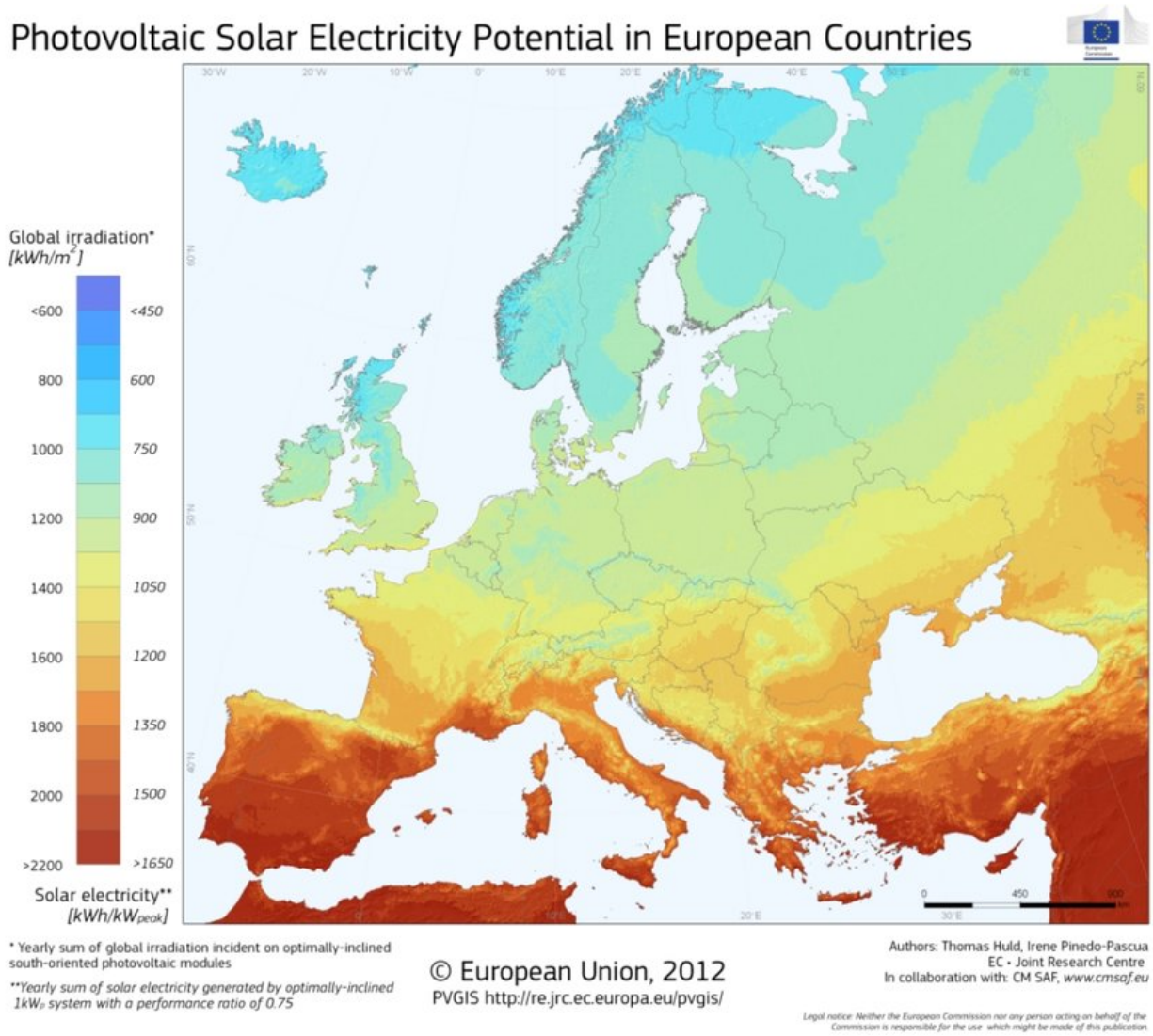

Figure 12. A map of European solar irradiation and energy potential (Mäki et al. 2015).

2.3.2 Functions of solar time

Several angles are used to simulate and calculate solar irradiance, determining the Sun's exact position in the sky based on the observer's location on the Earth's surface. Coordinates of longitude and latitude serve as the reference points for a location. For historical reasons, Greenwich in the UK is designated as the zero point of the meridian. Longitude is typically marked as E 0-180° or W 0-(-) 180°. The zero point of a latitude lies at the equator and can be represented similarly to a meridian, using a positive coordinate for north and a negative coordinate for south.

Solar time and time in different countries vary due to time zones and daylight saving time. Local time can be converted to solar time using transformation equations such as the local

time meridian, time equation, and time correction factor equations. Local solar noon is when the sun reaches its highest point in the sky. The longitude of local standard time (LSTM) is calculated from the Greenwich time zone using the formula 6. (Honsberg and Bowden 2019c)

$$LSTM = 15° \times \Delta T_{UTC} \quad (6)$$

where ΔT (UTC) represents the difference between local time (LT) and UTC in hours, specifically within the time zone. For instance, Finland falls under the UTC+2 time zone, which means Finland's LSTM is located at 30° E.

The time equation (E) is calculated using formula 7. It adjusts for the eccentricity of the Earth's orbit and the axial tilt of the Earth within half a minute (Honsberg and Bowden 2019c).

$$E = 9{,}87 \times \sin(2B) - 7{,}53 \times \cos(B) - 1{,}5 \sin(B) \quad (7)$$

where B is calculated with the following formula:

$$B = (n - 81)\frac{360}{365} \quad (8)$$

Where n represents the day number in a year. The time correction factor (TC) accounts for local time variations resulting from time zones and daylight saving time. It can be calculated using formula 9. All outcomes of the time equations are presented in minutes. (Honsberg and Bowden 2019c)

$$TC = 4(Longitude - LSTM) + E \quad (9)$$

Finally, local solar time (LST) is determined using the formula 10 (Honsberg and Bowden 2019c).

$$LST = LT + \frac{TC}{60} \quad (10)$$

2.3.3 The Position of the Sun

Figure 13 shows some angles necessary for determining the position of the Sun and its azimuth angle relative to the cardinal directions. The following angles are included in Figure 14:

- γ_s is the solar azimuth angle, which indicates the direction of direct radiation in relation to the horizontal plane. It is zero to the south, positive to the west, and negative to the east.

- β is the angle between the horizontal plane and the surface of a solar panel, for example.
- θ_z is the zenith angle, meaning the angle between the direct radiation and the zenith.
- θ_{El} is the angle of elevation of the Sun, which means it is the angle between the direct rays of sunlight and the horizontal plane. This angle complements the zenith angle.
- γ indicates the orientation of a local plane, such as a solar panel, relative to the horizontal plane in the southern direction, where the west is positive, and the east is negative. (Duffie and Beckman 2013, 12–13)

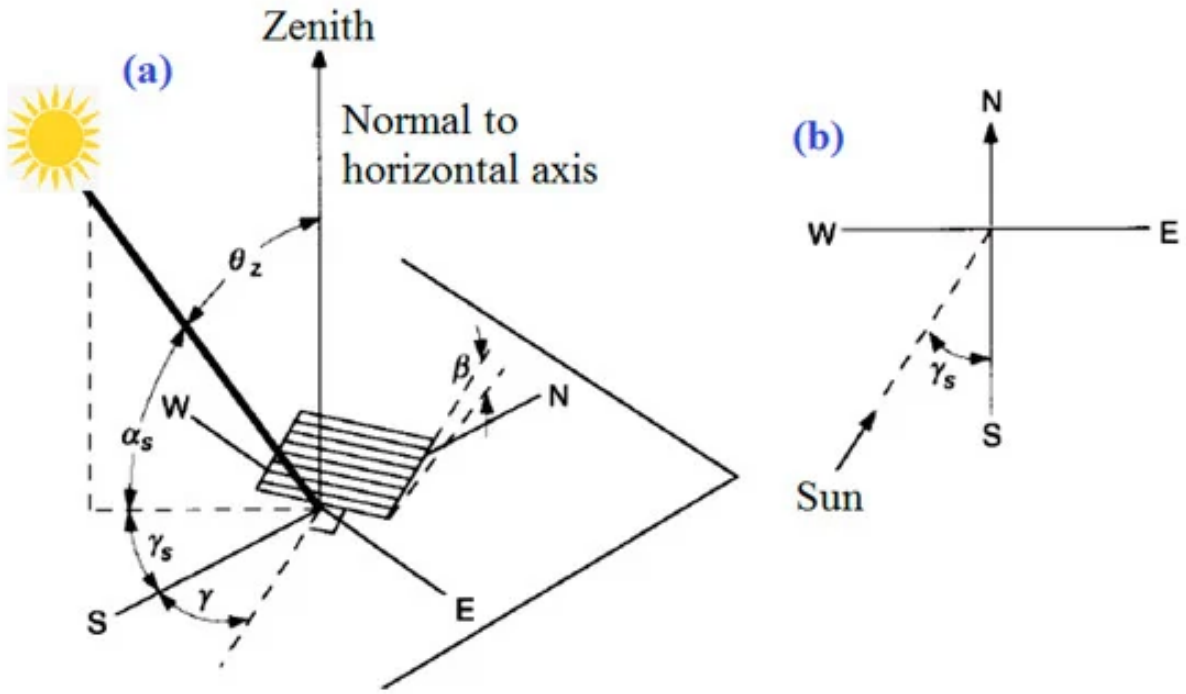

Figure 13. (a) Different radiation angles and (b) solar azimuth angle (Gomaa et al. 2020).

Other significant angles of the sun include:

- δ represents the angle of the sun's orientation at solar noon in relation to the equatorial plane, with $-23.45° \leq \delta \leq 23.45°$, where north is considered positive.
- ω represents the hour angle, indicating the Sun's displacement east or west of the local meridian at a rate of 15° per hour due to the Earth's rotation. It is positive in the morning and negative in the afternoon.

- θ is the angle formed between the incoming radiation and the normal to the surface, also known as the angle of incidence. (Duffie and Beckman 2013, 13)

Some of the angles mentioned above can be calculated using formulas. The declination angle can be determined using the following formula 11 (Duffie and Beckman 2013, 13).

$$\delta = 23{,}45 \times \sin\left(360\frac{264+n}{365}\right) \quad (11)$$

Where n represents the day of the year. The declination angle for the average day of the month is provided in Table 1. The only limitation for this declination application table is the location's latitude, which must be between -66.5° and 66.5°. (Duffie and Beckman 2013, 14). These values are used in the experimental part, where the average daily irradiance for a month is calculated on average days of the month.

Table 1. Recommended Average Days for Months and Values of n by Months (Duffie and Beckman 2013, 14)

Month	n for ith day of month	For average day of month		
		Date	n	δ
January	i	17	17	-20,9
February	31+i	16	47	-13,0
March	59+i	16	75	-2,4
April	90+i	15	105	9,4
May	120+i	15	135	18,8
June	151+i	11	162	23,1
July	181+i	17	198	21,2
August	212+i	16	228	13,5
September	243+i	15	258	2,2
October	273+i	15	288	-9,6
November	304+i	14	318	-18,9
December	334+i	10	344	-23,0

The hour angle can be determined using the local solar time, which is calculated with the formula 12.

$$\omega = 15°(LST - 12) \quad (12)$$

The solar azimuth angle is determined using the formula 13. The sign of this formula changes with the hour angle (Duffie and Beckman 2013, 15).

$$\gamma_s = sign(\omega)\left|\cos^{-1}\left(\frac{\cos\theta_z \sin\phi - \sin\delta}{\sin\theta_z \cos\phi}\right)\right| \quad (13)$$

Formula 14 represents the relationship between the angle of incidence and the angles mentioned above. The angle of incidence can exceed 90°, indicating that the sun is below the horizon. When calculating the angle of incidence, it's crucial to ensure that the hourly angle falls between sunrise and sunset. (Duffie and Beckman 2013, 14)

$$\theta = \cos^{-1}(\sin\delta \sin\phi \cos\beta - \sin\delta \cos\phi \sin\beta \cos\gamma + \cos\delta \cos\phi \cos\beta \cos\omega + \cos\delta \sin\phi \sin\beta \cos\gamma \cos\omega + \cos\delta \sin\beta \sin\gamma \sin\omega) \quad (14)$$

For horizontal surfaces, the angle of incidence equals the sun's zenith angle, θ_z. The zenith angle is calculated using formula 15 when the panel tilt angle is 0°. (Duffie and Beckman 2013, 14)

$$\theta_z = \cos^{-1}(\cos\phi \cos\delta \cos\omega + \sin\phi \sin\delta) \quad (15)$$

The Sun's elevation angle, also known as altitude angle, can be calculated from the zenith angle using the formula 16

$$\alpha_{El} = 90° - \theta_z \quad (16)$$

or by directly using the formula 17 (Kostić et al. 2010).

$$\theta_{El} = sin^{-1}(\sin\delta \times \sin\phi + \cos\delta \cos\omega \cos\phi) \quad (17)$$

All the above formulas can be easily calculated using pre-made calculators, such as the online Excel calculator available on the NOAA website, which was employed for the calculations in this thesis. The calculators require the location coordinates and the date, specifically the average day of the month, as shown in Table 1.

2.3.4 Types of solar radiation and recommended databases

Radiation levels are measured at weather stations and are now also quantified using satellite data. At weather stations, the total amount of radiation on a horizontal surface is typically measured with a pyranometer. Radiation can also be calculated from extraterrestrial radiation and either clear days or sunny hours. The radiation received on the horizontal surface is divided into direct radiation from the Sun and diffuse radiation from the atmosphere. (Duffie and Beckman 2013, 50; PVGIS, n.d.)

The free EU PVGis and NREL PVWatts programs and the SolarAtlas website can be used to download radiation data from various databases for the desired location. Radiation is typically expressed as total radiation on a horizontal surface, averaged over a month per hour or day. The average, calculated from multiple years of data, can also categorize radiation into different types, such as direct and diffused radiation, along with their ratio to total radiation. These programs can also calculate radiation amounts based on the panel's tilt angle and direction. (EU Comission 2024; Global Solar Atlas, n.d.; NREL, n.d.) Each of these programs is well-suited for general calculations of electricity production from solar panels. More accurate and specialized programs should be employed for more detailed, project-specific analysis.

Due to Finland's northern location, PVGIS utilizes the ECMWF's ERA5 database, which was developed based on a reanalysis of climate data. The reanalysis data have been generated by employing weather forecast models, re-running these models, and correcting known errors in meteorological measurements. The model's low resolution, which produces one value every 30 kilometers or more, limits its use to more general applications. The ERA5 database is used for the calculations in this work. (PVGIS, n.d.)

The average daily monthly radiation is often sufficient to evaluate the overall system. A typical meteorological year (TMY), usually derived from three decades of data, can be used for a more detailed analysis. In the TMY data, radiation is categorized into three components: global radiation on a horizontal surface, direct radiation on a surface perpendicular to the solar radiation, and radiation reflected from the ground. The TMY data also takes into account local weather, which significantly affects the annual yield of the solar panel. The TMY file for a specific location can be downloaded from PVGIS. Besides radiation data, TMY provides information on temperature, relative humidity, wind speed and direction, and barometric pressure. All these parameters affect the performance of the solar panel. (PVGIS, n.d.)

2.3.5 Radiation on a horizontal surface

In addition to existing measured radiation databases, radiation on a horizontal surface can also be calculated from the Solar Constant. Throughout history, the solar constant G_{sc} has been calculated and measured several times; however, a value of 1367 W/m² is frequently used in current literature. (Duffie and Beckman 2013, 9)

The monthly average daily horizontal extraterrestrial radiation for the mean day of the month can be calculated as follows (Duffie and Beckman 2013, 37):

$$H_0 = \frac{24\times3600G_{sc}}{\pi}\left(1 + 0.033\cos\frac{360n}{365}\right)\times\left(\cos\phi\cos\delta\sin\omega_s + \frac{\pi\omega_s}{180}\sin\phi\sin\delta\right) \quad (18)$$

In this formula, ω_s denote the mean day's sunset hour angle. This can be calculated with the formula 19. (Chandraprabu 2019)

$$\omega_s = \cos^{-1}(-\tan\phi\tan\delta) \quad (19)$$

The monthly average clearness index K is calculated as the ratio of the monthly average horizontal radiation to the horizontal radiation outside the Earth, as shown in formula 20 (Yadav and Chandel 2014). Global horizontal radiation (H_g) can be obtained from various databases mentioned in the previous chapter, local meteorological agencies, or by using measuring devices for solar radiation at a test site.

$$K = \frac{H_g}{H_0} \quad (20)$$

Several models and correlations have been developed in the literature for calculating diffuse radiation; the most widely used is the Erbs model. (Maatallah et al. 2011)

$$\frac{H_d}{H_g} = \begin{cases} 1{,}0 - 0{,}09K, when\ K \le 0{,}22 \\ 0{,}9511 - 0{,}1604K + 4{,}388K^2 - 16{,}638K^3 + 12{,}336K^4\ when\ 0{,}22 \le K \le 0{,}8 \\ 0{,}165\ , when\ K > 0{,}8 \end{cases} \quad (21)$$

Other models for diffuse radiation are presented and utilized, for example, in studies by Maatallah et al. (2011) and Dervishi & Mahdavi (2011). These models consider different correlations, resulting in varied outcomes. For a more generalised approach to approximating diffuse radiation in different climates, Kalyanam & Hoffmann (2020) employed various machine-learning algorithms to estimate diffuse radiation based on the Erbs model. By carefully selecting training data, machine learning programs accurately estimate diffused radiation at various locations.

2.3.6 Solar radiation on an inclined surface

The global solar irradiance on the inclined surface of the Earth is divided into several components: direct, diffuse, and reflected. Direct radiation is the solar radiation that reaches the surface without being scattered by the atmosphere. Diffuse radiation is light scattered by molecules and particles in the atmosphere. Reflected radiation refers to light that is bounced

back from the ground. The ratio of the different radiation components to the total amount is influenced by several factors, most notably the weather, cloudiness, humidity, time of measurement, and the sun's position in the sky. (Khan et al. 2022) Total radiation on the tilted surface can be expressed with formula 22, in which H_B is a beam, H_D is diffused, and H_R is ground-reflected radiation (Yadav and Chandel 2014).

$$H_T = H_B + H_D + H_R \tag{22}$$

In the isotropic model, diffused radiation is assumed to come uniformly from all directions. These models are simpler than the anisotropic models and are commonly used in the literature, although they are less accurate than the anisotropic models. The most used isotropic model, from Liu and Jordan, calculates total radiation with a formula 23. (Yadav and Chandel 2014)

$$H_T = H_b R_b + H_d \left(\frac{1+\cos\beta}{2}\right) + H_g \rho_g \left(\frac{1-\cos\beta}{2}\right) \tag{23}$$

The first term accounts for direct radiation, the second for isotropic diffuse radiation, and the third for radiation reflected from the ground. Symbol β is the tilt angle of the surface, and ρ_g denotes the ground's reflectivity or albedo, which typically measures around 0.2 but can reach as high as 0.6 to 0.8 in snowy regions. The third term remains the same across all models. (Venkatachalam et al. 2019) The geometric factor, *Rb*, is the ratio of the average beam radiation on an inclined surface to that on a horizontal surface, calculated using formula 24 (Khan et al. 2022).

$$R_b = \frac{\cos\theta}{\cos\theta_z} \tag{24}$$

The literature presents various anisotropic models that account for solar accentuation and horizon brightening, as illustrated in Figure 14. Examples of these models for diffuse radiation can be found in the study by Yadav & Chandel (2014) and the textbook by Duffie & Beckman (2013).

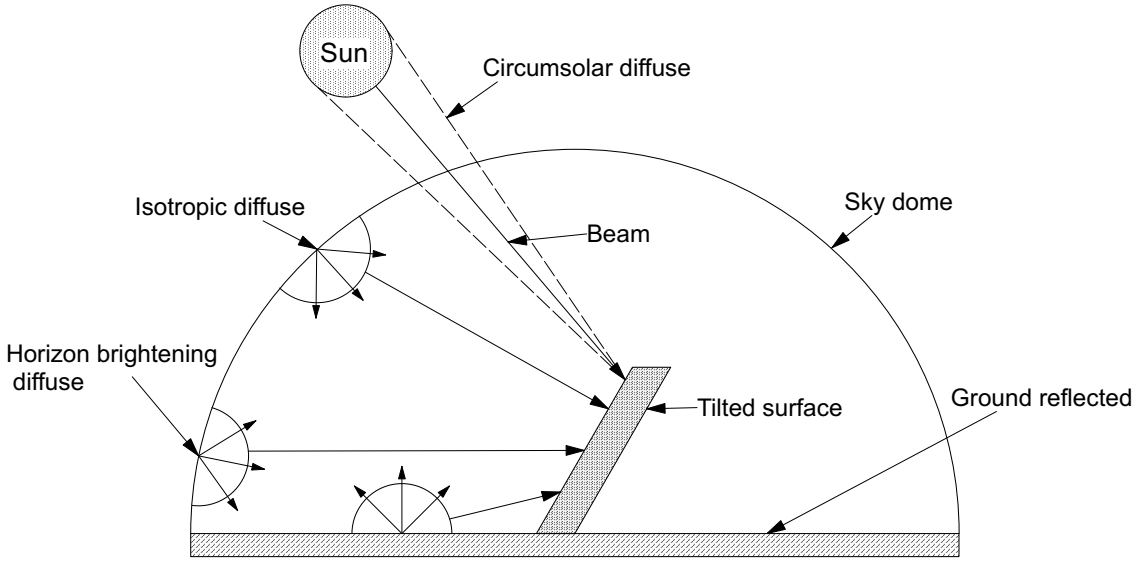

Figure 14. Different particle forms of radiation according to the anisotropic diffusion theory (based on Maatallah et al., 2011).

In the thesis's experimental section, the modified total isotropic plane of array irradiation (POA) is calculated with formula 25 from Nour et al. (2020).

$$\mathrm{POA} = \left(\frac{GHI-DHI}{\sin(\theta_{El})}\right) \times \cos(AOI) + \mathrm{DHI} \times \left(\frac{1+\cos\beta}{2}\right) + \mathrm{GHI} \times \rho_g \left(\frac{1-\cos\beta}{2}\right) \quad (25)$$

GHI and DHI refer to global horizontal irradiation and diffuse horizontal irradiation, respectively. Direct horizontal can be calculated by subtracting DHI from GHI.

The angle of incidence for solar panel arrays is determined using formula 26 (Nour et al. 2020).

$$AOI = \mathrm{acos}\big(\cos(\theta_Z) \times \cos(\beta) + \sin(\theta_Z) \times \sin(\beta) \times \cos\big(\gamma_s - \gamma_{array}\big)\big) \quad (26)$$

Where θ_Z is the solar zenith angle, β_t is the tilt angle of the PV panel, γ_s is the solar azimuth angle, and γ_{array} is the azimuth array angle.

2.3.7 The optimal tilt angle of the solar panel

The optimal azimuth angle for a solar panel in the northern hemisphere is south, as it captures the most sunlight at noon. Alternatively, solar panels can be installed facing east or west, which effectively utilizes the morning and evening sun. The most expensive option is the sun-tracking system, available in uniaxial and biaxial configurations. In uniaxial configurations,

the panel follows the sun only in elevation, while in the biaxial model, it also adjusts to track the sun's azimuth angle. (Maatallah et al. 2011)

The optimal angle for a solar panel without a reflector can be determined by conducting on-site tests to find the angle at which the panel performs best or by estimating total radiation using various algorithms, as noted in Khan et al. (2022). In this context, it is essential to consider the season, as there is a significant difference between the optimal angles in winter and summer, particularly at higher latitudes. Therefore, the optimal angle is the position that captures the most solar radiation, whether measured monthly, seasonally, or annually. The panel tilt angle can be adjusted each month, either automatically or manually. (Khan et al. 2022; Maatallah et al. 2011)

Kallioğlu et al. (2019) created an empirical algorithm to calculate the optimal solar panel angle for the Northern Hemisphere. Using this algorithm, they developed 12 functions based on declination angle and seven based on position latitude. The accuracy of these functions was verified through statistical methods and comparisons with previous studies, as well as results from NASA and PVGIS. In the Northern Hemisphere, the accuracy of the functions varies with latitude. The most accurate optimal angle functions for high-latitude locations (45° N - 65° N), which include Finland, are formulas 27 and 28. (Kallioğlu et al. 2019)

$$\beta_{opt} = 15{,}84ln(\phi) - 20{,}24 \tag{27}$$

$$\beta_{opt} = 3{,}0844(\phi)^{0{,}6594} \tag{28}$$

Symbol ϕ is the latitude of the installation site. The tilt angle of solar panels must be carefully considered, especially in large-scale installations, to ensure that the user receives the panels' full potential.

2.4 Basics of Reflectors

Several materials can serve as reflectors to enhance the yield of PV panels. Chapter 2.4.1 outlines various types, while Chapter 2.4.2 details key characteristics of these reflectors. Chapter 2.4.3 discusses common issues affecting reflectors. Chapter 2.4.4 describes the effects of shading that reflectors create on solar panels. Chapter 2.4.5 compares typical metal reflectors that can be used on roofs, and Chapter 2.4.6 analyzes key outcomes from various studies and sources.

2.4.1 Types of reflective surfaces

Research on reflector materials centers on developing and analyzing reflectors, or solar mirrors, intended for use in solar-thermal power plants. Mirrors are utilized in concentrating solar thermal power (CST) plants to focus solar radiation onto a receiver. This enables the energy from the sun's rays to turn water into steam, which then drives a steam turbine to generate electricity or to be used as heat in industrial processes. (Bellos 2019; U. S. Department of Energy 2022)

Hybrid systems, which combine photovoltaic (PV) and thermal power technologies, are also studied with reflectors. In hybrid systems, thermal power is utilized to cool the photovoltaic (PV) array. Researchers have shown increasing interest in utilizing mirrors alongside solar panels in recent decades. Mirrors and other reflective surfaces can enhance the energy directed toward solar panels. (Kostić et al. 2010; Michael et al. 2015)

Typically, reflectors are positioned on the ground between rows of ground-mounted solar panels. This effect is particularly significant in northern latitudes, where the distance between solar panel rows is greater due to the sun's lower position. (Brogren 2004) Mirrors are used less often on roofs due to limited space and the roof's angle.

Figure 15. shows the breakdown of solar mirrors by material. Metals, particularly silver and aluminum, are the most reflective materials. Steel can also be polished and coated to serve as a good reflector. Lighter polymer-based mirrors have also been developed for solar thermal power plants. (Malwad and Tungikar 2021). The mirrors used in solar power plants are optimized to reflect as much radiation as possible, as their energy production relies on capturing thermal radiation (García-Segura et al. 2016). Aluminum and stainless steel reflectors are more commonly used with PV technologies because they are cheaper and more durable than glass mirrors.

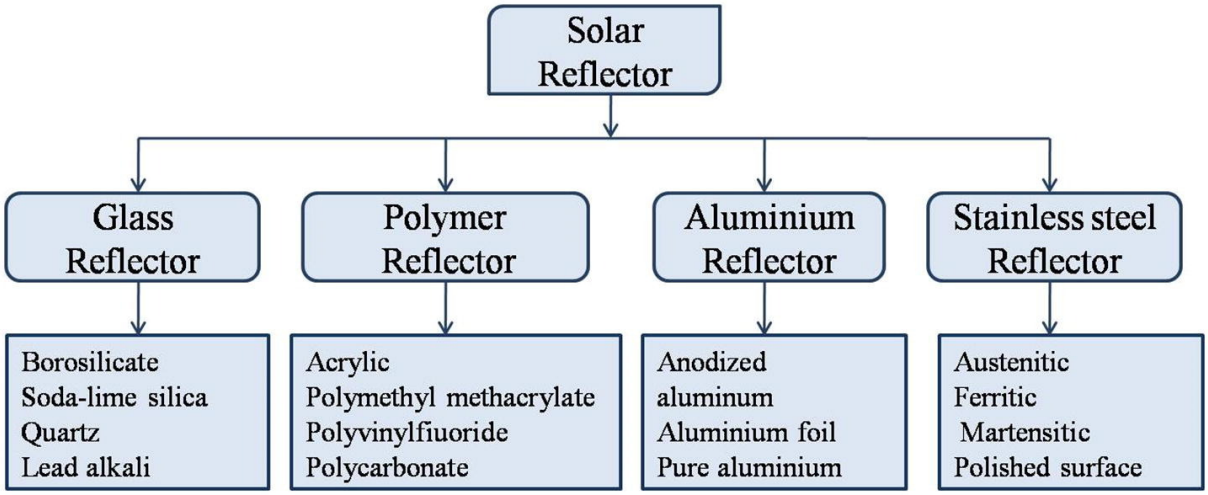

Figure 15. Classification of solar reflectors based on material (Malwad and Tungikar 2021)

2.4.2 Characteristics of reflector materials

Brogren (2004) states that a suitable reflective material should possess at least the following properties:

- High reflectivity.
- The reflector ought to cost less than the panel.
- The durability of reflectivity should ideally last for the panel's lifetime, approximately 20 to 30 years, or be easy to replace.
- Simple to clean.
- Mechanically strong and resistant to snow, rain, and wind.
- Fairly lightweight and simple to install.
- Environmentally friendly, contains no toxic substances.
- Visually appealing.

Reflectors designed for solar panels are typically simpler than CST reflectors, primarily due to cost considerations. Usual reflectors with PV panels are typically made from simple, polished stainless steel sheets or aluminum sheets. (Brogren 2004; García-Segura et al. 2016; Kostić et al. 2010) Some studies also use commercially available reflectors (Ahmed and Amer 2021). A solar panel reflector should be affordable, offsetting expenses through the additional revenue it generates. Cost effectiveness depends on the material, thickness, and size of the

reflector. Rooftop reflectors can be either temporary reflective materials or more permanent metal reflectors integrated into the roof. (Baccoli et al. 2018; Sultan et al. 2024)

2.4.3 Problems with reflectors

In their review article, García-Segura et al. (2021) assessed and identified the types of degradation in the reflectors used in concentrated solar thermal (CST) plants. They noted 16 distinct failure types and sources affecting the reflectors they examined. Figure 16 illustrates the 16 degradation types and their sources, along with example images. The primary causes of reflector deterioration are temperature fluctuations, the interaction between the reflector and humidity, and air pollution. These problems also impact reflectors used with PV panels, which must withstand the same outdoor conditions as mirrors in CST plants.

Many studies utilize aluminum as a reflector due to its relatively low cost, widespread availability, and superior reflectivity across a spectrum. However, the challenge with aluminum in outdoor applications is its reactivity with various molecules, which impacts its reflectivity over time. Due to this reactivity, an aluminum reflector must be protected through anodizing or, even better, by applying a varnish or polymer coating. (Brogren 2004; García-Segura et al. 2016)

Degradation types of reflector materials used in concentrating solar thermal systems

Defect type	Damaging agent	Example	Defect type	Damaging agent	Example
Abrasion	Contact cleaning		Corrosion spots	Humidity, chlorides, pollutant gases	
Erosion	Airborne particles	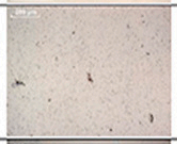	PVD-layer corrosión (observed for aluminum reflectors only)	Humidity, chlorides	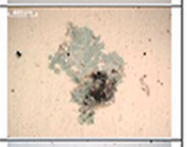
Stains on the glass	Humidity and chemicals		Micropitting (observed for aluminum reflectors only)	Humidity, chlorides	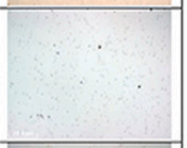
Deposits	Airborne particles and humidity	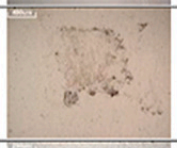	Tarnishing	Temperature, humidity	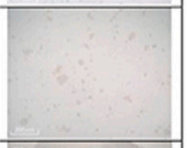
Paint deterioration	UV radiation		Blisters	Humidity	
Edge corrosion	Humidity, chlorides, pollutant gases	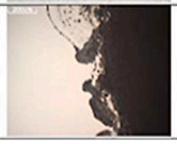	Delamination	Thermal cycling	

Figure 16. Reflector degradation types and their sources (García-Segura et al. 2021)

Brogren (2004) tested and analyzed six different aluminum reflectors in field experiments conducted over nine months under Swedish weather conditions, as well as in a climatic test chamber in a 2000-hour cycle. After the outdoor testing, the total reflectivity of the anodized aluminum samples decreased from approximately 88% to 83%. The 18-year-old test sample showed a decrease in specular reflectivity to 18% due to moisture damage. The reflectivity of anodized aluminum is affected by the thickness of the anodic layer. Thin-coated and lacquered aluminum performed better than bare aluminum in outdoor tests due to the protection it offered against the elements. The accelerated weathering cycle produced different outcomes than the outdoor tests. Therefore, test results should be carefully analyzed to understand the reasons behind the degradation of reflectivity observed in those tests. (Brogren 2004)

The reflector's downsides include possible shading and temperature increases in solar panels resulting from increased irradiance. For solar panels, a 1°C increase in temperature can reduce electrical efficiency by 0.125-0.5%, so most studies investigating reflectors also analyze the impact of temperature increases on solar panels. These factors also negatively impact the

lifetime of PV panels. Proper planning can mitigate most of the problems caused by shading and increased temperature, such as creating an air gap between the panel and the roof for cooling, and optimizing the reflector and panel angles to minimize shading. (Agyekum et al. 2021; Kabeel et al. 2019; Santiago et al. 2018)

Tabasi et al. (2019) calculated that a temperature increase resulted in a loss of approximately 1% in the annual electricity yield of a simulated reflector and panel system. Using natural convection, creating an air gap is the easiest way to cool a PV panel on a roof. The recommended size for an air gap is 150–200 mm, which can decrease the temperature of a PV panel by 10–20 degrees Celsius (Naghavi et al. 2021). Passive air gap cooling is usually sufficient in temperate climates, such as those in Northern Europe. In hot and dry climates, these temperature increases can also be mitigated with various cooling methods, including the use of phase change materials (PCMs), heat sinks, and hybrid systems that combine solar panels with solar thermal collectors (Bhakre et al., 2021; Lotfi et al., 2022).

2.4.4 Shading created by reflectors on solar panels

Reflectors can create shade on solar panels, reducing their energy output. Ground-mounted reflectors are typically positioned between rows of solar panels to prevent them from casting additional shadows. Row spacing calculations can be used to estimate the size of the reflector to analyse its effectiveness. Row spacing for the location is calculated during the winter solstice when shadows are longest. (Odungat et al. 2020)

The shading by the reflector is more pronounced on roofs and individual solar panels. Tabasi et al. (2019) discuss and optimize the shadows of solar panels equipped with reflectors. The shadows cast by reflectors on south-facing solar panels vary in the morning and afternoon, depending on the angle of the reflector. In-depth analysis examines the effect of the shadow cast by the reflector on the solar panel's output. The system's location influences the sun's general path across the sky, which means that the further north the panel is placed, the lower the average elevation angle to the sun. (Tabasi et al. 2019) A reflector affects solar panels in three ways, as mentioned by Tabasi et al. (2019) using reflector angle (α) and solar elevation angle (θ_{El}):

- The solar panel receives additional radiation from the reflector, $\alpha < \theta_{El}$
- The reflector does not affect the radiation received by the solar panel $\alpha = \theta_{El}$ and

- A reflector shades a solar panel, impairing its performance $\alpha > \theta_{El}$.

Agrawal et al. (2022) calculated the reflection and shadow surface functions based on the Sun's angles. The reflection and shadow areas on a solar panel depend on the system's tilt angles, the solar azimuth angle, and the angle of incidence. Illuminated and shaded areas produced by a reflector can also vary in shape on the solar panel. Figure 17 presents examples of areas and patterns from Agrawal's study and a figure containing the function definitions. The size and shape of the shadows are not analyzed further in this work.

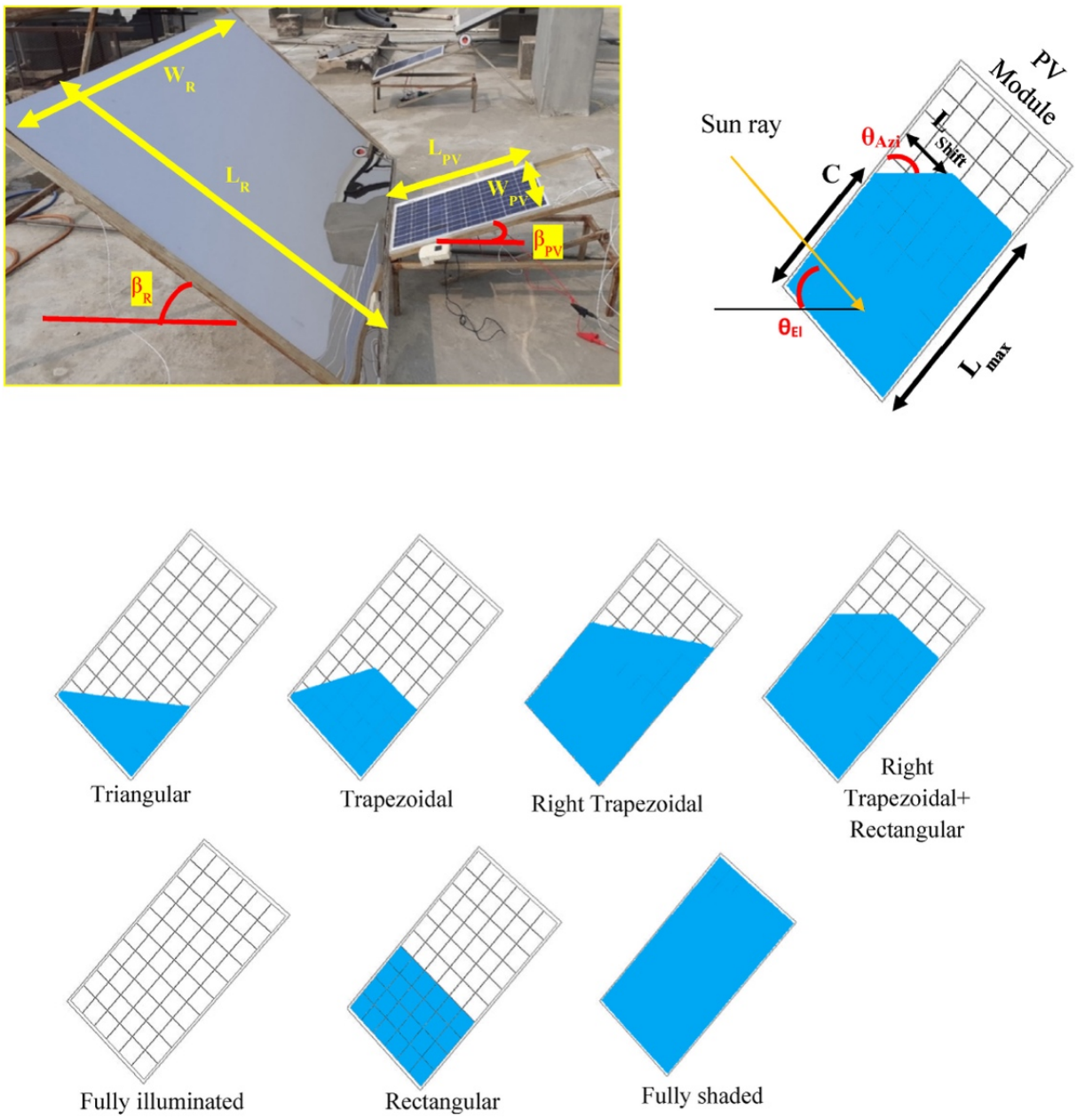

Figure 17. Reflection and shadow patterns caused by a reflector on a solar panel (Agrawal et al. 2022).

Multiple studies have examined the size of reflectors and optimized them to maximize the output of solar panels. The additional irradiance provided by the reflector increases rapidly as its size grows, reaching approximately three times the size of the solar panel, after which the additional irradiance slows down. (Baccoli et al. 2018; Rönnelid et al. 2000; Tabasi et al. 2019) Optimizing the reflector's size is a delicate balancing act between maximizing yield and minimizing land and rooftop use. It is also important to consider land use when designing a solar panel system, allowing for smaller solar panels if space is limited, along with proportionately smaller reflectors. Additionally, the optimal size of the reflector is influenced by the angle between the reflector and the solar panel, which can be adjusted according to the season or month (Baccoli et al. 2018).

2.4.5 Reflectors in research

Table 2 summarizes studies that have analyzed the effects of reflectors on solar panels at different tilt angles. These studies frequently differentiate between the additional irradiance provided by the reflector and the increased electricity production of the solar panel. Due to significant methodological differences, these studies cannot be directly compared. Some studies evaluate individual days, as seen in Setiawan & Dewi (2013), while others calculate the whole year's production growth for a test site, as in the study by Tabasi et al. (2019). Some of these studies adjust the angles of the reflector and PV panel to determine the optimal combination for maximum power. Test locations also vary between studies concentrated on latitudes 25°–50°N, which can skew the results because they are heavily influenced by location.

Table 2. Overview of the reflector studies used in the thesis (Viljami Kukkola)

Study	Tested tilt angles of surfaces (Reflector is α and panel is β)	Output improvement (%)	Location	Comments
Abed et al. (2020)	Both 30°	On one test day, the average power increased by 22.4%	Baghdad, Iraq, 33.3°N, 44.4°E	CIGS PV solar system tested—evaluation of system power parameters.
Agrawal et al. (2022)	Several scenarios	30,22 % increase when β =45° and α=13°	Jaipur, India, 26.86° N, 75.81° E	Reflector size effect and calculation of the optimum angle. Model for 20°-30° latitude, reflector stainless steel

Study	Tested tilt angles of surfaces (Reflector is α and panel is β)	Output improvement (%)	Location	Comments
Baccoli et al. (2021)	Changed every month	EF: 6-17% improvement	Cagriali, Italy, 39,16° N, 9,7° E.	Analysis of the reflector size impact. The difference between the model and the tests was about 3.4%.
Kim et al. (2021)	α is 15,5° and β changes 30°, 45° and 60° and 75°	4% to 23% depending on the angles of the panel and reflector	Calgary, Canada, 51.05° N, –114,06°E	The reflector has a semi-circular shape that minimizes shadows.
Lewis et al. (2024)	Varies according to the day.	0,9–4,5 % per year	Golden, Colorado, 39.8° N	Bifacial solar tracking panel backside add-on yield and economic assessment
Malik & Chandel (2020)	α changes according to the time of year and β is 31°.	10-19.84% in summer and 10-13.23% in winter	Hamirpur, Himachi Pradesh, India	Differentiated sunny and cloudy days
Matsushima et al. (2003)	The angle between the panel and the reflector is 90° and the whole system is at an angle of 20–30°.	50 % increase at noon	Indoors and outside conditions tested	Results calculated using midday values. Mirror, reflection coefficient 0.95.
Nour et al. (2020)	Optimization of angles and reflector length	Radiation increases between 8,5 % and 28,7 % depending on the size of the reflector	Sirta, Palaiseau, Paris, France.	0.8 reflection coefficient, calculated and tested only for the increase in radiation from the reflector
Odungat et al. (2020)	α is 37° and β is 20	Energy generation up 30.3%	South India, 10.8°N, 78.8°E	System performance and economic analysis
Pavlović & Kostić (2015)	β is 45° and α is optimized to maximize output	Solar irradiance increased about 50% with two reflectors and close 80% with all four during summer.	Niš, Serbia, 43°N, 21°E	The study uses two or four Al sheet reflectors fixed to panel sides. Optimizes reflectors' tilt angles.
Rönnelid et al. (2000)	In the ideal scenario, the angle of the reflector changes;	20-25% increase, variable up to 40% with angle	Stockholm, Sweden, 59.4° N	The effect of reflector size on the result. A

Study	Tested tilt angles of surfaces (Reflector is α and panel is β)	Output improvement (%)	Location	Comments
	otherwise, β = 50° and $\alpha \approx$ 6-8°			simple economic assessment.
Setiawan & Dewi (2013)	Reflector angle varies, panel is horizontal	Stainless steel 21,5 % and aluminium foil 31,5 %	Depok, West Java, Indonesia, 6.36° S, 106.82 E	Reflector effect on the I-V curve of the panel
Tabasi et al. (2019)	S1: None, 0° S2: None, 35° S3:α is 0° and β is 69.084° (optimized)	S1: 216, 67 kWh S2: 283, 33 kWh S3: 613.89 kWh	Tehran, Iran	Angle optimisation algorithm, shadow analysis and temperature effect

Studies conducted with reflectors in northern latitudes (+50° N) are rare; however, according to available studies, yearly yield improvements are concentrated in the summer season due to the low irradiance in winter. Rönnelid et al. (2000) investigated the use of reflectors under northern low-sun conditions. They found a 20% to 25% increase in annual production with reflectors that have a reflectance of 0.8. Using a superior reflector and adjusting its tilt angle according to the month can enhance yields by up to 40% at Swedish latitudes. Kim et al. (2021) studied a unique half-circle reflector in Calgary, Canada. Its impact on solar panel output varied depending on reflector tilt angle, but the best increase was 17% to 23%.

Field experiments are conducted to verify the results of studies that developed a calculation model. Some reviewed studies were validated using statistical methods, such as the mean absolute error (MAE) and expected mean error (EMAE). The accuracy of the model can be estimated using bias error and mean bias error (MBE and RMBE). Differences of less than 10% can be considered acceptable for the studies examined, given the numerous variables involved (Nour et al. 2020). Most models generally overestimate the amount of radiation compared to field tests. For example, Baccoli et al. (2018) created a model that yielded an additional approximately 3.4 percentage points higher than that of a field experiment. The differences arose from elevated solar panel temperatures and uneven irradiance.

Different solar panel technologies exhibit varying outputs, so the additional radiation from the reflector will affect each type in distinct ways. Ahmed & Amer, (2021) compared three types of panels: amorphous, single-crystalline, and thin-film, which are the most common varieties. The study found that the yield of the panels increased by approximately 35% to 45%, with the

thin-film panel showing the best performance. Moreover, the thin-film panel was least influenced by temperature increases that impact solar panel performance.

Research indicates that the additional yield from a reflector placed beneath a solar panel ranges from 20% to 40%, depending on the previously mentioned parameters. Generally, reflectors provide a cost-effective way to enhance electricity output from solar panels, provided there is sufficient space for the reflector. Reflectors are also a cheap way to boost the output power of a smaller, off-grid system, where the position and angles of reflectors can be adjusted easily. Local conditions significantly influence these studies, making analytical estimates and measurement results often indicative rather than definitive.

2.5 Irradiation Analysis of Solar Panels with Reflectors

Calculating the additional irradiation is crucial for assessing the reflector's impact on the operation of PV panels. Chapter 2.5.1 examines the reflector's overall effect. As detailed in Chapter 2.5.2, the reflector must be positioned at the correct angle relative to the solar panel to optimize its performance. Chapter 2.5.3 outlines a more comprehensive workflow and the calculation of the reflector's radiation, which is used in the Experimental Section of the thesis. Finally, Chapter 2.5.4 provides the calculation formulas for determining the potential shadow cast by the reflector.

2.5.1 The impact of reflectors on irradiation

Various mirrors and reflectors can enhance the radiation received by solar panels. The most common type is flat reflectors, which are the focus of this study. Researchers have also developed various types of reflectors, including parabolic reflectors, V-reflectors, and Fresnel reflectors, each with its own advantages and disadvantages. (Shanks et al. 2016)

The use of reflectors with solar panels has been studied since the 1970s, when the first mathematical models were created to calculate reflected radiation. The simplest way to estimate the amount of radiation a reflector receives is to employ various geometric models to determine the total radiation from the reflector. One such model is utilized in the experimental section and presented in the following Chapter. More detailed analyses consider the effects of temperature and the influence of shadows on the solar panel's electricity output.

This thesis does not delve deeply into the theory of light and reflection, but several considerations must be made when designing a reflector for a solar panel. Reflection can be

understood as comprising two distinct types: specular and diffused reflection. Reflection also depends on surface roughness. Rough surfaces diffuse light, scattering it in all directions, whereas specular reflection occurs on a mirror-like surface. Most materials have a combination of these two types. (Heimsath and Nitz 2019; Hermany, n.d.)

The most effective reflector materials, such as aluminum, exhibit high reflectivity across the entire electromagnetic spectrum, with total reflectivity reaching over 90%. However, numerous studies suggest that for solar panels, more stable materials that reflect a higher proportion of diffused radiation—such as stainless steel—should be used as reflectors because mirrors can cause the solar panel to form hot spots on the surface and mismatch losses, ultimately reducing its output (Michael et al. 2015; Tripanagnostopoulos et al. 2002).

Several studies have demonstrated that using a tilted reflector can enhance the radiation reaching the solar panel, as shown in Table 2. The impact of the reflector angle on the solar panel is also the focus of various studies, as the optimal angle of the reflector depends on the Sun's position (Pavlović and Kostić 2015; Tabasi et al. 2019). Reflectors are more frequently utilized in solar thermal technologies, which capitalize on the thermal radiation of the Sun's rays. Direct solar radiation is primarily used in thermal applications, while diffused radiation is harnessed in solar panels and PV/T technologies. The radiation should be evenly distributed across the entire surface of the solar panel since the current of series-connected solar cells is determined by the lowest current of the series. (Michael et al. 2015)

A PV panel with a reflector reduces the radiation reflected from the ground to nearly zero, especially when the reflector is positioned at an angle to the panel. However, several studies, such as those by Kim et al. (2021) and Nour et al. (2020) still incorporate the radiation reflected from the ground into their mathematical models.

2.5.2 Placement of the solar panel and reflector

The most common and cost-effective combination of reflector and solar panel is illustrated in Figure 18, which features a flat additional reflector mounted on one side of the solar panel (c). These reflectors can be used between rows of ground-mounted solar panels (a and b). Also depicted in the same figure is a curved reflector developed by researchers that directs more radiation into the solar panel (d) than a straight flat reflector, but it creates a hotter spot in the horizontal direction. This drawback can be minimized by selecting a solar panel design with cells connected horizontally. (Choi et al. 2019)

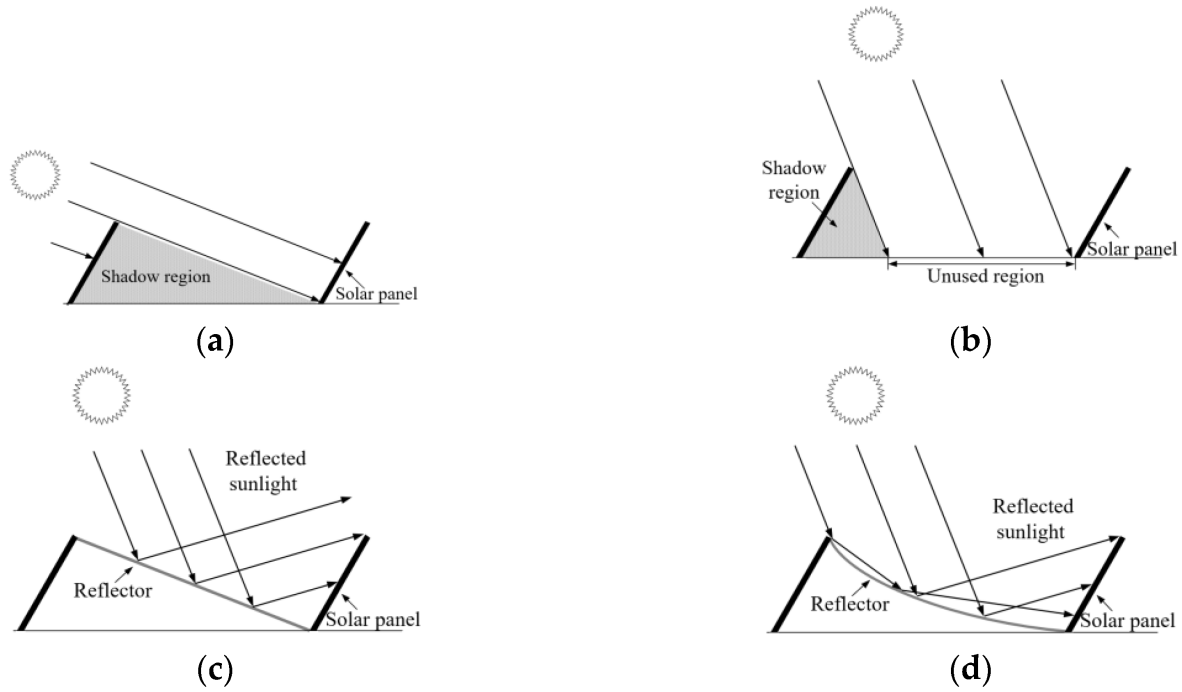

Figure 18. Location of an additional reflector between solar panel rows (Choi et al. 2019)

Reflectors can be used almost anywhere. They can also serve as ground reflectors for vertical and sun-tracking bifacial PV panels (Durković and Đurišić 2021; Lewis et al. 2024). In an urban environment, reflectors can be incorporated into the architecture and to minimize land use by utilizing overhanging reflectors with PV panels near buildings and fences (Al-Ghussain et al. 2023). Another way to utilize reflectors is to install smaller reflectors on each side or on opposite sides of the solar panel. This method works well for individual panels, such as the solar tracking panels shown in Figure 19. (Manosroi et al. 2020)

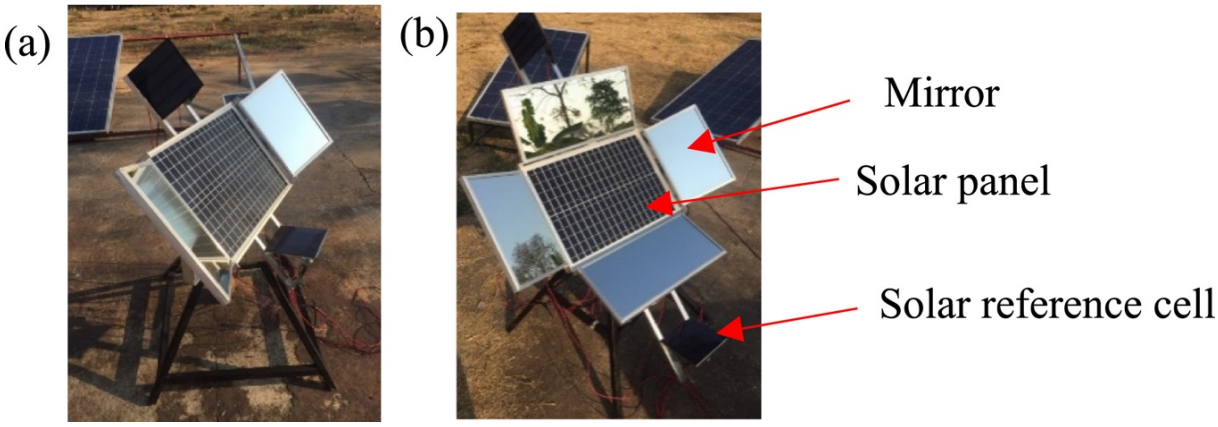

Figure 19. Reflectors with two short sides (a) and all sides (b) (Manosroi et al. 2020)

The irradiation gain of bifacial solar panels can be enhanced by utilizing reflectors, as demonstrated by the roof-mounted product from the Spanish company FutureVoltaics and a study by Lewis et al. (2024). Durković & Đurišić (2021) compared a similar vertical arrangement of bifacial panels and reflectors to standard south-facing bifacial panels. Al-

Ghussain et al. (2023) suggested an overhang reflector for panels near a wall or fence. Reflectors can be applied in various locations for solar panel arrays of different sizes. A common barrier to using reflectors on site is often the lack of an optimization tool and the limited availability of practical and commercial reflectors.

2.5.3 Irradiation from reflectors to a solar panel

Several models have been developed over the decades to calculate the additional radiation from a reflector, but they follow a general formula shown in Figure 21. Most models also consider the potential shadow created by the reflector and the increased temperature of the solar panel when calculating the yield (Agrawal et al. 2022; Tabasi et al. 2019). Many studies have created a model in MATLAB to expedite the calculation (Baccoli et al. 2018). Some studies utilize models based on bidirectional reflectance distribution function (BDRF), which was designed for isotropic rough surfaces. This approach works best when the reflector functions as a diffuse reflector. (Andrews et al. 2013)

Figure 20 summarizes a general workflow for calculating and analyzing the effect of a reflector on irradiation and a solar panel's output. The analysis begins with the coordinates of the selected location, the horizontal radiation values at that location, the time scale, usually one year, and the chosen solar panel angle, which can be optimized separately. These parameters are typically available in databases. Next, the reflector's length, angle, and reflectivity coefficient are determined. The length and angle of the reflector are usually optimized based on the total radiation. (Wijesuriya et al. 2017; Iskandar et al. 2023; Malik and Chandel 2020) The sun angles are calculated using a predefined calculator or according to the formulas from Chapter 2.3.3.

The total irradiation is then calculated using user-selected formulas. The total irradiance is also affected by any shading created by the reflector, whose size and impact must be estimated. The increase in panel output varies depending on the model, and the influence of temperature is generally considered here.

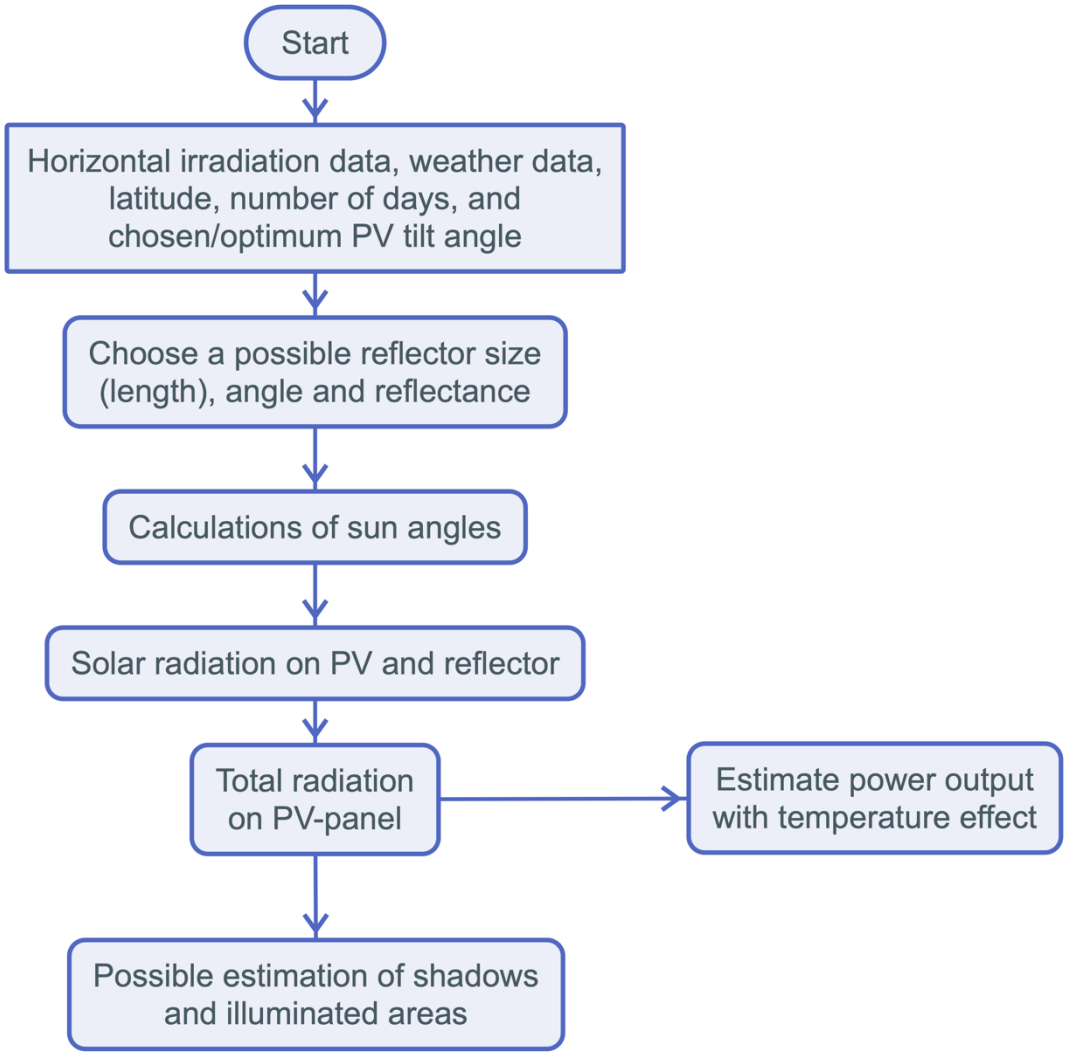

Figure 20. The basic workflow for calculating irradiation

The primary distinction among studies is in how they calculate the radiation from the reflector to the solar panel. Ultimately, the various components of the radiation are summed to determine the total radiation. The total radiation, temperature change, and panel efficiency can be used to estimate the increase in panel yield. In most studies, the computational analysis is validated by practical measurements, which also ensure the model's accuracy at that location.

Nour et al. (2020) assessed the impact of a plane reflector on the total amount of radiation. The researchers optimized the design of the reflector and the solar panel, including the angles and the length of the reflector to the solar panel's length. Solar radiation is divided into three components: direct, diffuse, and radiation reflected from the ground. In addition to these components, the plane reflector reflects both direct and diffuse radiation onto the panel. The

calculations involve determining the solar angles and the surfaces of the design. The model is relatively simple and considers the shadows and light beams created by the reflector, which is particularly important at northern latitudes. (Nour et al. 2020)

This calculation model is utilized in the experimental part of the thesis across three Finnish cities. The analytical radiation calculation begins with the angle of incidence, as determined by formula 25, and the view factors from the reflector to the solar panel, as well as from the panel to the reflector, which are calculated using formulas 29 and 30. (Nour et al. 2020)

$$VF_{R_{PV}} = \frac{\left(L_{PV}+L_R-\sqrt{\left({L_{PV}}^2+{L_R}^2-2\times L_{PV}\times L_R\times\cos\theta_{PVR}\right)}\right)}{2\times L_R} \tag{29}$$

$$VF_{PV_R} = VF_{R_{PV}} \times \frac{L_R}{L_{PV}} \tag{30}$$

L_{PV} is the PV panel's length, and L_R is the length of the reflector. Gelegenis et al. (2015) calculated the solar elevation angle and azimuth angle for the reflector as follows:

$$\alpha_1 = \alpha_s - \text{atan}(\tan(\zeta) \times \cos(\gamma_s)) \tag{31}$$

$$\gamma_1 = \text{atan}(\cos(\zeta) \times \tan(\gamma_s)) \tag{32}$$

Where ζ is the reflector tilt angle. The sun's profile angle is calculated using formula 33.

$$\alpha_p = \text{atan}\left(\frac{\tan(\alpha_s)}{\cos(\gamma_s)}\right) \tag{33}$$

from which the profile angle of the reflector is calculated with the following formula 34

$$\alpha_{p1} = \alpha_p - \zeta \tag{34}$$

The coefficients m1, m2, and m3 can be calculated by functions 35, 36, and 37.

$$m_1 = \sqrt{\tan(\gamma_1)^2 \frac{1}{\tan(\psi+\alpha_{p1})^2}} \tag{35}$$

$$m_2 = \frac{\cos(\alpha_{p1})}{\sin(\psi+\alpha_{p1})} \tag{36}$$

$$m_3 = \sqrt{\tan(\gamma_1)^2 \frac{\sin(\psi)^2}{\sin(\psi+\alpha_{p1})^2}} \tag{37}$$

Where ψ is the angle between the PV panel and reflector. Finally, the angle of incidence of the reflector on the solar panel can be calculated using the coefficients m1, m2, and m3 according to formula 38. (Gelegenis et al. 2015)

$$AOI_{R,PV} = \text{acos}\left(\frac{m_2^2+m_3^2-m_1^2}{2\times m_2\times m_3}\right) \quad (38)$$

The extra radiation from the reflector is determined by combining the radiation reflected off the ground with the viewing coefficient and separately calculating the directly reflected and diffusing radiation. (Nour et al. 2020)

Ground-reflected incident radiation is calculated using formula 39.

$$GRISR = GHI \times \rho_g \times \left(\frac{1-\cos(\theta_{tilt})}{2} - VF_{PV_R}\right) \quad (39)$$

The direct reflected beam irradiance is calculated using formula 40.

$$DRBI = R \times BHI \times \frac{\cos(AOI_{R,PV})}{\cos(\theta_Z)} \quad (40)$$

Diffuse reflected radiation is calculated using formula 41.

$$DRSR = \left(1 - VF_{R_{PV}}\right) \times DHI \times \frac{1+\cos(\beta)}{2} + GHI \times \rho_g \times \frac{1-\cos(\alpha)}{2} \times R \times VF_{PV_R} \quad (41)$$

Where β is the solar panel's tilt angle, α is the reflector's tilt angle, and BHI is beam radiation to a horizontal surface. (Nour et al. 2020)

The analysis estimates the additional radiation from the reflector using three different cases in which the radiation levels vary due to the radiation and shadows created by the reflector.

Case 1: The additional reflected radiation covers or exceeds the solar panel. Formula 42 includes all terms.

Case 2: The additional reflected radiation covers part of the panel, resulting in zero DRBI. In this case, the non-uniform radiation activates the bypass diodes, ignoring the directly reflected radiation.

Case 3: When a reflector partially or completely shades a solar panel, only the diffuse radiation from the sky and the reflector is considered in Formula 42. (Nour et al. 2020)

The length of reflected radiation for a solar panel can be calculated by Tabasi et al. (2019) using the formula 42. This can be used to estimate which case should be used.

$$I_{ref,max} = I_m \times \frac{\cos(\theta+\alpha)}{-\cos(\theta+\beta+2\alpha)} \quad (42)$$

where I_m represents the reflector length, θ the incident angle, α the reflector angle, and β the solar panel angle. A negative result indicates a shadow on the solar panel.

Finally, the general radiation formula and the additional reflector radiation formula are combined according to formula 43. Cases 1 to 3 must be considered when calculating the final radiation. (Nour et al. 2020)

$$POA_{Mir} = \frac{GHI-DHI}{\sin(\theta_{El})} \times \cos(AOI) + DHI \times \frac{1+\cos(\theta_{tilt})}{2} + GRISR + DRBI + DRSR \quad (43)$$

2.6 Economic and Environmental Assessment of Solar Panel Systems

An economic evaluation of solar panel systems should be conducted when considering solar panels for a site. Chapter 2.6.1 provides a brief description of solar panel system planning. More detailed information on installing solar panel systems can be found in the international standard IEC 62548. The economic viability assessment will impact both the investment decision and the actual size of the system. The most common assessment parameter is the levelized cost of electricity (LCOE) calculation, which is discussed in Chapter 2.6.2. The concept of net present value is defined in Chapter 2.6.2.

The environmental assessment primarily focuses on reducing greenhouse gas emissions through solar energy. Chapter 2.6.3 discusses a life cycle assessment (LCA) tool that can be used to conduct a more comprehensive and detailed environmental analysis. This chapter also introduces the Energy Payback Time (EPBT), which estimates how quickly a system generates the energy it consumes during its manufacturing. Each viability assessment is further influenced by the subsidies that the project receives.

2.6.1 System design principles

The careful design of a solar panel system is essential for ensuring an efficient and productive solar plant. The design's scope is mainly influenced by the system's size and intended use, such as a residential property, a commercial use, or a power plant. Figure 21 illustrates the

process diagram used by Boulahia et al. (2021) to estimate a residential property's solar capacity. However, this study lacks the economic and environmental assessments that are often conducted separately from the solar power yield evaluation.

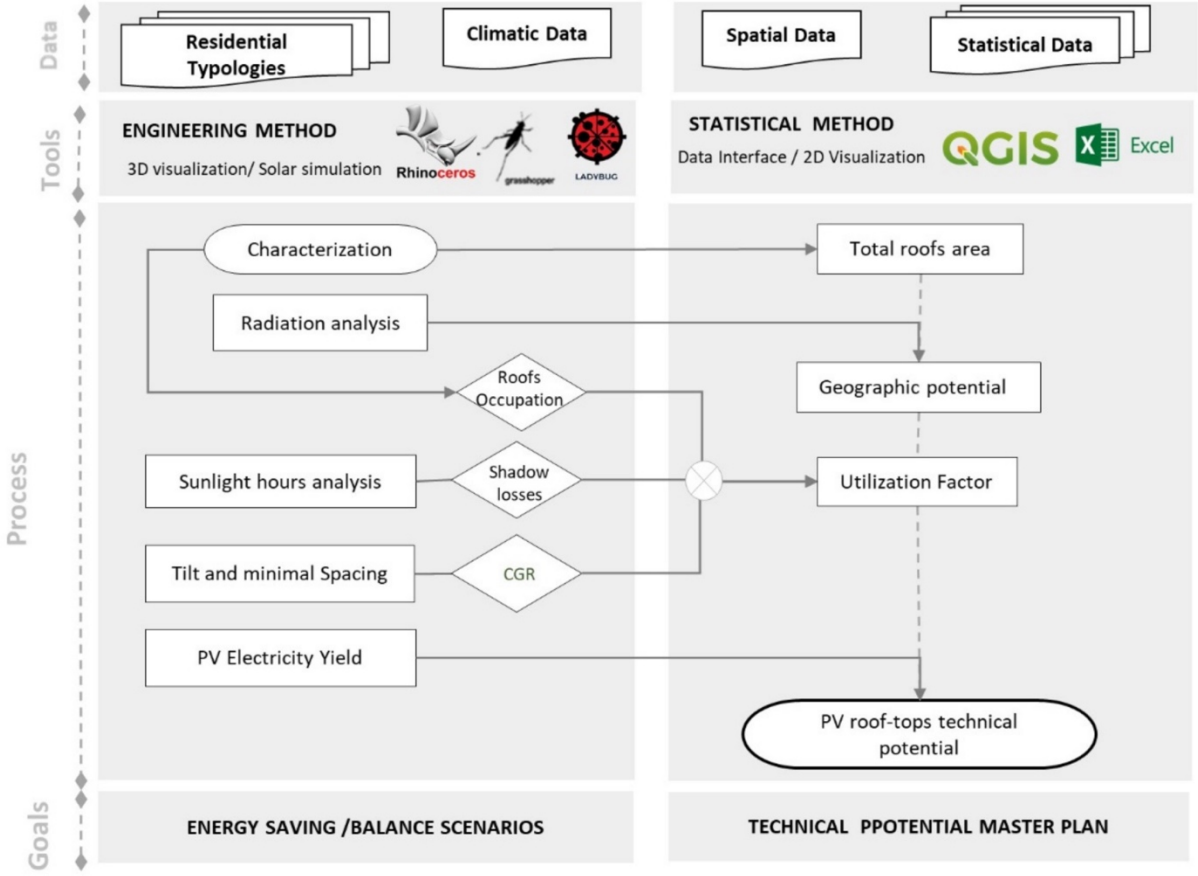

Figure 21. Process diagram for assessing the solar energy potential of a residential building (Boulahia et al. 2021)

The design of a solar panel system begins with assessing the location; the factors influencing this are summarized in Figure 22. The most significant factor is the amount of radiation, which is also affected by environmental shadows. (Vasel and Iakovidis 2017) Software such as PVSyst can be used to analyze the site's exposure and shadows at various times of the year. Suitable sites for solar panel farms can be estimated using geographic information systems (GIS) and various analysis tools. Common criteria for these analyses include:

- Energy criteria include irradiation and ambient temperature,
- geographical elements such as location, land use, and grid connections, and
- environmental criteria such as protected and culturally significant areas. (de Luis-Ruiz et al. 2024; Mokarram et al. 2020)

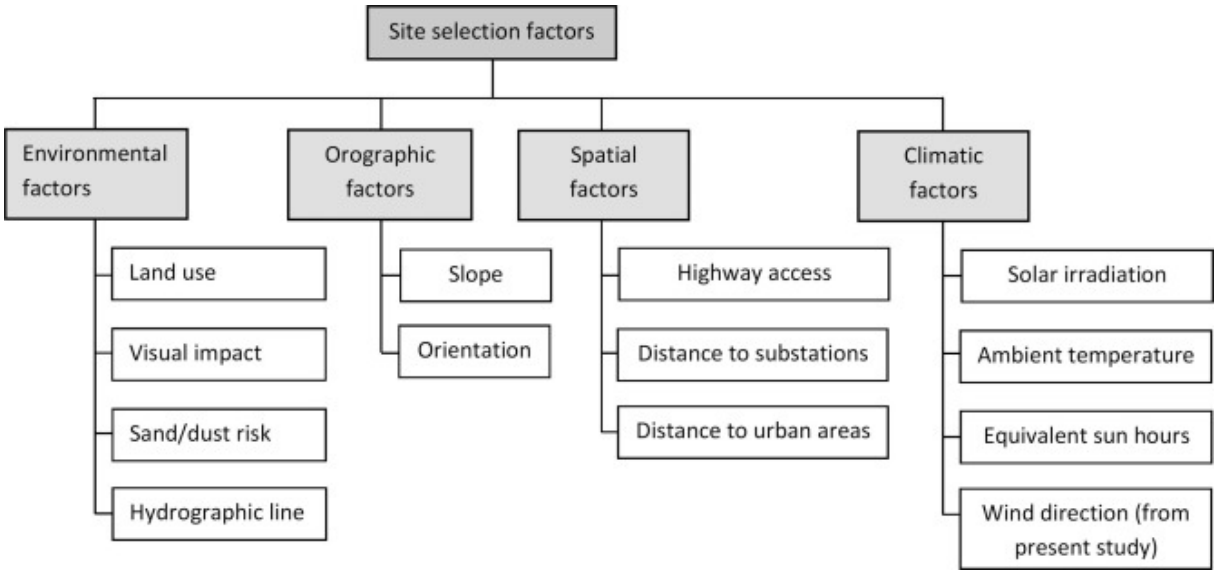

Figure 22. Location criteria for PV panel systems (Vasel and Iakovidis 2017)

The size of the system will be proportional to electricity consumption. The variability of solar panels' energy output should also be considered, depending on the time of day and the season. Energy storage, such as batteries, can compensate for production differences, though these systems have high investment costs. (Lai and McCulloch 2017) In addition to assessing solar power potential, the project must conduct an economic evaluation using methods like LCOE and payback period as described in the following chapters.

2.6.2 Economic evaluation of a PV system

The economic sustainability of solar energy systems can be measured and analyzed in various ways, often concurrently. The most common analytical measure is the levelized cost of electricity (LCOE). The free, but login-required, SAM program, maintained by NREL, is a valuable tool for conducting economic analyses of renewable energy sources, which can be used to calculate LCOE. The LCOE calculated for a project is typically compared to the price of available energy (Zainali et al. 2023).

The LCOE calculation is a versatile tool for analyzing projects of any size. It represents the actual cost of energy produced by a power plant, which can be generally described using the formula 44.

$$LCOE = \frac{\sum_{t=1}^{n} \frac{Total\ costs\ over\ service\ life\ (€)}{(1+r)^t}}{\sum_{t=1}^{n} \frac{Total\ energy\ production\ over\ service\ life\ (kWh)}{(1+r)^t}} \quad (44)$$

Where *n* is the expected lifetime of the system and *r* is the discount factor.

Zainali et al. (2023) analyzed the LCOE distribution in Swedish single-family houses, also using a Monte Carlo simulation to calculate LCOE metrics and to present the variability of various economic parameters. The study identified that the primary risk factor is *CAPEX*, referring to capital costs. This has been recognized since the project's inception. A solar panel project may be abandoned or postponed if the estimated capital expenditure (CAPEX) of the system exceeds the levelized cost of energy (LCOE) that is feasible. The *CAPEX* of a solar panel system is fixed and can be influenced by the buyer, for instance, through tendering.

A significant part of LCOE involves reinvestments for solar panel repairs and inverter replacements, which have a 15-year lifespan. Most repairs occur within the first five years, while solar panels typically last between 20 to 30 years. The initial electricity efficiency of solar panels decreases by approximately 0.1% to 0.5% each year, which negatively impacts the PV system's levelized cost of energy (LCOE). The degradation rate is affected by the panel type, environmental conditions, and the climate at the installation site. (Zainali et al. 2023)

Due to the volatility of the energy market and Finland's small size and low energy prices, profits from electricity sales are rare. Therefore, consumers and businesses should consider replacing the energy they purchase with solar energy. Vartiainen et al. (2024) compared the attractiveness of solar panels in the European electricity market. Their analysis utilized LCOE and solar PV self-supply data from five European countries: Finland, France, Germany, Italy, and Spain. They also divided their findings into market segments: residential, commercial, and industrial producers. The analysis revealed that Finland was the only country in which the average electricity price (P_{ave}) did not exceed the LCOE at higher discount rates, as shown in Figure 23.

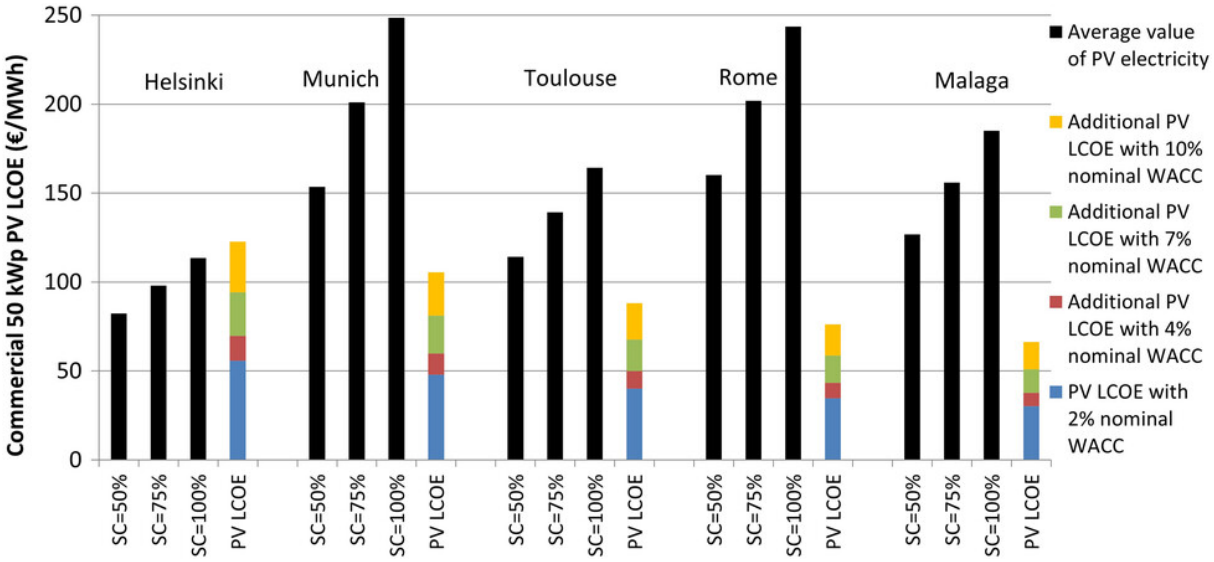

Figure 23. Comparison of commercial rooftop solar panel systems in five cities in 2023 EUR (Vartiainen et al. 2024)

The discount factor is the second-largest risk factor after *CAPEX*, and its size depends on the specific project and the interest rate set by the central bank. For larger projects, some studies use the weighted average cost of capital (WACC) instead of the discount rate. In countries with high radiation levels, such as Greece, solar panel projects may not be economically viable due to their elevated weighted average cost of capital (WACC) Kenttä (Bódis et al., 2019). The discount factor remains somewhat uncertain, as interest rates may experience significant fluctuations in the future; however, the discount factor used in studies for LCOE typically ranges from 0% to 8%. (Abdelhady 2021; Hirvonen et al. 2015; Vartiainen et al. 2024; Zainali et al. 2023)

Abdelhady (2021) analyzed the levelized cost of electricity and net present value (NPV) of a solar PV power plant in Egypt. The proposed power plant's net present value was calculated, demonstrating the project's economic feasibility. A positive NPV suggests the project is feasible, while a negative NPV indicates infeasibility, as shown in formula 45.

$$NPV = \sum_{i=1}^{n} \frac{C_i}{(1+r)^i} - TIC \quad (45)$$

In the formula, C_i represents net cash flow in year i, including revenues and costs, while *TIC* stands for total investment costs. *NPV* is generally used for larger power plants; however, the same principle can also be applied to estimate the economic viability of small power plants. Therefore, the calculations aim to determine whether the system is profitable over its lifetime and economically feasible. (Abdelhady 2021)

2.6.3 Environmental impacts of solar panels

The environmental impact of solar panel systems can be evaluated through life cycle assessment (LCA). This method examines a product's environmental effect across its entire life span, from raw material extraction to final use, recycling, and external effects. LCA is affected by solar panel technology, system size, and location, so studies typically focus on specific types and sizes of solar panels across different countries and conditions. Conducting a thorough LCA requires extensive reliable data on raw materials, manufacturing, transportation, installation, the whole life cycle, and disposal processes, often involving assumptions and estimates in the analysis. (Bhandari et al. 2015; Kim et al. 2014; Koppelaar 2017)

The most common indicators used to assess the environmental impact of solar panels are the Energy Payback Time (EPBT) and various greenhouse gas emission indicators, which are typically compared to the country's overall energy mix. EPBT is the time required for a system to generate enough energy to offset the energy used in its production throughout its life cycle. This is calculated using the following formula 46. (Kim et al. 2014)

$$EPBT(year) = E_{requiment}/E_{annual\ generation} \tag{46}$$

According to a report by the European Technology and Innovation Centre (ETIP), under the radiation conditions in Northern Europe and Finland (approximately 1100 kWh/m2/year), the EPBT ranges from 1 to 4 years. Under Southern European conditions (1700 kWh/m2/year), the EPBT ranges from 0.7 to 3 years.

In their review articles, Koppelaar (2017) and Bhandari et al. (2015) estimated the energy payback time (EPBT) of solar panels to be between 1 and 4 years. However, this is influenced by key variables, including solar panel technology, manufacturing processes, and radiation levels. Studies also highlight factors such as the lifetime of the solar energy system (25 years), the energy mix of the system, the type of installation, and the efficiency of the solar panels when calculating the EPBT. Another common reference parameter is the energy return on energy invested (EROI), calculated using formula 47 (Bhandari et al. 2015).

$$EROI = \frac{lifetime\ energy\ output}{Embedded\ energy} \tag{47}$$

The EROI compares the energy generated by a source to the energy required to produce it. It is a unitless ratio used to assess the profitability of various energy sources. According to

Bhandari et al. (2015), EROI is a more appropriate measure than EPBT for evaluating the long-term sustainability of an energy source. When EROI is less than 1:1, the energy source is not a viable investment. The minimum EROI for industrialized countries is 3:1 for oil, which also applies to other energy sources. The average EROI ranges from 8.7 to 34.2 for solar panels, depending on the technology and study, making solar panels a highly viable energy source.

Agarwal et al. (2023) designed a 42 kWp solar power plant in Udaipur and evaluated, among other factors, the EPBT. The EPBT of the power plant designed by the researchers is over 8 years, significantly higher than that reported in other studies. The high EPBT may be attributed to the batteries and other initial energy costs associated with the power plant. The EPBT of the entire solar panel system, including any batteries, inverters, and electrical wiring, must be considered when assessing the system. (Agrawal et al. 2021)

Several studies have examined the environmental impact of solar panels using parameters beyond EPBT, such as various greenhouse gas indicators. Typically, studies use LCA to assess the CO2 emissions reduced by solar panels compared to fossil fuels, resulting in similar findings. The emission reductions from solar panels are significantly greater in developing countries that rely heavily on fossil fuels than in Europe, where countries incorporate more renewable energy sources, including nuclear, hydro, and wind, into their energy mix. (Kim et al. 2014; Rajput et al. 2018; Tan et al. 2023)

2.6.4 The impact of reflector costs on the PV system

The economic impact of using reflectors has been assessed using standard parameters like Levelized Cost of Energy (LCOE) and payback period. Buying and installing a reflector increases the initial investment cost of a solar power project. The studies aim to determine how well the extra revenue from the reflector offsets this higher investment.

Hamed et al. (2022) optimize the reflector geometry to maximize solar panel output on the ground. Researchers conducted a levelized cost of energy (LCOE) analysis of rear reflectors integrated with the panels, examining variables including reflector angles and reflection coefficients. The LCOE of a panel with a reflector remained nearly the same as that without one, but it increased as both the reflection coefficient and panel angle were raised. Increasing the angle of the solar panel increased investment costs due to greater land use. (Hamed et al. 2022)

The effect of the reflector on LCOE is generally small, with a variation of about 5% in either direction; however, it usually shortens the payback period by a couple of years. Several factors influence this variation, including the size, cost, additional yield, and location of the reflector. (Hamed et al., 2022; Wijesuriya et al., 2017) Reflectors can also enhance a solar power plant's internal rate of return (IRR), making investment in reflectors more economically viable. Since the size of a solar panel system is typically designed to meet the user's electricity needs, reflectors can reduce the number of solar panels required, thus lowering initial investment costs. Land efficiency can also be improved by installing inter-row reflectors in existing PV plants. Kenttä (Agrawal et al., 2022; Mansoor O et al., 2020; Matsushima et al., 2003) Overall, reflectors are an affordable way to boost power generation in both new and existing solar power facilities.

2.7 Literary Summary

The use of solar panels as an energy source has grown exponentially over the past twenty years, driven by lower costs and improved efficiency. The first solar panels were developed in the 1960s, but they became widely used in the 1980s and 1990s as governments in various countries began supporting their broader adoption. By the 2000s, solar panel efficiency had increased enough for consumers to benefit from solar energy. The decreasing prices of solar panels and the global energy crisis have also boosted consumer demand for solar panels.

Electromechanical parameters help us understand how solar panels work and the factors influencing their performance. The I-V curve and the power curve, often shown together, are the most common diagrams used to illustrate panel efficiency. When radiation hitting the solar panel increases, its power output also goes up. However, the panel's temperature rises too, which can reduce its efficiency. By measuring electrical parameters, we can analyze and optimize solar panel output and spot potential malfunctions.

To optimize the operation of a solar panel, it is essential to know the amount of solar radiation reaching the ground. For this purpose, various functional programs have been developed to calculate and determine the optimal orientation and angle for a solar panel system. Several research organizations have compiled radiation databases using measurements from the Earth's surface and satellite data, covering the entire planet. These databases are based on years of data and typically represent the average radiation values at specific locations. Variations in local weather are accounted for in the TMY data. Different theories and

calculation methods have been developed for estimating the radiation on a tilted surface, with varying levels of accuracy and complexity.

The amount of sunlight hitting the solar panel can be increased by using one or more reflectors. The size and angle of the reflector relative to the solar panel will affect the additional output, making it important to optimize these parameters. Reflectors are usually flat, straight surfaces, but research has shown that their effectiveness can be enhanced by using a concave design or reducing shading with a semi-circular reflector.

Studies on additional reflectors for solar panels can be categorized into two groups: those that employ algorithms to calculate and optimize solar panel systems, and those that test the effects of reflectors in outdoor settings. The accuracy of these algorithms is typically assessed through outdoor testing. The results regarding the growth of solar panel and reflector system output are significant, as solar panel output is heavily influenced by location, weather conditions, and time of year. Well-optimized and multiple reflectors can boost the yield of the solar panel by more than 50% annually, although enhancements for flat single reflectors typically range from 15% to 40%.

Materials used in reflectors vary based on reflectivity, durability, and cost. The best options are aluminum-based reflectors coated with a thin protective film. Polished and coated steel also works well for solar panel systems that need lower concentration. Applying lacquer or plastic coating to reflector materials boosts their durability. When designing a reflector, it's important to consider how easy it is to clean and whether the surface might need replacement if its properties begin to decline.

Solar panels are installed on roofs, on the ground, on walls, and on balconies. Ground-mounted panels are arranged in rows, with reflectors placed between them. These solar panel systems take up land, making them ideal for out-of-town locations with lower land costs. Reflectors are rarely used on roofs due to space restrictions. They are usually used with smaller off-grid systems to boost the power output of solar panels, especially where land use isn't a major concern. Large commercial reflector solar projects are uncommon, and reflectors are often optional or built into the product's structure, such as solar canopies. The limited commercial use of reflectors probably comes from the low cost of solar panels, which makes it cheaper to invest more in the panels themselves rather than in complex systems with reflectors.

When designing a solar panel system, an economic assessment must be performed to determine the system's levelized cost of energy (LCOE), which compares the financial expense of solar panels to the cost of electricity purchased. For larger projects, using net present value (NPV) is helpful, for example, to assess the investment's feasibility. The environmental impact of solar panels is often evaluated by their ability to reduce greenhouse gas emissions. Regarding energy yield, the energy payback time for solar panels is calculated, which indicates how long it takes for the panels to generate the energy required for their manufacturing. The additional benefit from reflectors should be balanced against their cost to decide if their installation is financially justified. Both LCOE and payback periods are used to compare production costs and the efficiency of different power plants.

Solar panels and their use as a source of energy are broad and constantly evolving fields. This work focuses on the effects of reflectors on solar panels in general and specifically in Finland. Under Finnish conditions, reflector surfaces increase the available radiation, especially during summer. The next section presents the effects of reflectors on the radiation and output of a solar panel using a calculation model and outdoor testing.

3 The Experimental Section

In the experimental section of the thesis, the tools and functions introduced in the theoretical section are used to calculate solar radiation. This also includes calculating the additional radiation from the reflector. First, the climate type and annual mean temperature of the target country, Finland, are described. The availability of solar energy in Finland is evaluated based on annual radiation hours.

Chapter 3.1 describes Finland's overall climate and radiation levels. Chapter 3.1.3 identifies the best angles for solar panels without reflectors using three different methods. Chapter 3.2 shows the results of the analytical calculations, which evaluate the extra radiation from the reflector, as explained in Chapter 2.5.3. The analysis also considers the effect of angles and the reflector coefficient on the additional radiation. Lastly, the energy production of the panels is assessed.

Chapter 3.3 outlines the installation of PV panels and reflectors on the roof, as well as the dimensions of an insulator. The analysis also includes the influence of the roof's angle on radiation.

Lastly, Chapter 3.4 compares radiation measurements taken in Southern Finland with various reflector materials to the calculated values and studies referenced earlier. The two best reflectors, aluminum and stainless steel sheets, are tested further. The potential angle of the roof is not considered in these tests, nor are the angles of the solar panel or reflector changed during testing.

3.1 Evaluation and Calculation of Solar Radiation in Finland

The amount of solar radiation and the efficiency of solar panels are greatly affected by a location's climate and average temperature. Chapter 3.1.1 covers Finland's climate, average temperature, and sunlight hours. Chapter 3.1.2 provides radiation levels on the horizontal surface in five Finnish cities. In Chapter 3.1.3, the ideal angle for the solar panel is calculated, and Chapter 3.1.4 analyzes how the solar panel’s tilt angle impacts radiation.

3.1.1 Finland’s climate and typical temperature

The electricity production and profitability of solar panel projects are heavily influenced by the site's climate and the country's climate, especially air temperature and sunlight hours.

Finland, in Northern Europe, according to the Köppen classification, experiences a cold, wet winter climate characterized by snow and forests. The typical annual maximum temperature in Finland is around 35 degrees Celsius, while the minimum can drop below -40 degrees Celsius, with significant variations between years and locations. Finland receives moderate rainfall throughout the year. Figure 24 shows the yearly average temperatures at two measurement points, Helsinki Kaisaniemi and Sodankylä, over the past 100 years. During the period from 1991 to 2020, the average temperature was 6.5°C in Helsinki and 0.3°C in Sodankylä, as shown in Figure 27.

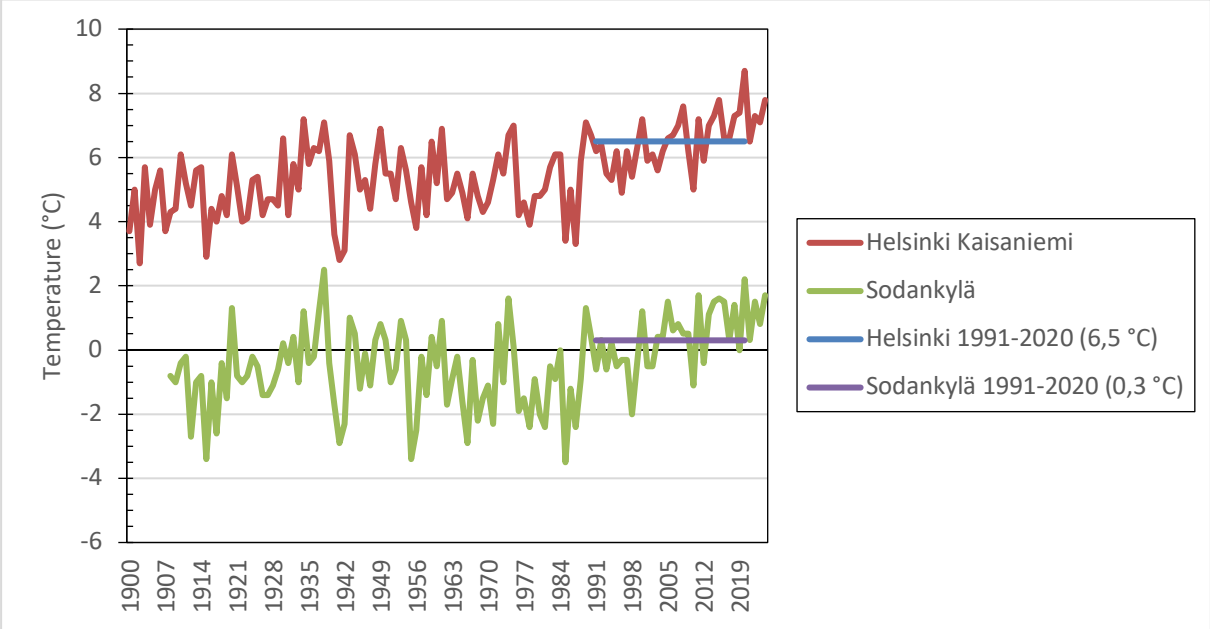

Figure 24. Yearly average temperatures in Helsinki and Sodankylä from 1900 to 2019 (Ilmatieteen Laitos, n.d.-b).

Finnish Lapland is partly situated north of the Arctic Circle, where it experiences continuous summer nights and winter days without sunlight. Sunshine hours in Finland are mainly focused in summer, when clear skies are common, with daylight lasting up to 19 hours, even in southern Finland. These longer daylight periods are especially beneficial for solar-tracking panels. Autumns, winters, and springs are often rainy, and during winter, there can be only about 6 to 7 hours of daylight in southern Finland. In winter, cloud cover and the sun's low angle further decrease the efficiency of solar panels. Figure 25 illustrates the average monthly sunlight hours for three cities over a 30-year period from 1991 to 2020. As expected for a southern city, Helsinki gets the most sunshine, while Sodankylä receives the least. Sun hours can also help estimate the annual radiation in a location if no other data are available.

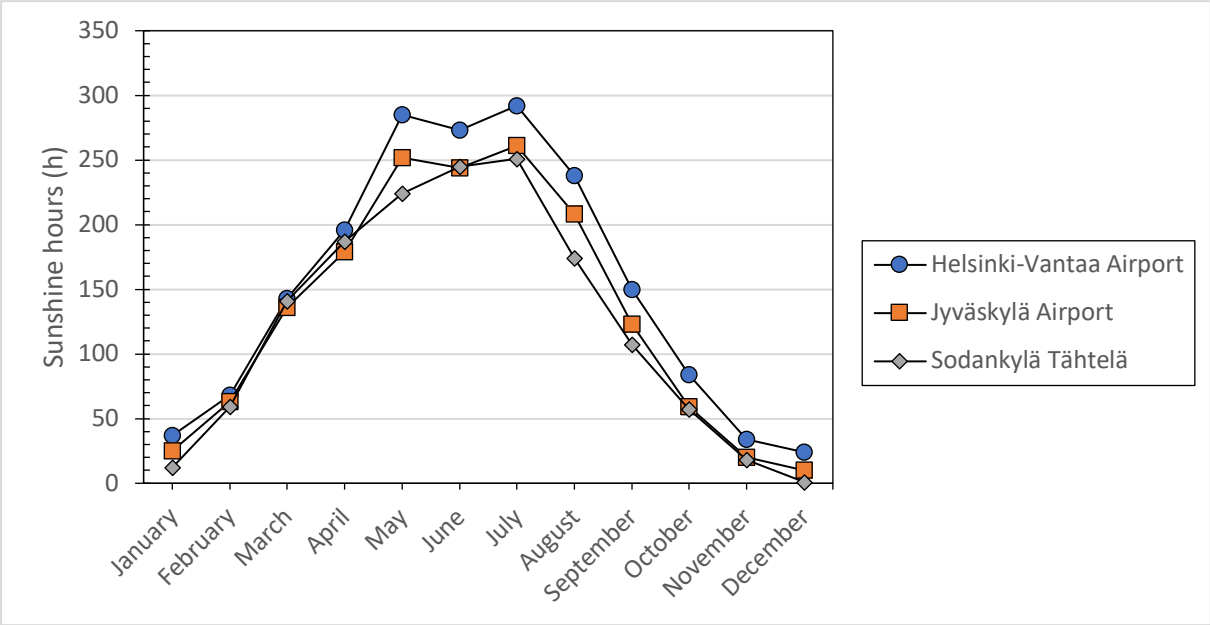

Figure 25. Monthly average sunshine hours from 1991 to 2020 in Finland (Ilmatieteen Laitos, n.d.-a, graph made by Viljami Kukkola)

The reflector casts shadows when in use, except when positioned horizontally. In studies, shadows produced by reflectors are often classified into distinct shadow patterns. A south-facing panel reflector creates shadows only in the morning and evening, leading to a relatively small effect on irradiance and output. During December and January, the reflector can completely block direct sunlight from reaching the solar panel if its angle exceeds the Sun's elevation angle. This effect is minimal in winter because sunshine hours are limited, averaging about 30 per month in Helsinki. In winter, most radiation is diffused, contributing little to the total annual irradiance.

The best locations for solar panels in Finland are along the coast and in southern Finland, where the annual energy output is generally highest. This is clear from the irradiance data, which compares the levels of sunlight in major coastal cities to those inland, as shown in the next chapter. In Finland, temperatures rarely go above 30°C, so the average temperature does not greatly reduce the efficiency of solar panels. Additionally, the temperature rise of solar cells caused by reflectors is minimal because of Finland's temperate climate.

3.1.2 Radiation in Finnish cities

Either databases or local measurements are used to estimate radiation. A simple and cost-effective method is utilizing existing solar radiation databases, which incorporate weather station and satellite data. This approach provides a relatively accurate and global database of solar radiation. The radiation database from PVGIS has been used in this work. PVGIS also

separates total radiation into direct and diffuse components, which accelerates the calculation of other radiation parameters.

Finland is situated in Northern Europe, partially within the Arctic Circle. Due to its northern location, only the PVGIS-ERA5 database is available for Finland, except for its southernmost areas. Cities across various parts of Finland were chosen as measurement points to give a broad overview of radiation levels. The measurement sites include Helsinki (60.167 N, 24.943 E), Jyväskylä (62.239 N, 25.746 E), Vaasa (63.096 N, 21.616 E), Joensuu (62.601 N, 29.759 E), and Oulu (65.012 N, 25.472 E), which are marked in red on the map of Finland in Figure 26. The green spot shows the outdoor test location. The PVGIS-ERA5 database features measurements from 2005 to 2020. A more detailed description of ERA5 can be found in Chapter 2.3.4.

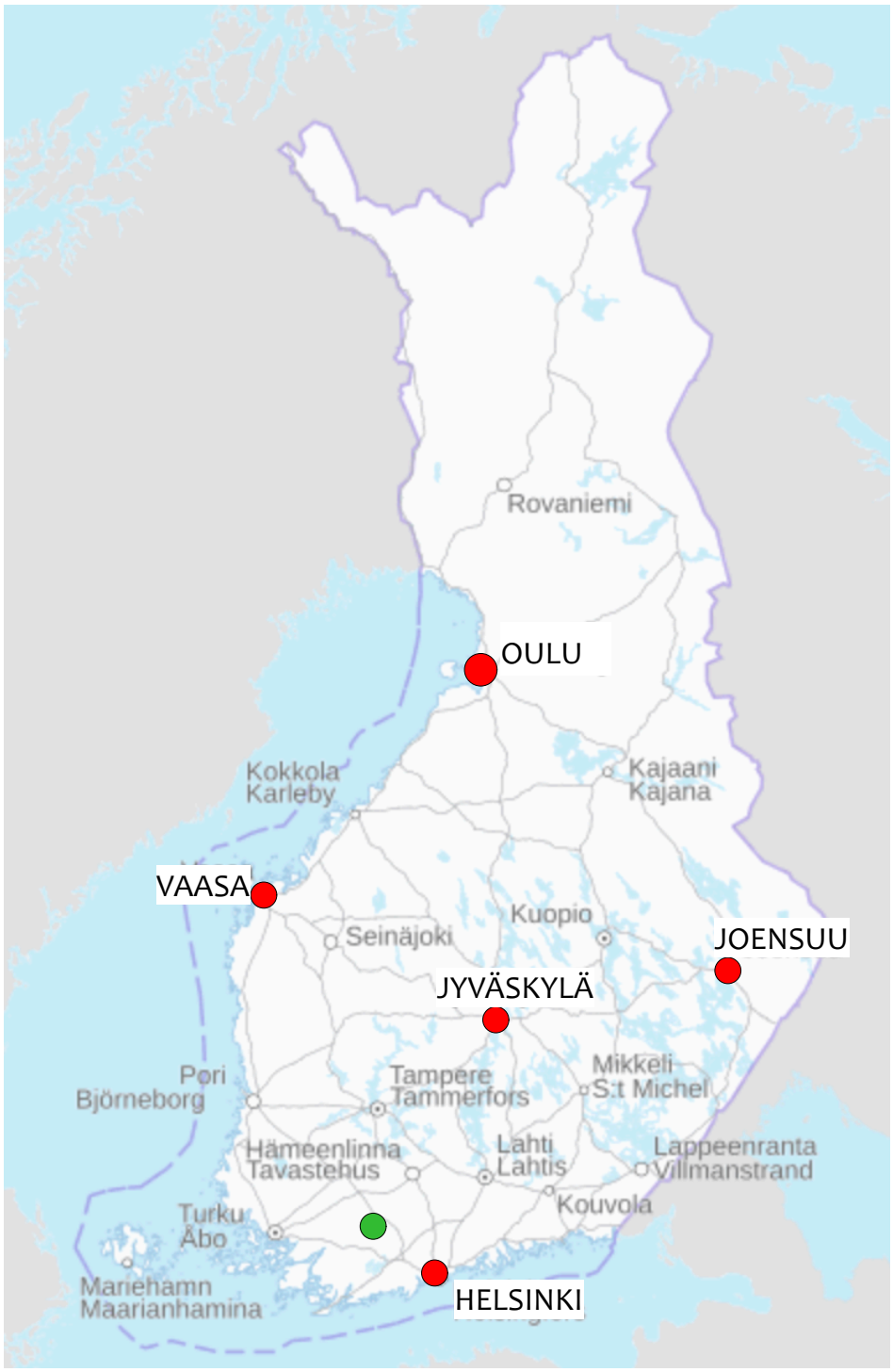

Figure 26. Location of the five cities in Finland

Figure 27 shows a line chart of the average daily horizontal solar radiation levels in five Finnish cities. The chart indicates that Helsinki has the highest radiation levels, peaking at just over 6 kWh/m² per day. Coastal cities Vaasa and Oulu also receive more radiation than the inland cities Jyväskylä and Joensuu. Interestingly, Oulu gets more summer radiation than Jyväskylä and Joensuu, even though it is much further north. This is due to Oulu's position by the Baltic Sea and the fact that summer days last over 20 hours.

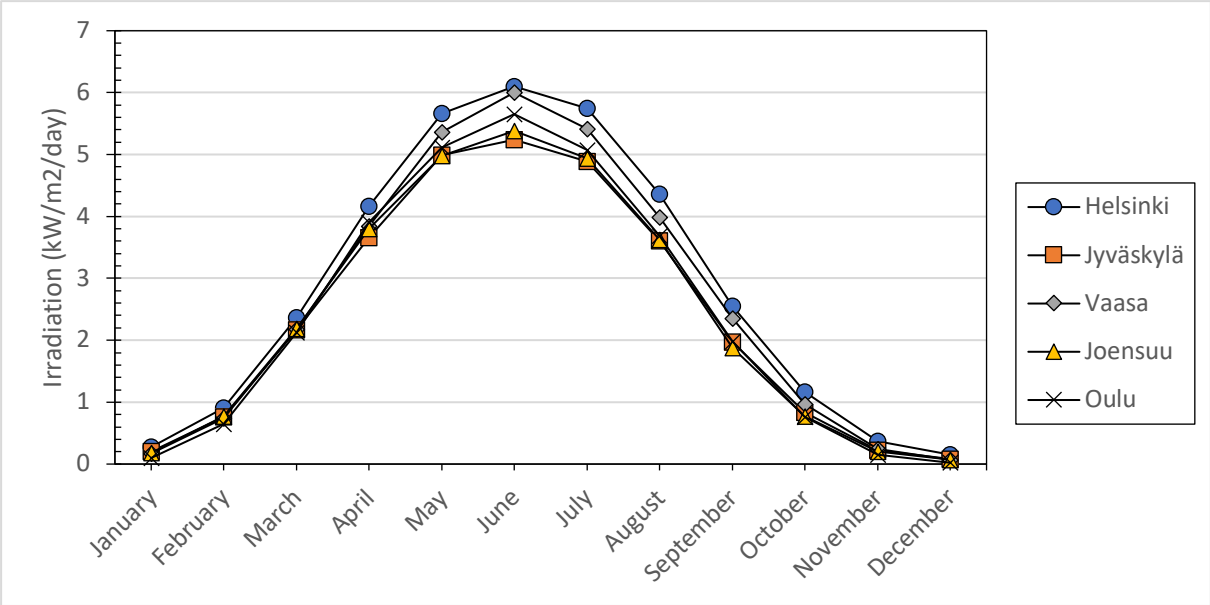

Figure 27. Average daily global horizontal irradiation in Finland (Viljami Kukkola)

Figure 27 shows how radiation levels are also affected by the time of year. Months are divided into four three-month periods. During winter, from November to January, solar radiation is at its lowest due to cloudy weather and the low path of the Sun. Spring, from February to April, and autumn, from August to October, are transitional periods with rapidly changing day lengths affecting radiation levels. In summer, from May to July, solar radiation reaches its peak, and solar panel output is at its highest. There is a notable difference between summer and winter in terms of radiation and daylight hours at Finnish latitudes. This difference decreases as we move closer to the equator.

3.1.3 Optimal angles for solar panels in Finland

When designing a solar panel system with a reflector, the panel orientation (azimuth) and the reflector angle must be carefully considered. If the solar panels face east or west, meaning they catch the morning or evening sun, placing the reflector above the panels is the best way to enhance the yield. With the panels facing south, the goal is to maximize radiation when the sun is at its highest, allowing the reflector to be positioned below the panels. The reflectors that follow the sun's path can be placed on either side of the panels. (Manosroi et al. 2020)

In the studies discussed in Chapter 2.4.6, either the angles of the solar panels and the reflector are optimized simultaneously using algorithms, or different configurations are selected and tested in field experiments. The panel's angle can also be set at an optimal position to test reflectors at various angles. Reflector placement largely depends on the surroundings of the solar panels. The optimal angles for both the reflector and the solar panel will vary with the

seasons. In winter, a smaller angle is recommended for the reflector and a larger angle for the solar panel. Conversely, in summer, the reflector angle can be larger and the panel angle smaller compared to winter.

The optimal angle for solar panels at these locations has been calculated using the formulas presented in Chapter 2.3.7. The programs mentioned also calculate the optimal angle of the solar panel; however, these optimal angles can vary significantly by location. All the optimal angles in Table 3 are between 44° and 48°.

Table 3. Optimal solar panel angles by location without reflector (Viljami Kukkola).

Location, latitude	Formula 26.	Formula 27.	PVGis
Helsinki, 60.175° N	44,66°	45,97°	43°
Jyväskylä, 62,239° N	45,19°	47,01°	44°
Vaasa, 63.096° N	45,40°	47,42°	45°
Joensuu, 62.601° N	45,29°	47,19°	45°
Oulu, 65.012° N	45,89°	48,28°	48°

3.1.4 Effect of solar panel angle on radiation

Figures 28–30 display line charts that illustrate how the angle of solar panels affects radiation levels in three cities: Helsinki, Jyväskylä, and Oulu. The diagrams represent radiation on a flat surface and at four different angles: 30°, 40°, 50°, and 60°, which are essential for the design of the reflector insulator. Generally, solar panels are not installed at angles steeper than these.

Due to Finland's northern position and the Sun's lower altitude, steeper angles are more effective in winter than in summer. In summer, the optimal angles for each city range between 35 and 45 degrees.

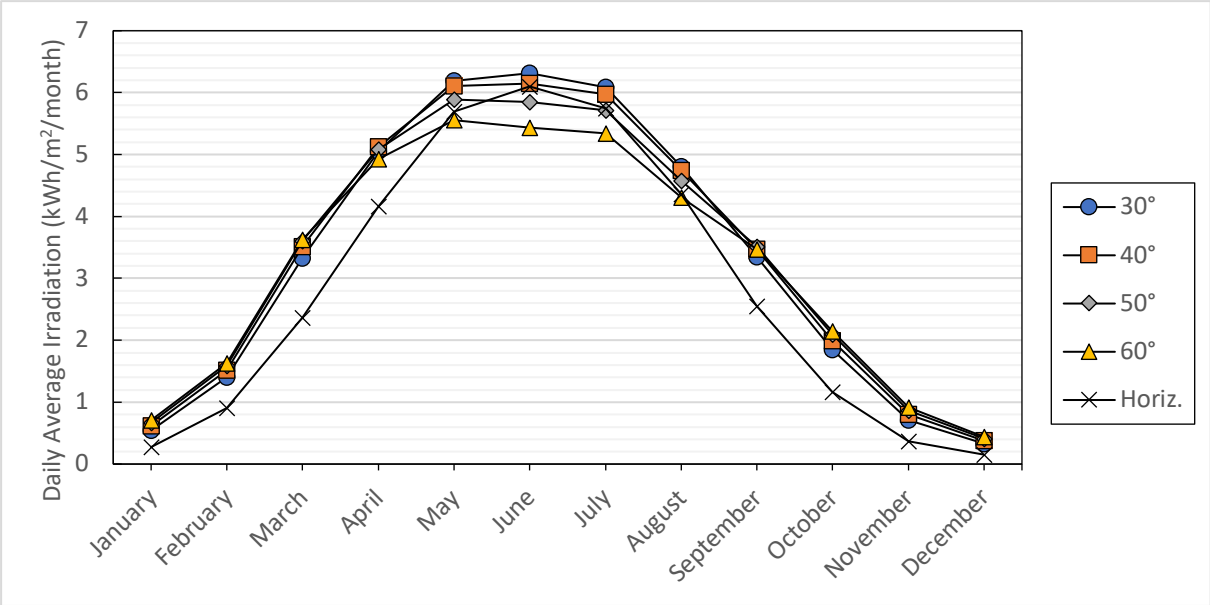

Figure 28. Monthly average daily radiation in Helsinki at different tilt angles (Viljami Kukkola)

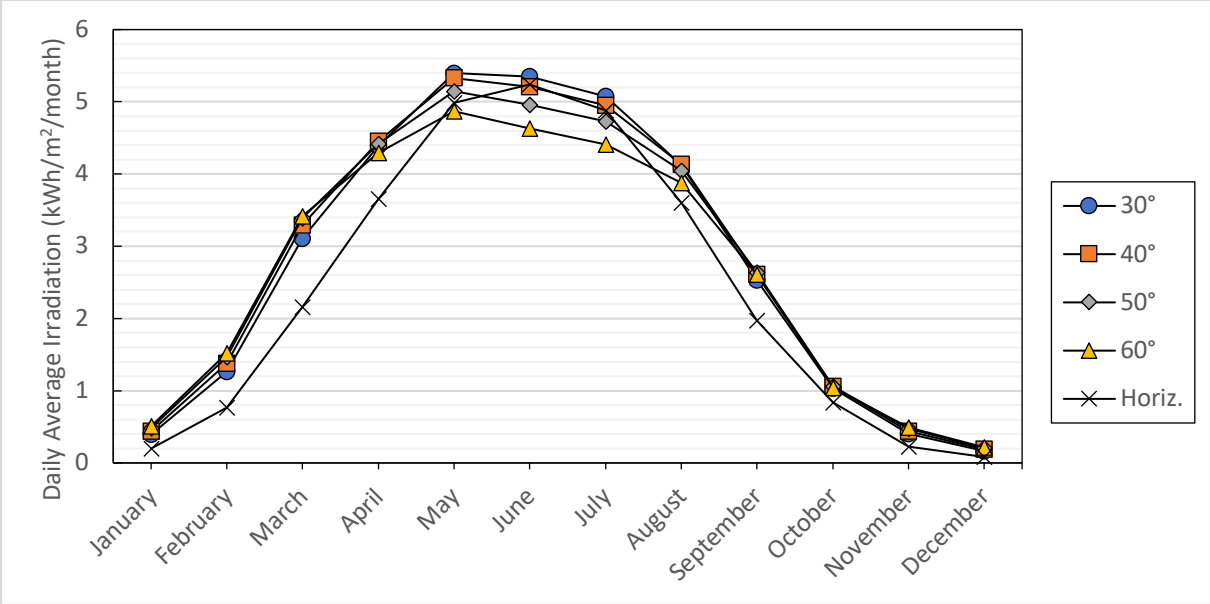

Figure 29. Monthly average daily radiation in Jyväkylä at different tilt angles (Viljami Kukkola)

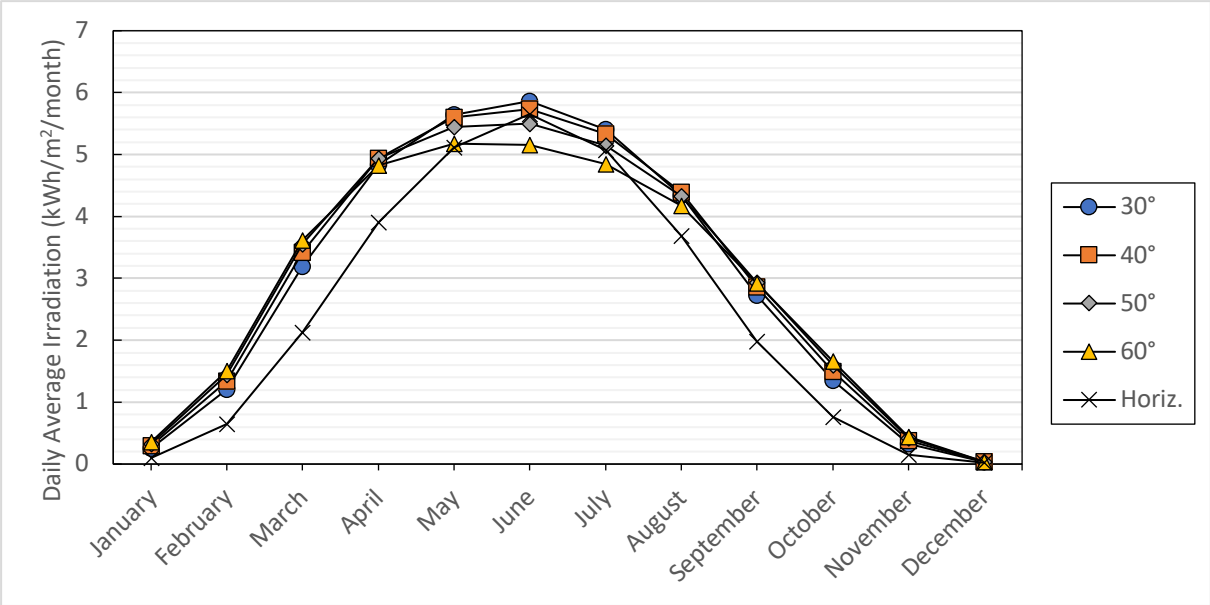

Figure 30. Monthly average daily radiation in Oulu at different tilt angles (Viljami Kukkola).

Installing a solar panel at an optimal angle can enhance radiation absorption by 10-30% compared to a horizontal surface in Finland. According to the diagrams above, the optimal angle for a solar panel in Finland varies depending on the calculation method. The additional irradiance provided by the reflector can be computed in several ways, but in this thesis we will use the functions described in Chapter 2.5.3.

3.2 Simulation Model

The results of the Nour et al. (2020) calculation model, presented in Chapter 2.5.3, are detailed in Chapter 3.2.1. A more comprehensive analysis of the monthly reflector irradiance is provided in Chapter 3.2.2. The geometry and angles of the reflector and solar panel depend on the insulator block design, as mentioned in the previous chapter.

3.2.1 Annual irradiance from the reflector

The model calculations assume that diffuse radiation is isotropic, meaning it comes from all directions evenly. The reflector has an assumed reflection coefficient of 0.7, while the ground has a coefficient of 0.2. Additional reflection from winter snow is not accounted for. A reflection coefficient of 0.7 simulates a more diffuse reflective stainless steel. In this case, a lower reflection coefficient results in a more realistic outcome in longer outdoor scenarios.

The length of the solar panel in the analysis is set at 1.2 meters. Table 4 presents the reflector's corresponding angles relative to the panel’s angle, as the reflector's angle in the

analysis depends on the panel's angle. The calculations for the angles and reflector's dimensions are discussed in greater detail in Chapter 3.2.3.

Table 4. Corresponding tilt angles of solar panel and reflector (Viljami Kukkola).

Panel's tilt (°):	30	40	50	60
Reflector's tilt (°):	11,5	14,1	15,9	17

The optimal angle of the PV panel is determined by the maximum radiation. Figure 31 illustrates the average annual increase in radiation at different solar panel angles in three Finnish cities. The optimal angle for the solar panel with a reflector is approximately 32°, which is significantly less than the optimal angles derived from the previously presented functions. This difference stems from the reflector angle, which varies with the size of the wedge. The reflector can boost annual radiation by approximately 35% at this optimal angle.

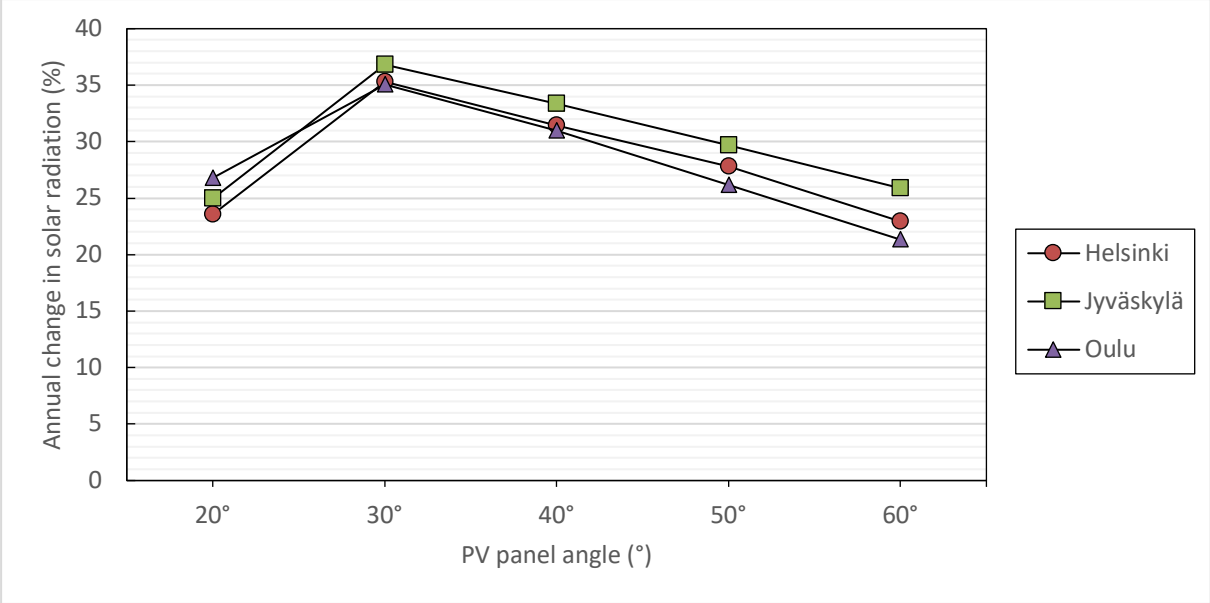

Figure 31. Annual increase in irradiation with reflector in Finland (Viljami Kukkola).

The analysis used the angles from Table 4 for three different cities: Helsinki, Jyväskylä, and Oulu, as examples. Figures 32–34 show an estimate based on the analysis of the reflector's effectiveness in capturing additional radiation. The figures also include a panel at an optimal 45° angle without a reflector and a horizontal panel for comparison. The reflector can increase the irradiance on the PV panel by approximately 3 to 4 kWh, depending on the angles and location.

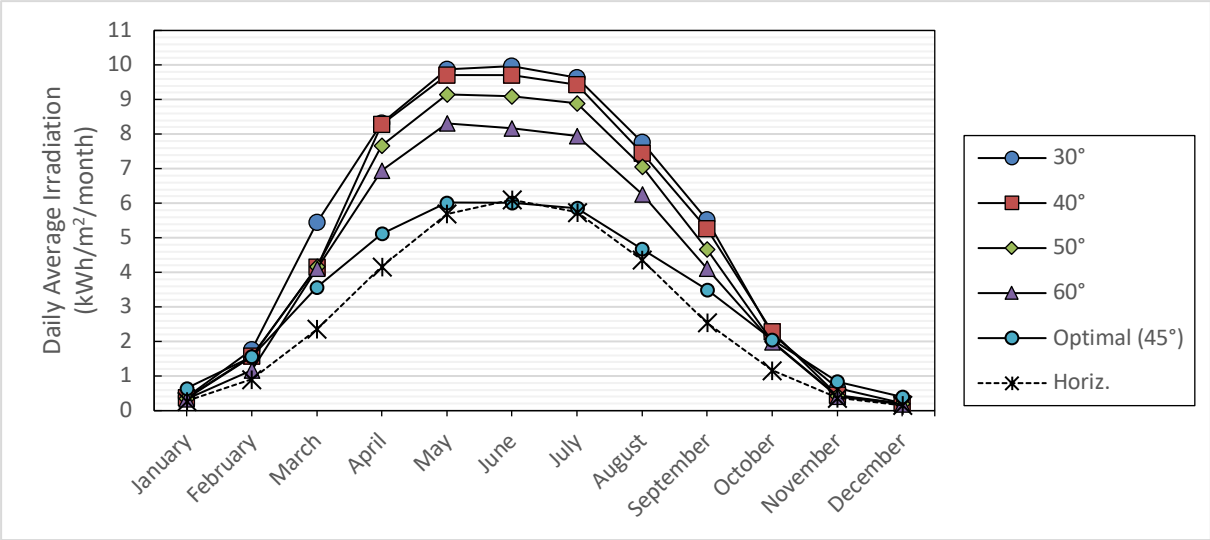

Figure 32. Daily average monthly irradiance with a reflector at various panel tilt angles in Helsinki (Viljami Kukkola).

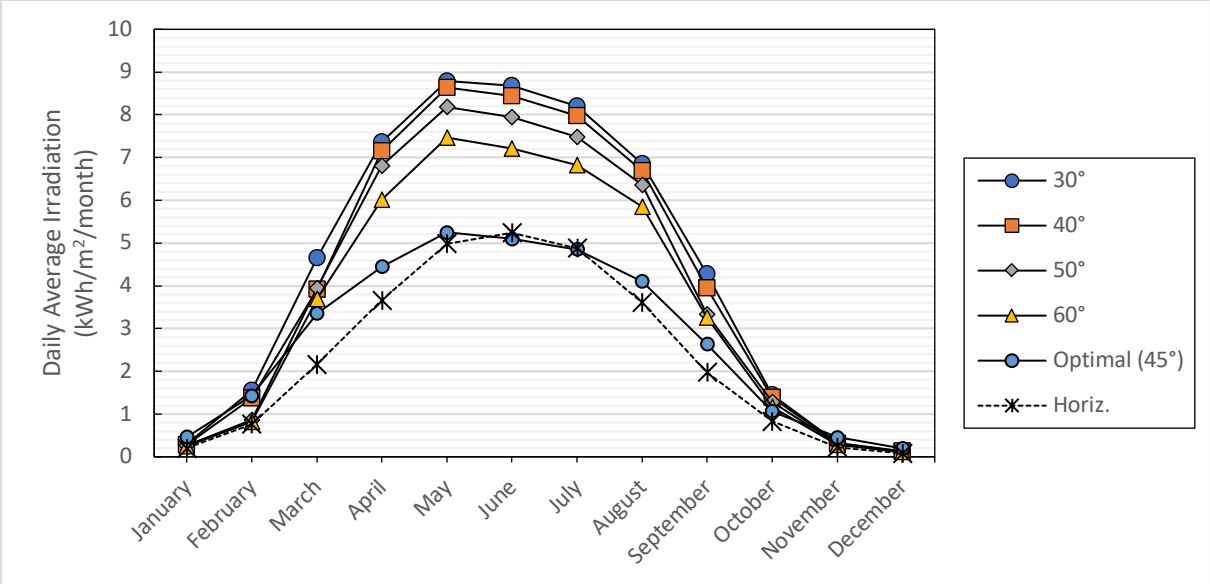

Figure 33. Daily average monthly irradiance with a reflector at various panel tilt angles in Jyväskylä (Viljami Kukkola).

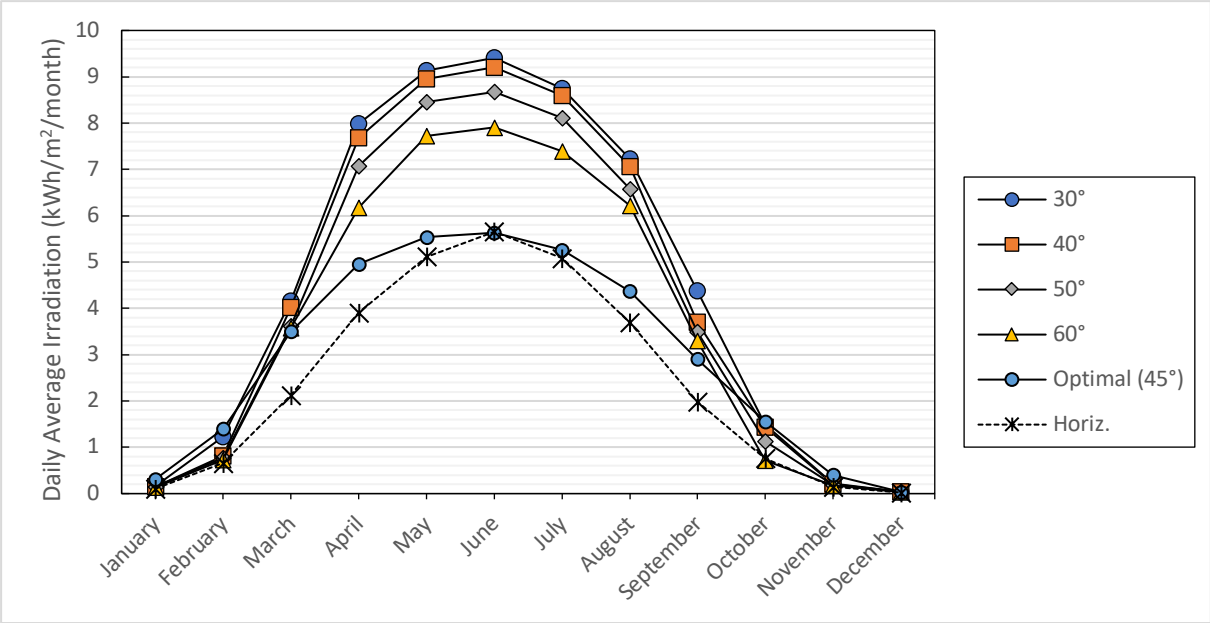

Figure 34. Daily average monthly irradiance with a reflector at various panel tilt angles in Oulu (Viljami Kukkola).

3.2.2 Monthly change in irradiance with the reflector

Figures 35 to 40 illustrate the additional radiation received per month due to the reflector. Figures 35, 37, and 39 show the total impact of the reflector on irradiance. Figures 36, 38, and 40 show the exact percentage changes in irradiance. In Helsinki, the most significant increase is approximately 3.5 kWh/m² during the summer. This analysis reveals that the increase in irradiance varies significantly, by as much as 40%, and is influenced by factors such as location, time of day, and the angles of both the reflector and the solar panel. This increase aligns with findings from other studies.

The irradiance gain from the reflector sharply decreases when the solar panel angle exceeds 40°. The optimal angle, approximately 30°, differs from other angles in late winter, specifically in February and March, because it maintains a lower reflector angle, allowing for increased irradiation to the panel. A significant loss in irradiance, exceeding half of the total, occurs during the winter months when the reflector shades the panel, allowing only diffuse radiation to reach it. The lost irradiance is less than 1 kWh/m² per day, so its impact on annual total irradiance is only a few percent.

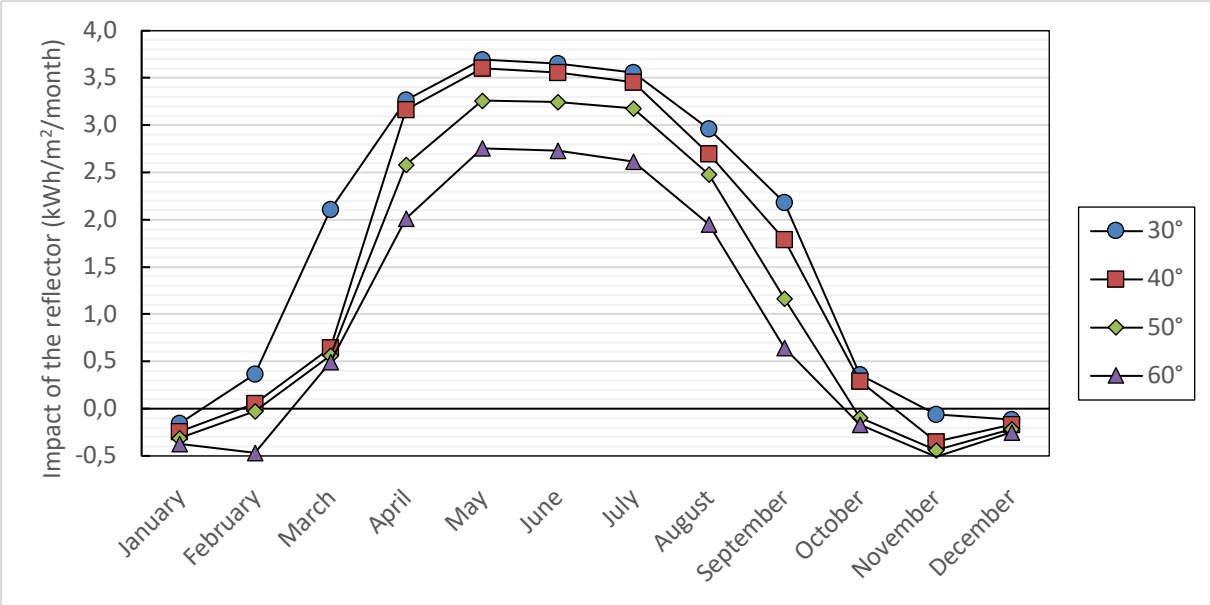

Figure 35. Total impact of the reflector in Helsinki (Viljami Kukkola)

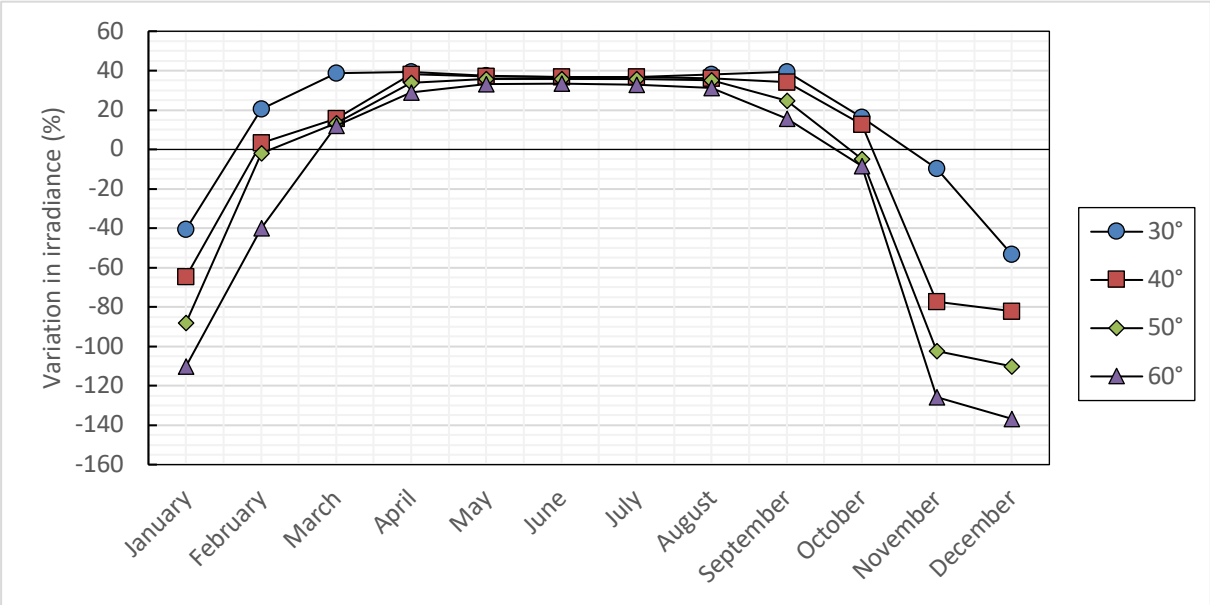

Figure 36. Reflector effect on irradiation in Helsinki (Viljami Kukkola).

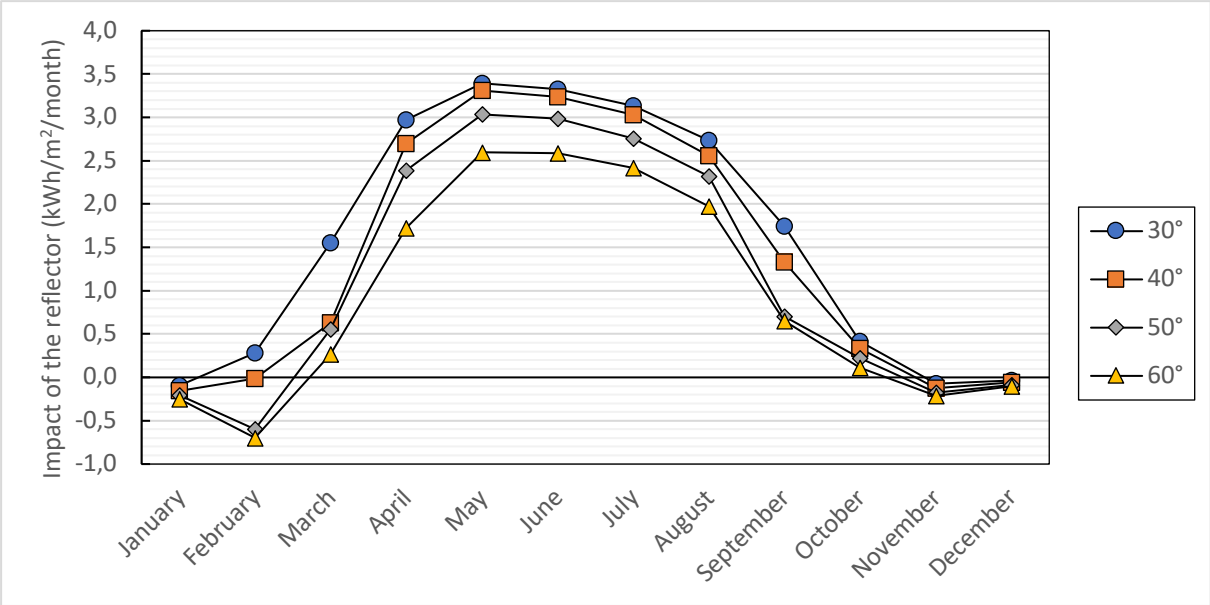

Figure 37. Total impact of the reflector in Jyväskylä (Viljami Kukkola).

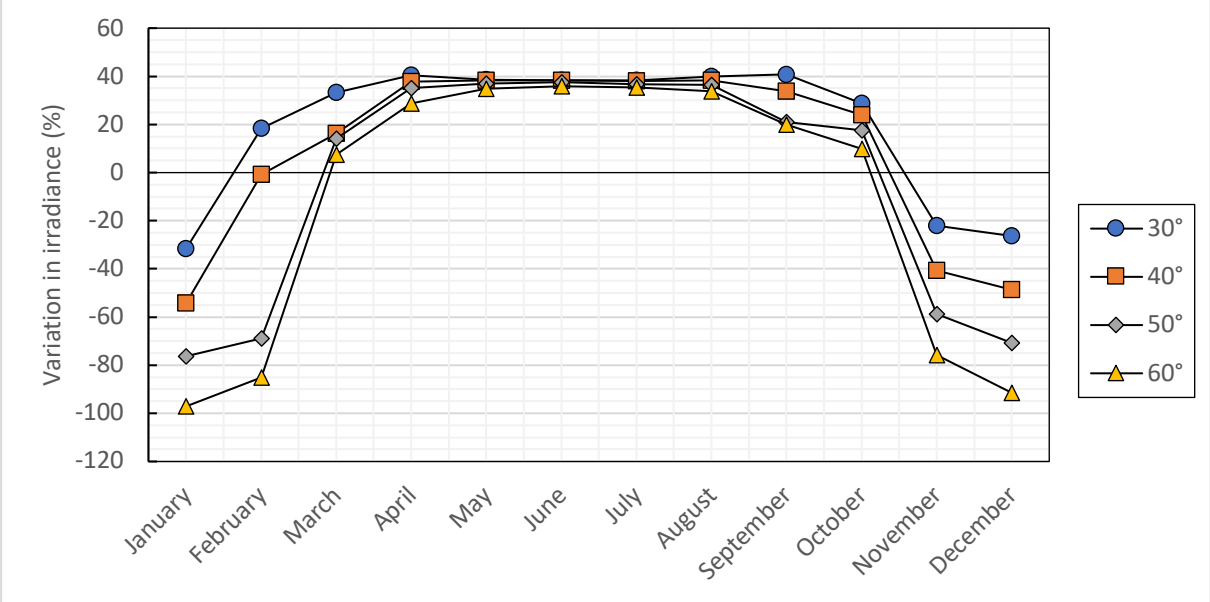

Figure 38. Reflector effect on irradiation in Jyväskylä (Viljami Kukkola).

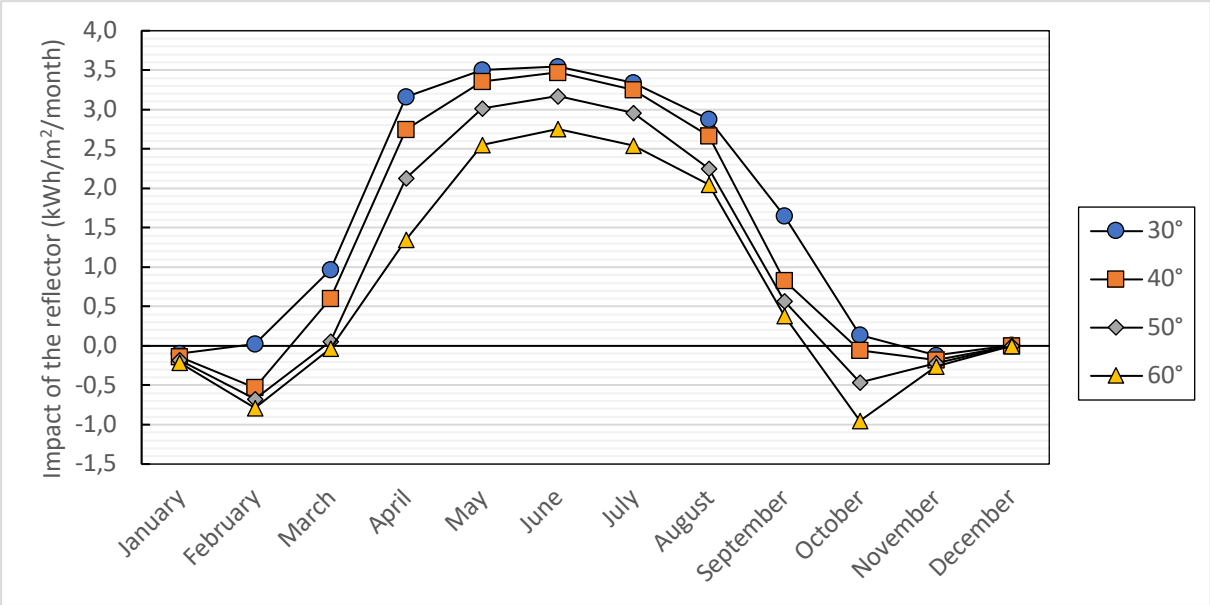

Figure 39. Total impact of the reflector in Oulu (Viljami Kukkola).

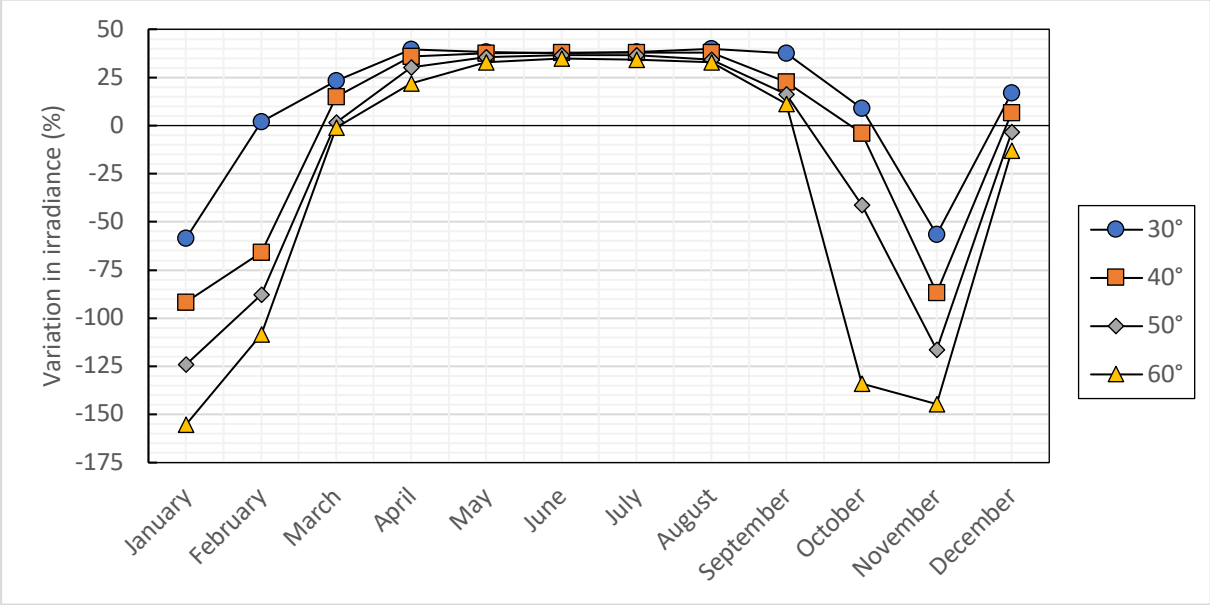

Figure 40. Reflector effect on irradiation in Oulu (Viljami Kukkola).

The analysis also examined how the reflection coefficient affects additional radiation. In Helsinki, the radiation level increases by only about 4-6% from April to September, as the reflection coefficient increases from 0.5 to 0.7, then from 0.7 to 0.9. This pattern is similar in other cities and at different tilt angles. The reflection coefficient used in the calculations comes from the same material with identical properties, varying only in the reflection coefficient.

Practical tests reveal differences between reflector materials, such as steel and aluminum, with variations in radiation levels of several tens of percent. For instance, aluminum reflects

uniformly across the spectrum and exhibits higher specular reflectance compared to steel. This implies that it reflects more direct radiation, which constitutes most of the total radiation.

3.2.3 The effect of roof tilt angle on solar irradiation

The small pitch angle of flat roofs influences the amount of radiation received by the solar panel by a few percentage points. Calculations show that the panel's angle must also increase as the roof angle rises to keep the optimal position. These calculations assume that the roof slopes downward toward the south, which raises the solar panel's angle and reduces the reflector's angle from a horizontal position.

Figures 41–43 compare the relative increase in radiation at different roof angles in Finland. The specified tilt angles for solar panels are measured from the horizontal. Figure 45 illustrates how the radiation on a 30° solar panel with a reflector decreases, especially at higher roof angles. This phenomenon is due to the sun's higher position and the small angle of the reflector relative to the panel. The loss levels off once the panel tilt angle exceeds 35°, which can be seen in figure 46.

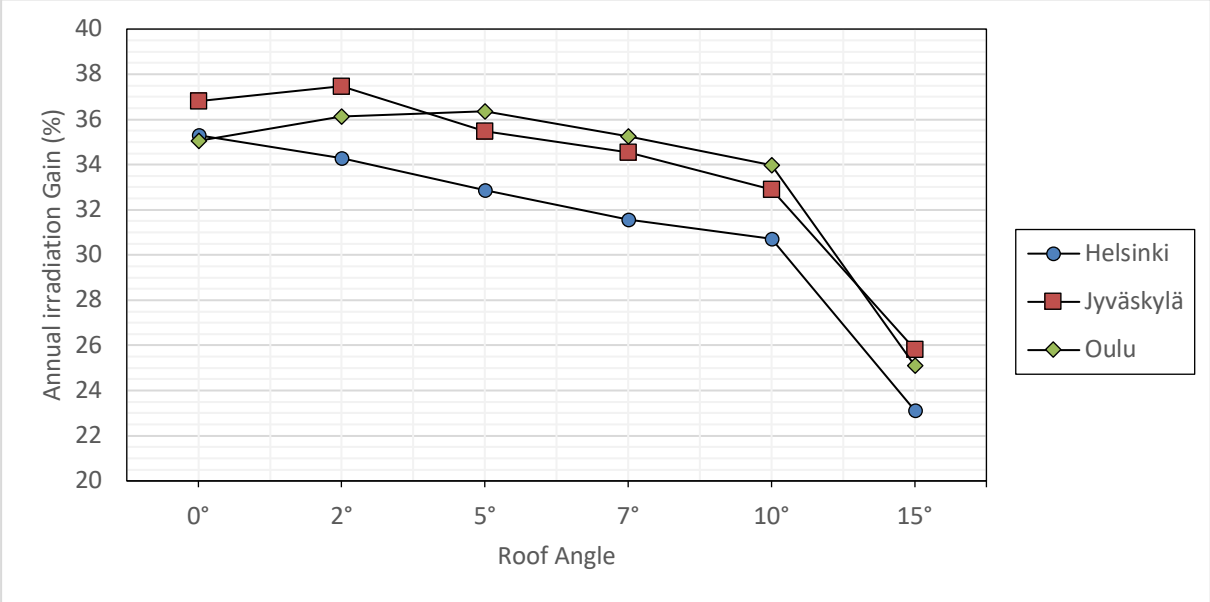

Figure 41. Irradiation change of a 30° solar panel with a reflector at different roof angles (Viljami Kukkola)

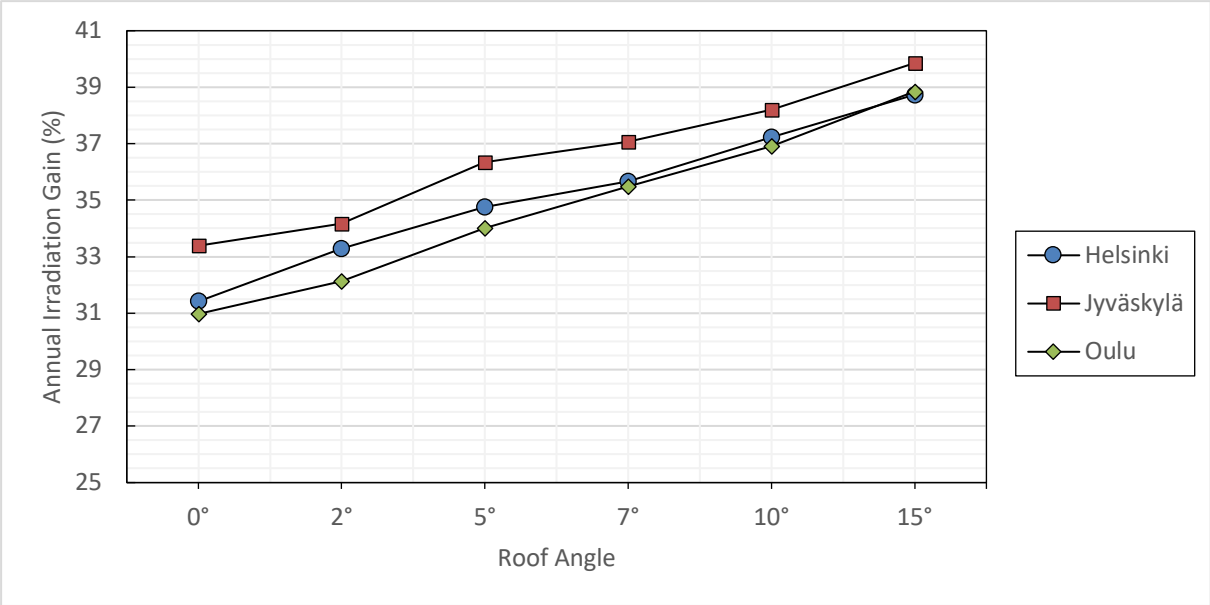

Figure 42. Irradiation change of a 40° solar panel at different roof angles (Viljami Kukkola)

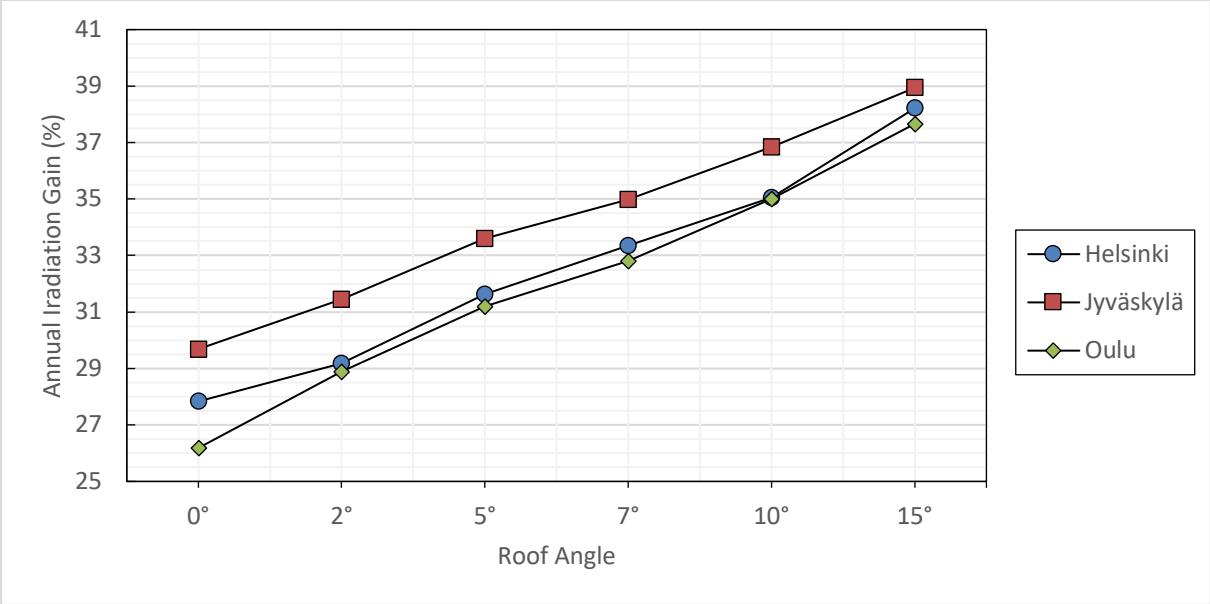

Figure 43. Irradiation change of a 50° solar panel at different roof angles (Viljami Kukkola)

The angle of the solar panel should be aligned with the roof angle for optimal performance. As the roof pitch increases, installing the insulating piece becomes more difficult. Based on calculations, the ideal tilt angle for a solar panel on a flat roof ranges from 35° to 40°. On steeper roofs, the panel's angle needs to be increased to compensate for the steeper roof and the low angle of the reflector.

3.3 Outdoor Tests

The outdoor tests for this thesis were conducted in Southern Finland, as explained in more detail in Chapter 3.3.1. Chapter 3.3.2 describes the test solar panel, the measuring instruments, and their accuracy. The outdoor tests took place before the simulations, so the test angles of the reflector and solar panels were not based on simulations; instead, they were estimated from previous studies mentioned in Chapter 2.4.5.

3.3.1 Location and Setup

The outdoor test compares and evaluates various reflector materials alongside the solar panel to assess their effect on the panel's electricity output and radiation. The site, located in Somerniemi, southern Finland, as shown in Figure 45, is surrounded by trees such as birches and pines, and the terrain resembles a garden.

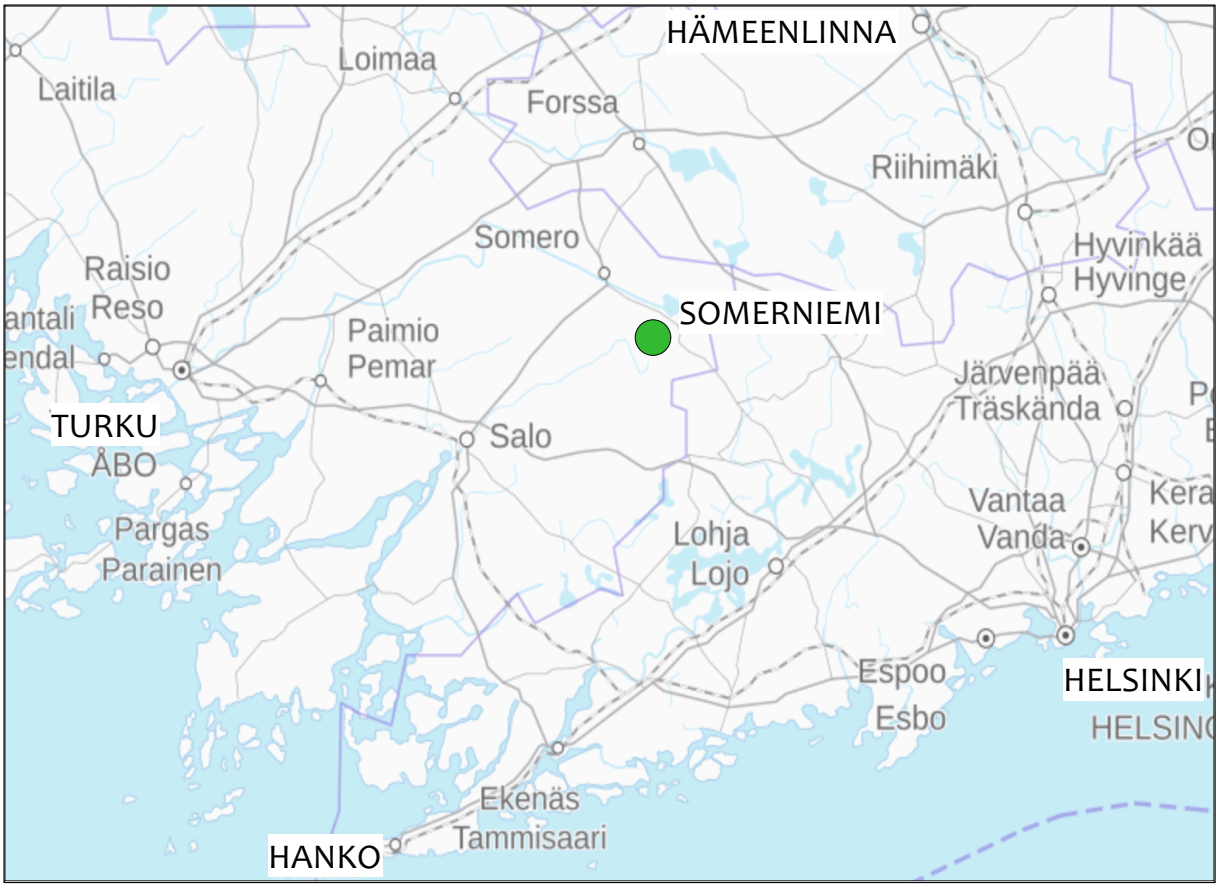

Figure 45. The Location of the test site in Southern Finland (Viljami Kukkola)

The test platform is made of wood and is mounted horizontally, facing south, as shown in Figure 46 the reflectors are tilted at approximately 15 degrees, while the solar panels are tilted at 55 degrees. This angle was expected to be close to the optimal angle, as indicated by the

studies in Table 2. Mathematical simulations conducted after these tests showed a significantly lower optimal angle of 30–35 degrees for the designed rooftop reflector in Finland. The reflector consists of four sheets measuring 0.6 x 1.0 m, making them easy to handle, transport, and store. These are positioned on a few centimeters of plywood and secured with two-sided tape. Another similar solar panel, located about three meters away from this one and without the reflector, allows for measuring the difference between a standard solar panel and one equipped with a reflector.

Picture 46. Solar panel and reflector of the experimental setup. (Viljami Kukkola)

The comparative test of reflector materials was conducted on June 28, 2024, a week after the summer solstice. On the day of the test, the weather was hot with light winds and a few clouds in the afternoon. Measurements were taken hourly, and each reflector material was measured separately. Temperature readings were taken on-site, while wind speed and humidity data were gathered from a nearby weather station.

The second tests were performed on August 13 and 14, 2024, using the two best-performing reflectors from the previous test: stainless steel and aluminum sheets. Each reflector was

tested over a day, allowing for the assessment of its overall impact on the solar panel. The reference panel was used for the same measurements every 0.5 to 1.0 hours.

The measurements were taken using various instruments, which are further explained in the next chapter. The test evaluated solar irradiance, ambient and panel temperatures, and the panel's electrical metrics. Identical measurements were recorded for both panels: Pmax, Vmp, Imp, Voc, and Isc. These measurements are usually taken to verify the solar panel's proper function. A significant deviation from the STC in the measurements indicates that the panel may not be functioning correctly. This direct measurement method can also be used to determine the values for individual panels. The panel temperature was recorded from the back of the panel between the conductors of the cells. Solar irradiance on the panels was measured at the center of each panel, while horizontal irradiance was measured at the front of the reference panel.

P_{max}, V_{mp}, I_{mp}, and V_{oc} were measured using the same meter, the Frogbro EY1600W Solar Panel Meter, by connecting the panel wires to the instrument's corresponding MC4 connectors, as shown in Figure 50. Measurements were taken after about half a minute to allow the results to stabilize. I_{sc} was measured with a Uni-T UT203R AC/DC meter by connecting the panel wires and measuring the direct current (DC) using a clamp, as shown in Figure 51. During these measurements, the solar panel must not be under load. Measurements of the installed solar panel system can be conducted directly from the solar panel using a multimeter and a digital clamp meter. Additional testing can be performed at the controller and combiner boxes if the system shows a downgraded output and voltage. (SunWize, n.d.)

3.3.2 Testing equipment and materials

The total size of the test reflector with four sheets is approximately 2000 x 1200 mm, making it slightly larger than a solar panel. The reflectivity of the metal sheets had not been measured previously. The aluminum sheets had some scratches, but still reflected solar radiation very effectively. The galvanized steel had a coating that was often spotty and frosted. The paint on the sheet was likely semi-dull, which hindered its ability to reflect light. The stainless-steel sheets were protected with plastic, keeping them clean and scratch-free. For the test, the protective plastic sheets were removed. There were a few marks on the sheets after handling

them, despite using gloves. The reflectors were wiped clean of loose dirt and dust before the tests. Photos of each sheet are included in Appendix 1.

The reflector materials being used consist of four types suitable for roofing materials, with each sheet measuring 600 by 1000 mm:

- stainless steel sheet, thickness 0.6 mm,
- galvanized steel sheet, thickness 0.64 mm,
- aluminum sheet, thickness 0.6 mm, and
- white steel sheet RR-20, thickness 0.45 mm.

The solar panel used in the test was the LONGi Hi-MO5 410W panel, measuring 1722 x 1134 x 30 mm and comprising 108 monocrystalline solar cells (6 x 18). The panel specifications are given in Table 5 under two test conditions.

Table 5. LONGi LR5-54HPB-410M module specifications (LONGi 2023)

Testing Condition	STC (AM1.5, 1000 W/m2, 25 °C)	NOCT (AM1.5, 800 W/m2, 20 °C, 1 m/s)
Maximum Power (Pmax/W)	410	306,5
Open Circuit Voltage (Voc/V)	37,40	35,17
Short Circuit Current (Isc/A)	13,84	11,19
Voltage at Maximum Power (Vmp/V)	31,42	29,19
Current at Maximum Power (Imp/A)	13,05	10,50
Module efficiency (%)	21,0	

A Frogbro Solar Panel Meter EY1600W in Picture 47, and a Uni-T digital clamp meter UT203R in Picture 48, were used to measure current, voltage, and power. The Frogbro solar panel meter operates over 5-1600 W, 12-60 V, and 0-60 A, making it ideal for evaluating solar panel performance. While this model does not specify a margin of error, similar solar panel meters typically show errors of about 1.5% + 10. Solar irradiance, back-of-panel temperature, and ambient temperature were recorded using the Seaward Solar Survey 200R, which included a calibration certificate. Seaward's Solar Survey 200R also features a compass and a tilt meter to orient the solar panel to the required angle. (Seaward, n.d.)

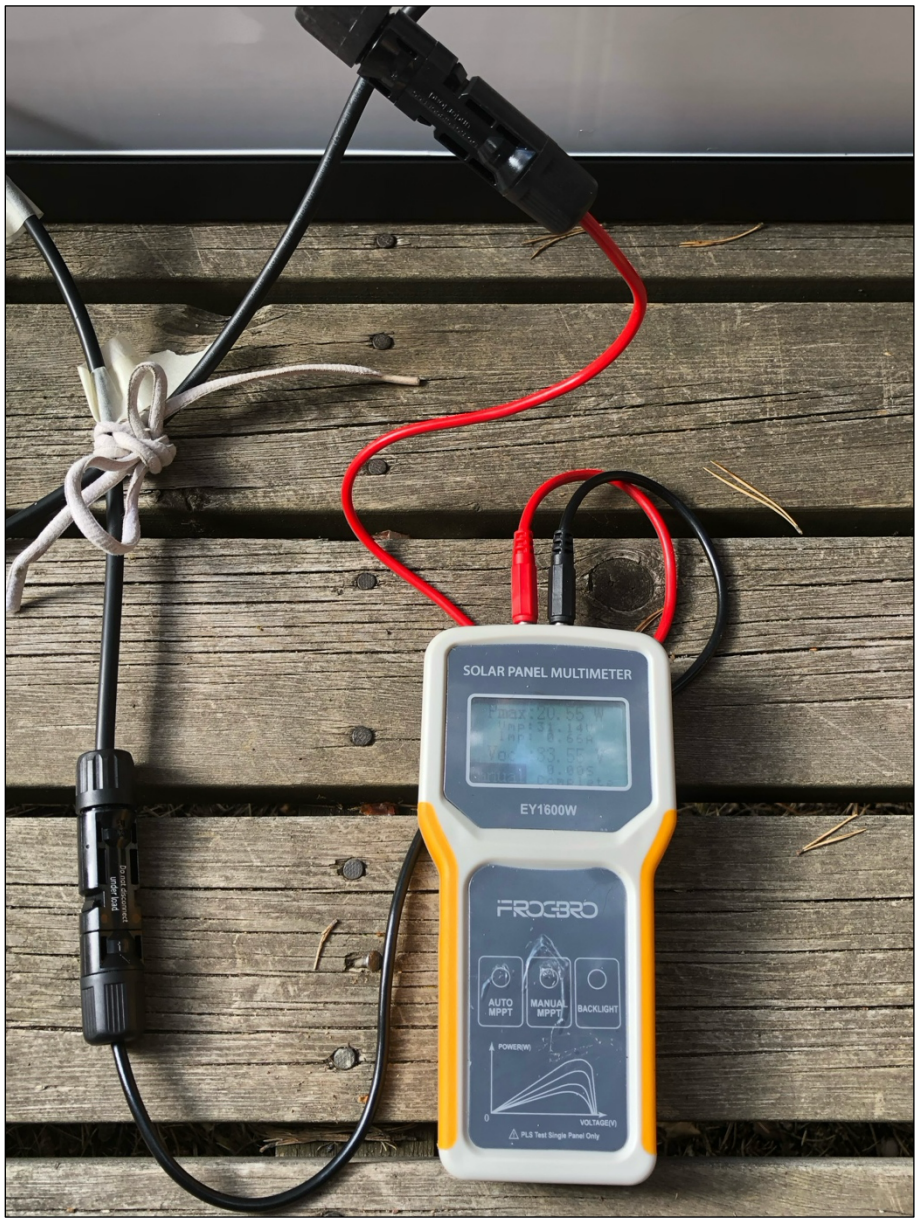

Picture 47. Measuring with a solar panel multimeter (Viljami Kukkola)

Picture 48. Measurement of closed-circuit DC using a clamp meter (Viljami Kukkola)

Table 6 presents the calculated uncertainties and accuracies for each parameter, sourced from the websites of different manufacturers. The standard uncertainty for equipment is calculated using formula 48 (Agyekum et al. 2021; Bell 2001).

$$Y = \frac{Z_n}{\sqrt{3}} \tag{48}$$

Table 5. Accuracy and Uncertainty of Measurement

Parameter	Accuracy	Uncertanty (%)
Irradiation (W/m2)	± 5	2,89
Temperatures (°C)	± 0,5	0,29
AC Current (A)	± (2 %+5)	2,90
AC Voltage (V)	± (0,8 %+2)	1,16
Power, Vmp and Imp (W,V,A)	± (1,5 %+10)	5,78

3.3.3 Comparison test of reflector materials

The first experiment tested four different metallic reflectors suitable as roofing materials: stainless steel, aluminum, zinc-coated sheet, and white steel sheet. The tests were conducted five times throughout the day, specifically between 10:40 a.m. and 6:35 p.m. The measurement times were chosen to align with the additional reflector gain, enabling observation of the resulting changes. As a result, reflector gain is lowest in the morning and evening when the panel faces south. Figure 49 shows the humidity, wind speed, and direction at the nearest weather station, located about 15 km from the test site, based on data from a weather app. The wind was very light at the test site, and a few clouds appeared in the afternoon; however, they did not cast shadows on the test panels. Before each measurement, the panels were lightly wiped to remove loose dust and dirt.

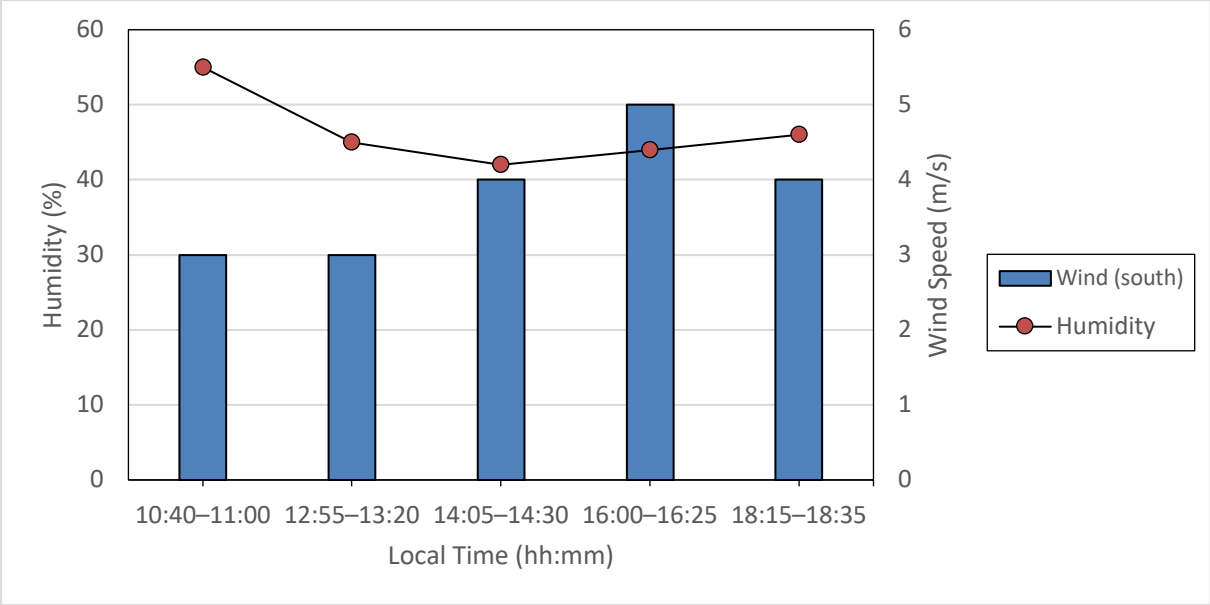

Figure 49. Relative humidity, wind speed, and direction from weather app during the comparison test (Viljami Kukkola)

Figure 50 shows the air and test panel temperatures. The test day was one of the hottest days of 2024 in Finland, with temperatures exceeding 30 degrees Celsius. The test panel's temperature peaked at around 63 degrees Celsius. The rise in temperature caused by the reflectors was minimal, as they were used only part of the day. The amount of radiation affects a solar panel's temperature; therefore, when the panel is in the shade, its temperature drops quickly, while additional radiation increases it.

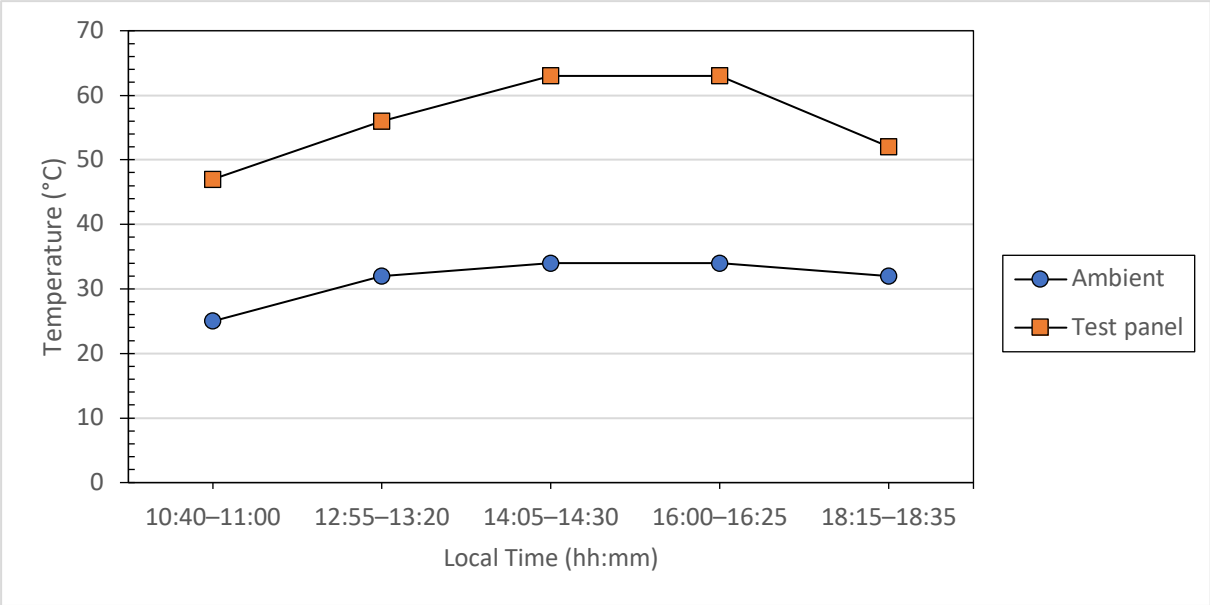

Figure 50. Test panel and ambient temperatures during the comparison test (Viljami Kukkola)

Figure 51 shows the radiation levels for different reflectors, the reference panel, and the horizontal surface. The highest additional irradiance comes from aluminum, followed by stainless steel, galvanized steel, and white sheet metal. Daytime radiation on the reference panel is about 850 W/m², increased by the reflectors.

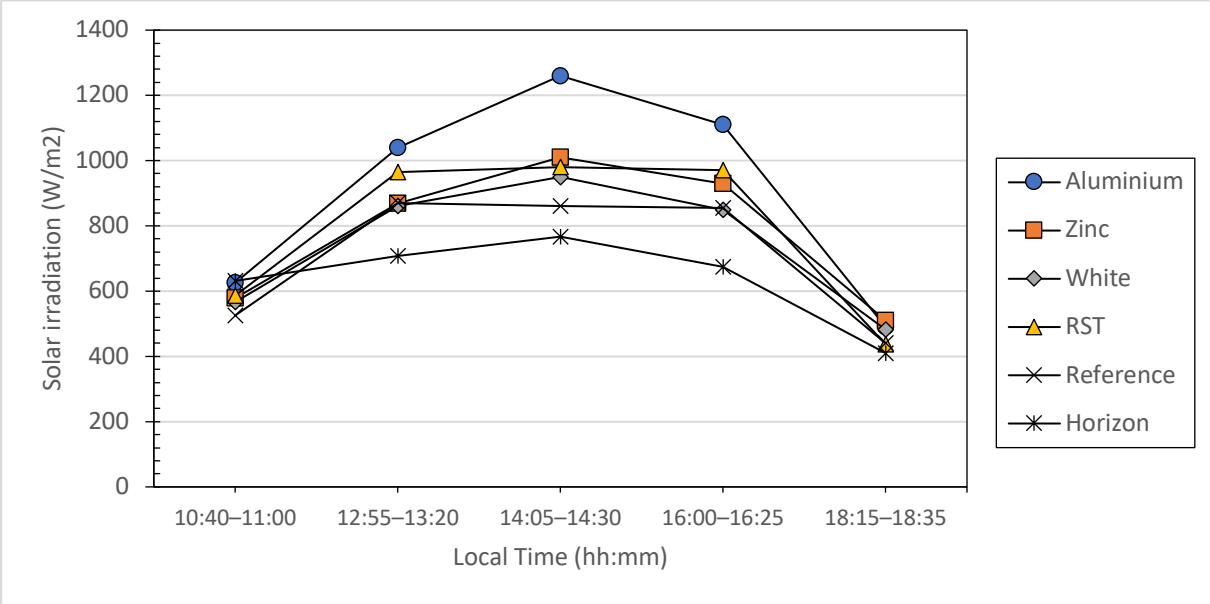

Figure 51. Radiation from different reflectors on a solar panel and in horizontal during the comparison test (Viljami Kukkola).

Figure 52 shows the extra radiation from the reflectors compared to the radiation received by the reference panel. Aluminum can add up to 400 W/m² of radiation, boosting total radiation by about 47% during the peak time of day. The RST sheet keeps a steady radiation level throughout the day, with just over 100 W/m² more than the reference.

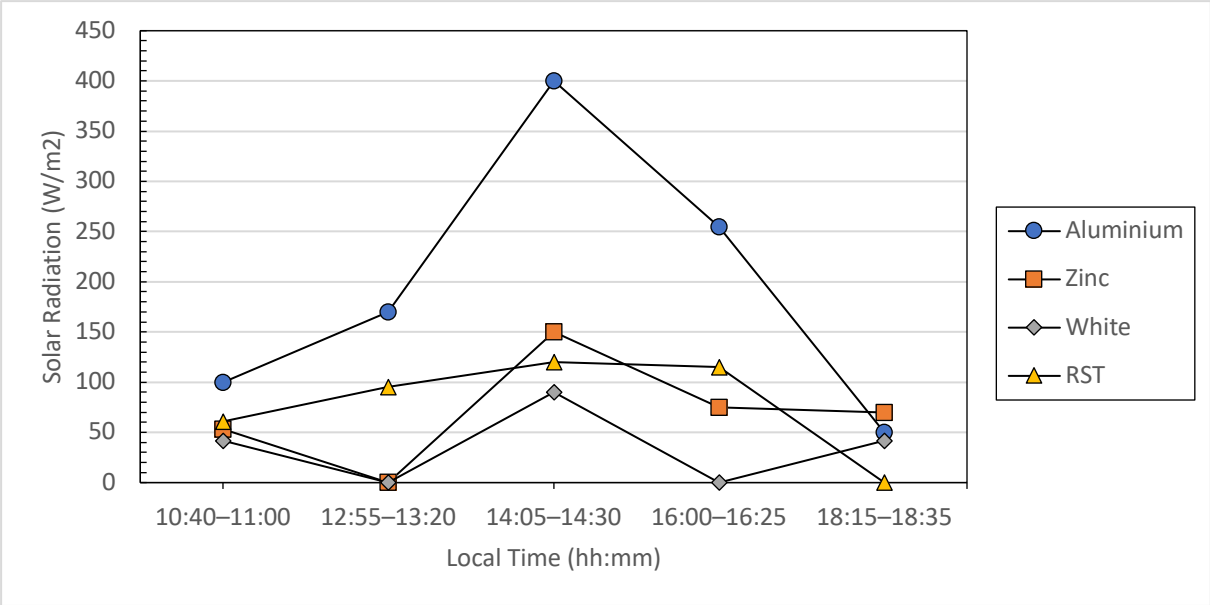

Figure 52. Increased irradiance relative to the reference panel given by reflectors (Viljami Kukkola).

Next, the electrical measurements for the solar panels are shown in Figures 53-58. An important parameter, the solar panel power, is displayed in Figure 53, and the power gain from the reflectors is shown in Figure 54. The maximum power gain of the aluminum reflector was about 70 W at 14.05, which is a significant gain for Finnish conditions, and 410 W for the solar panel. As a consistent and high-quality reflector, stainless steel contributed an extra 18-29 W. Galvanized and white reflectors provided, at most, well over 20 W and 30 W, respectively.

Figures 55 and 56 display the voltages and currents of each reflector at maximum power. Figures 57 and 58 illustrate the impact of the reflectors on open-circuit voltage and closed-circuit current. In the voltage diagrams, note that the y-axis does not start from zero because the voltages remain nearly constant regardless of the measurement. Open-circuit voltage (VOC) was also the only quantity that showed slight variations on the meter.

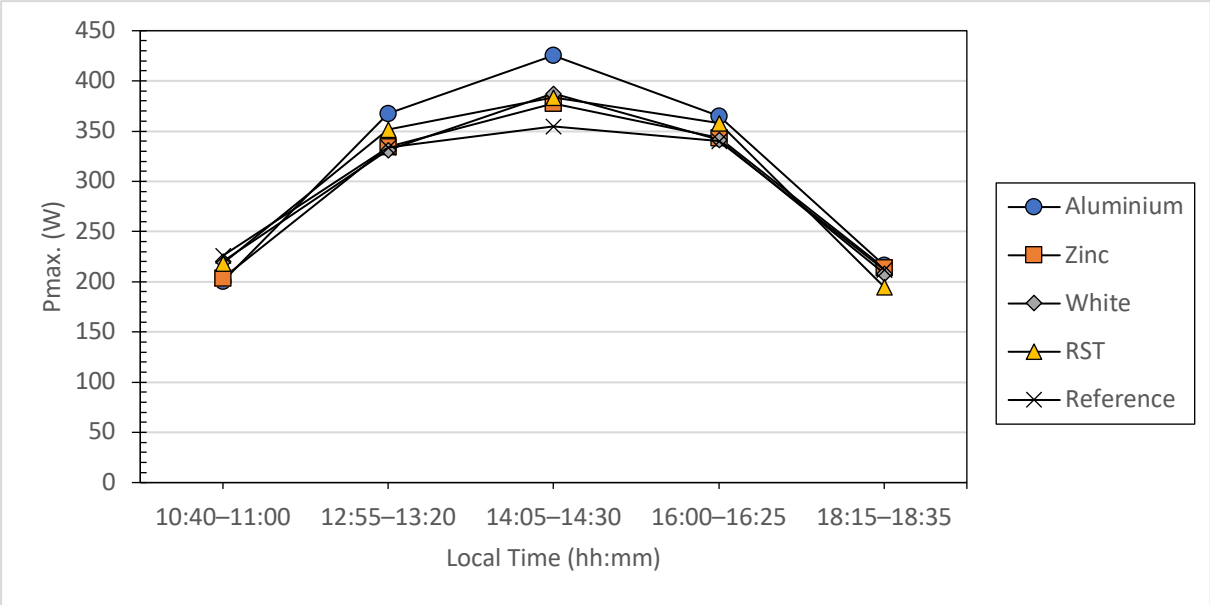

Figure 53. Maximum output of a solar panel during the comparison test (Viljami Kukkola).

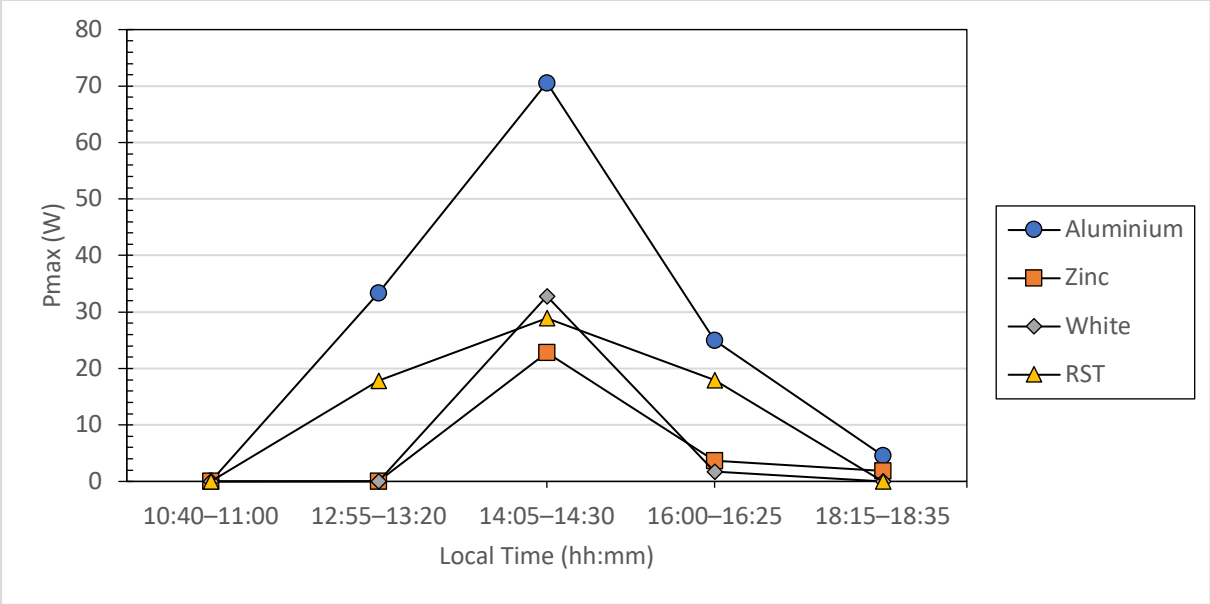

Figure 54. Solar panel power gain compared to the reference panel during the comparison test (Viljami Kukkola).

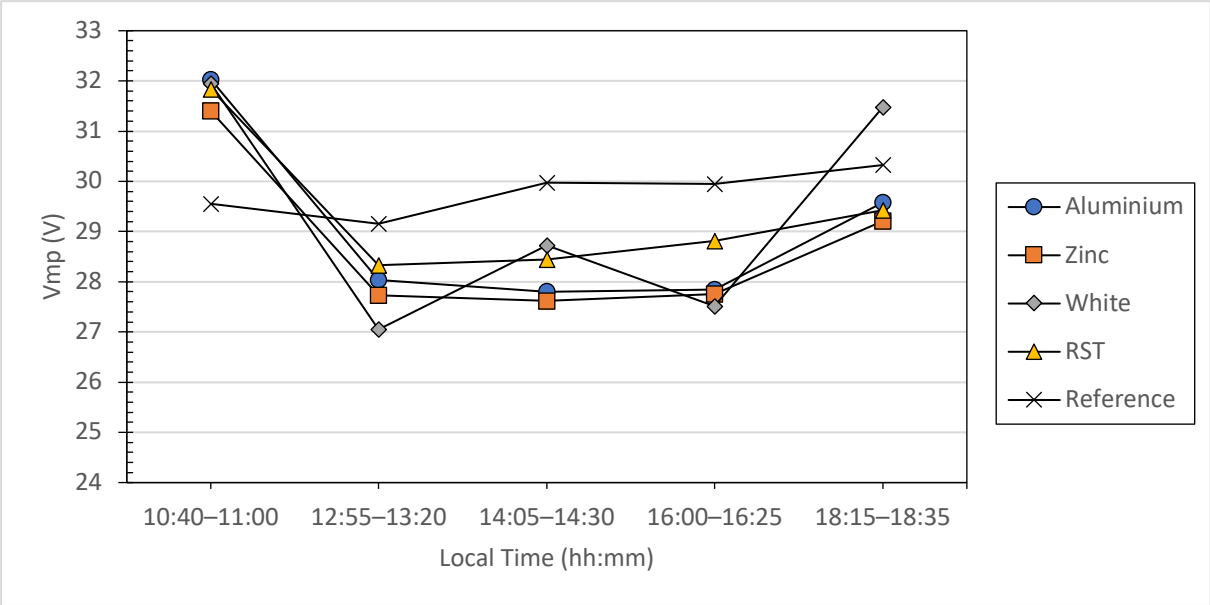

Figure 55. Voltage at maximum power during the comparison test (Viljami Kukkola).

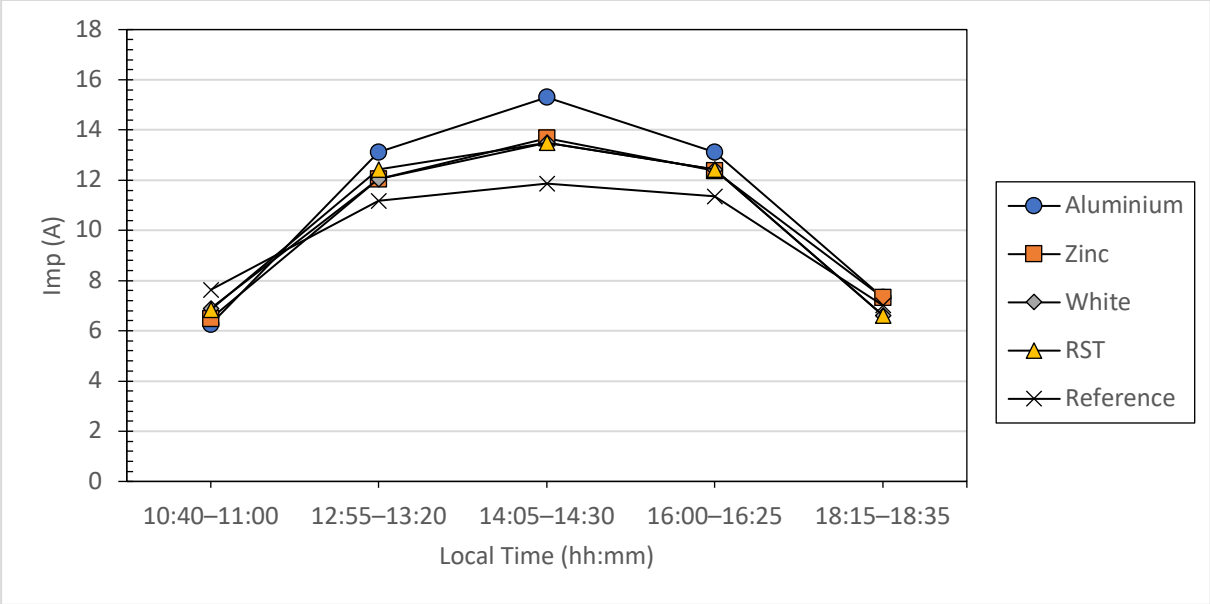

Figure 56. Electrical current at maximum power during the comparison test (Viljami Kukkola).

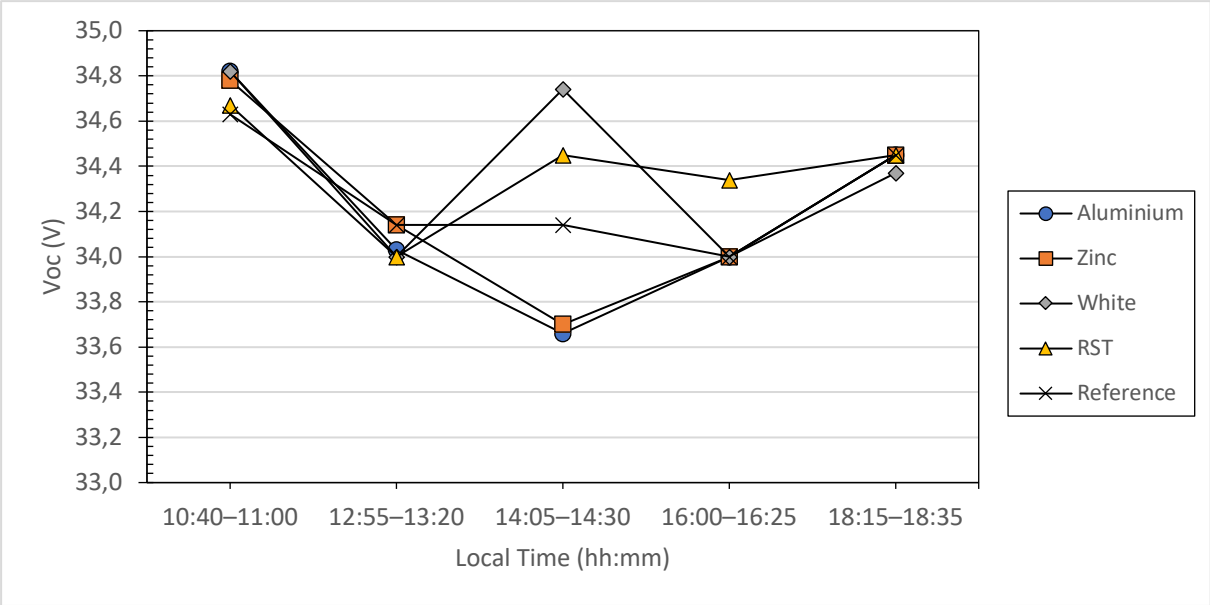

Figure 57. Open circuit voltage during the comparison test (Viljami Kukkola).

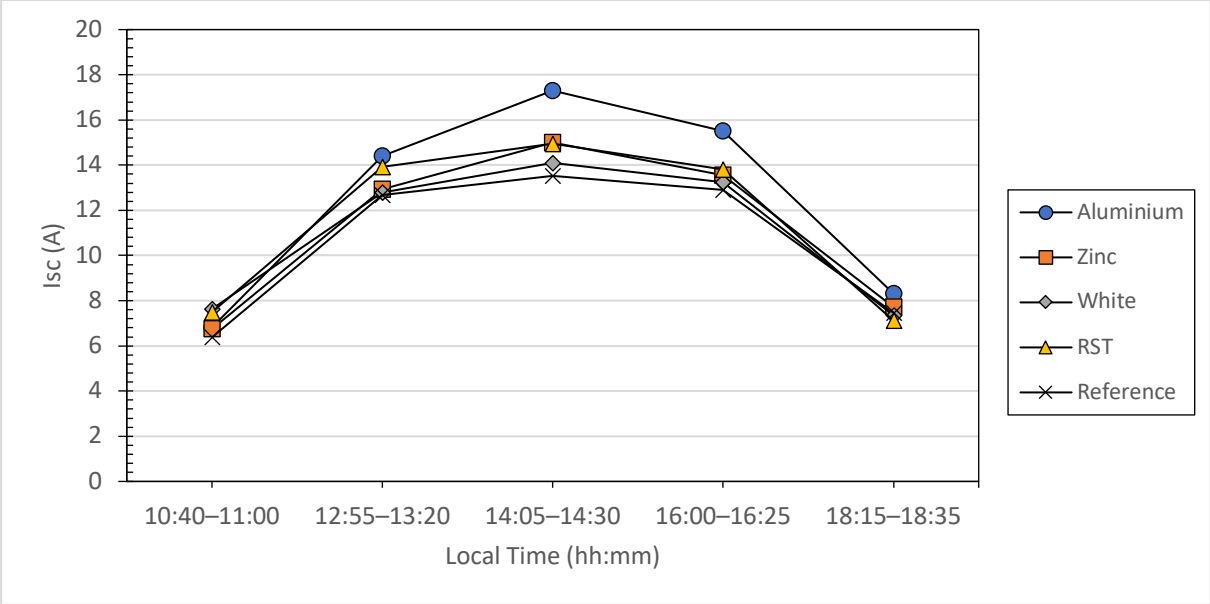

Figure 58. Short-circuit current during the comparison test (Viljami Kukkola).

3.3.4 Reflection test with stainless steel

An additional test on stainless steel sheets was conducted on August 13, 2024, lasting just over six hours. This test also helps us evaluate the reflector's impact on the solar panel temperature. Figure 59 displays the test panel, the reference panel, and the ambient temperatures. The stainless-steel reflector raised the solar panel temperature by a few degrees, as expected.

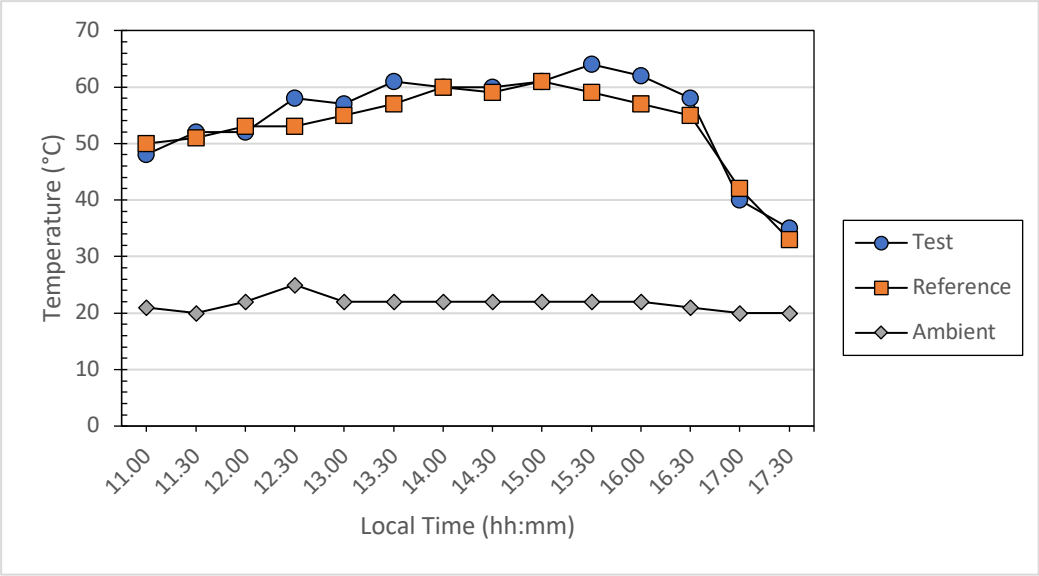

Figure 59. Test and reference panels and ambient temperatures during the RST test (Viljami Kukkola).

Figure 60 illustrates the radiation levels for the solar panel with a reflector and the reference panel, along with the differences between them and the horizontal radiation. The additional radiation provided by the reflector ranges from approximately 100 to 220 W/m². At 17:00, a cloud obscured the sun, affecting the radiation levels. During the measurements, it was noted that the reflector's additional radiation does not cover the entire solar panel; however, at noon, it covers about two-thirds of it. This is influenced by the relatively large reflector angle of 15°, its size relative to the solar panel, and the test date, when the sun is significantly lower than in midsummer. This also negatively affects the electrical measurements and the solar panel's temperature, as the radiation is unevenly distributed across it.

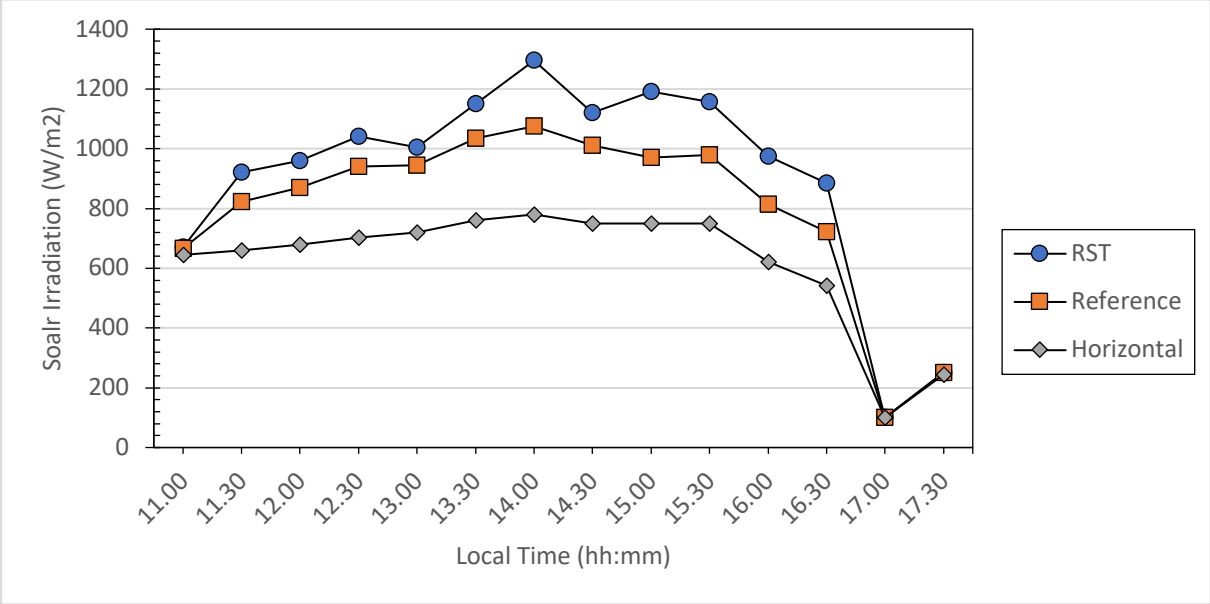

Figure 60. Solar irradiance on various solar panels and the horizontal plane during the RST test (Viljami Kukkola).

Figures 61–65 show the electrical measurements. Figure 61 displays the maximum power of the solar panels, while the extra power from the reflector ranges from 8 to 38 W. The maximum power increase was just over 10% compared to the reference panel. The noticeable drop in the evening reading at 17:30, down to 72.3 W, was caused by the tree canopy's shadow affecting the reference panel. Figures 62 and 63 present the maximum current and voltage, respectively. Figures 64 and 65 also show the open-circuit voltage and short-circuit current. Note that the voltage y-axis does not start at zero.

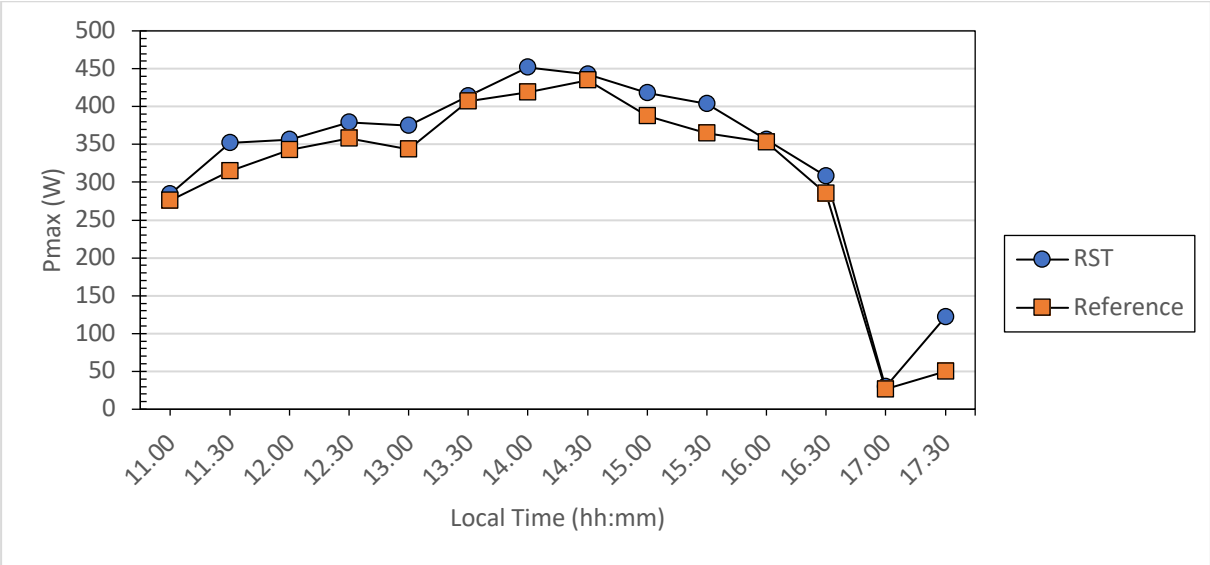

Figure 61. Maximum power of a solar panel during the RST test (Viljami Kukkola).

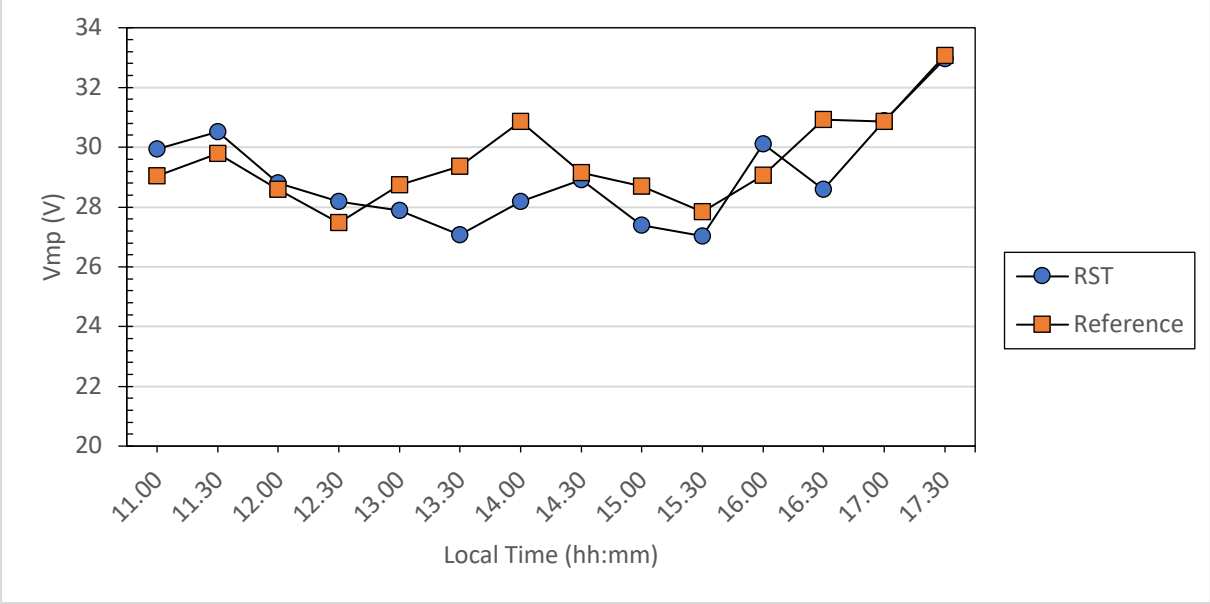

Figure 62. Voltage at maximum power during the RST test (Viljami Kukkola)

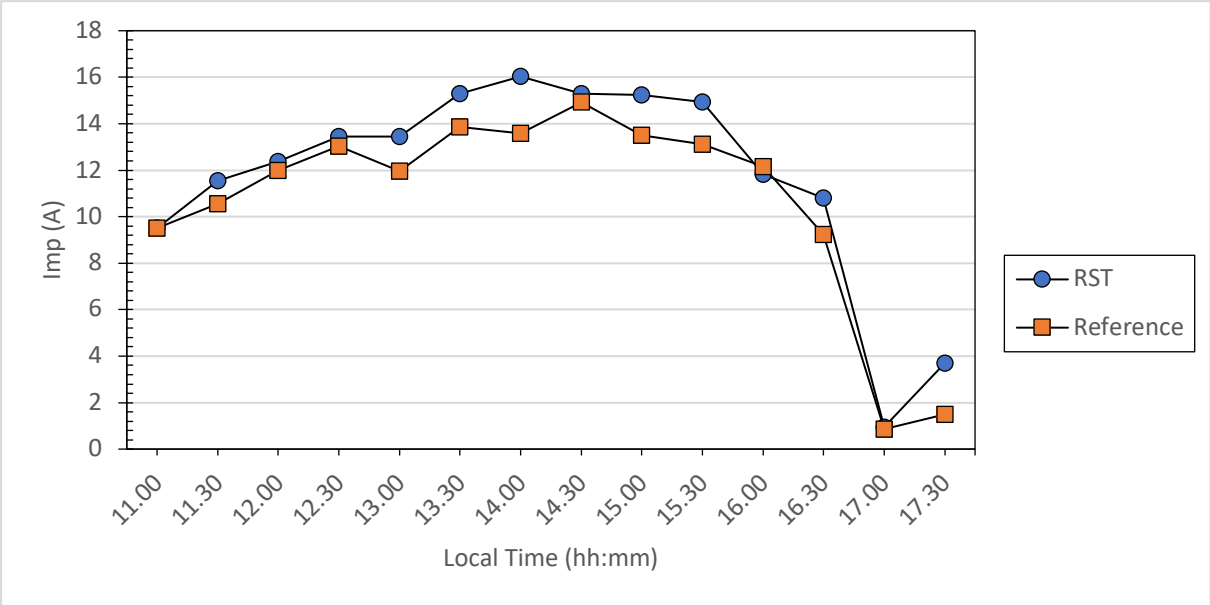

Figure 63. Electrical current at maximum power during the RST test (Viljami Kukkola)

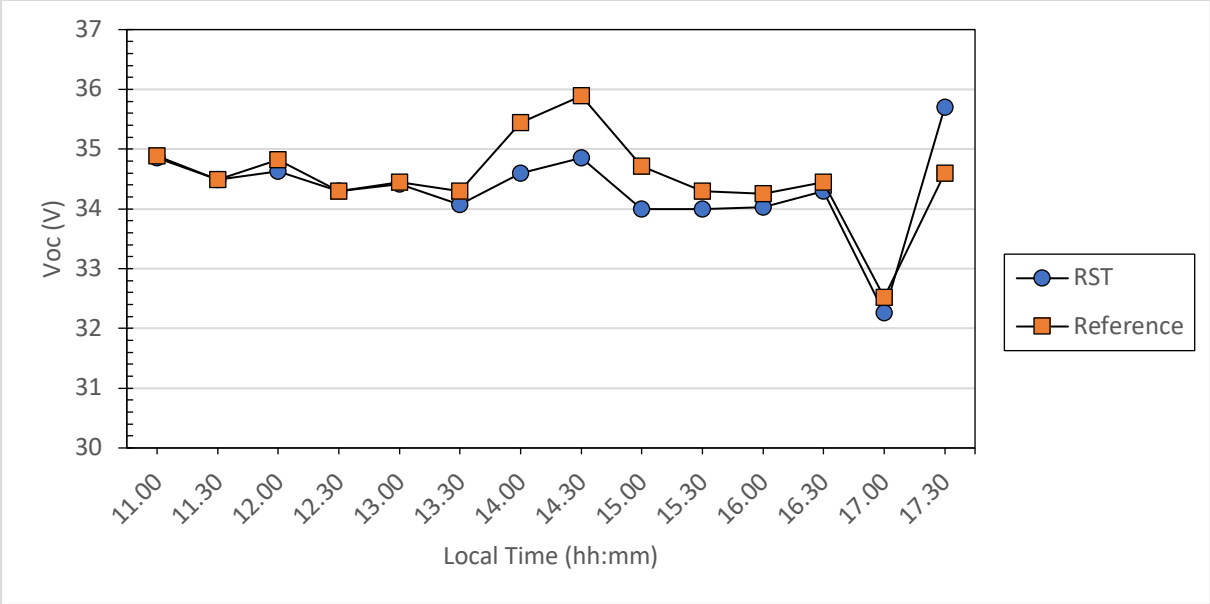

Figure 64. Open-circuit voltage during the RST test (Viljami Kukkola).

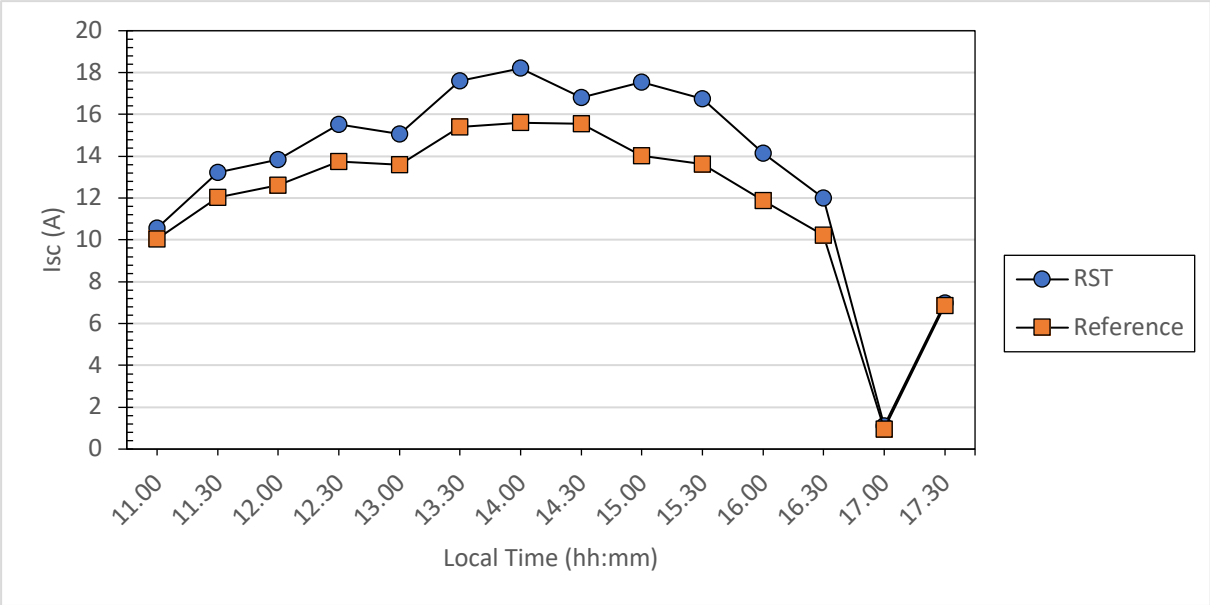

Figure 65. Short-circuit electrical current during RST test (Viljami Kukkola).

3.3.5 Reflection tests with the aluminium sheets

For the most effective reflector material tested, aluminum, an all-day test was conducted to assess the impact of an aluminum sheet on the solar panel and its temperature. The test occurred on August 14, 2024. Figure 66 illustrates the temperature of the solar panel with the reflector, the reference panel, and the ambient temperature. Aluminum also reflects more thermal radiation when the solar panel's temperature exceeds 70°C at 14:00. The temperature rises by about 8 degrees compared to the reference panel, slightly reducing panel efficiency. Testing of the aluminum wed earlier than that of the RST sheet due to shadows cast by cloudy skies and nearby trees.

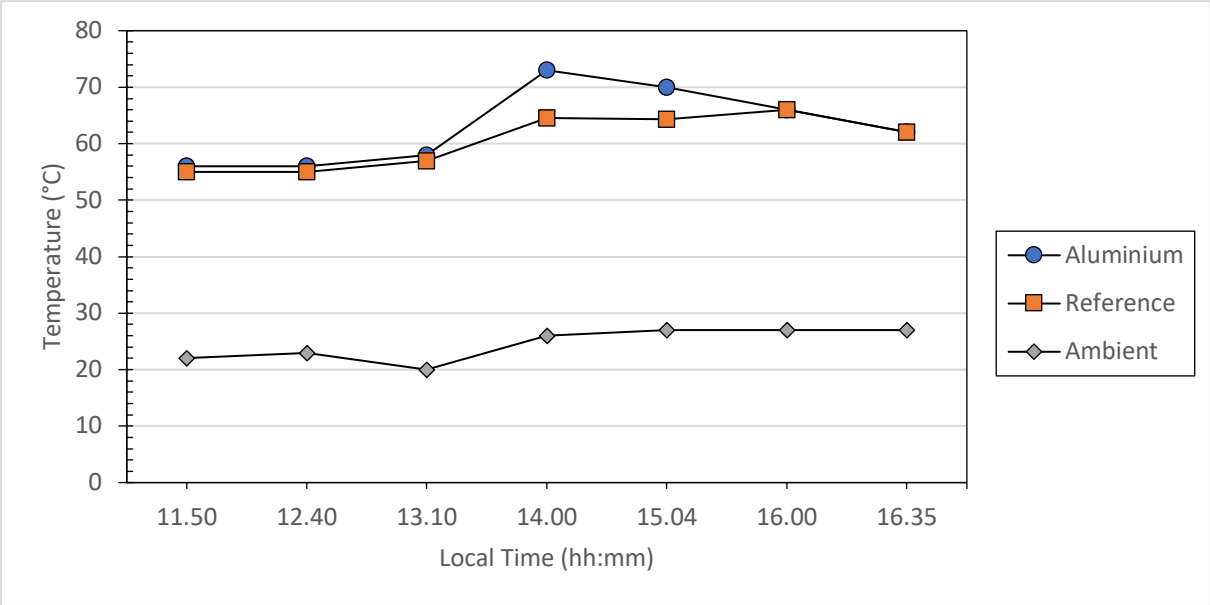

Figure 66. Test and reference panels and ambient temperatures during the aluminum test (Viljami Kukkola).

The amount of solar radiation on different solar panels and on the horizontal surface is shown in Figure 67. At 13:10, a small shadow cast on the reflector, causing a brief decrease in radiation. Using an aluminum reflector increases the radiation on the solar panel by approximately 200-360 W/m², or nearly 40%, which is twice as much as the RST sheet. Aluminum reflects similarly to RST, meaning its reflection covers about two-thirds of the solar panel. The radiation measurements are taken from the edges or the center of the panel, where the extra radiation from the reflector hits.

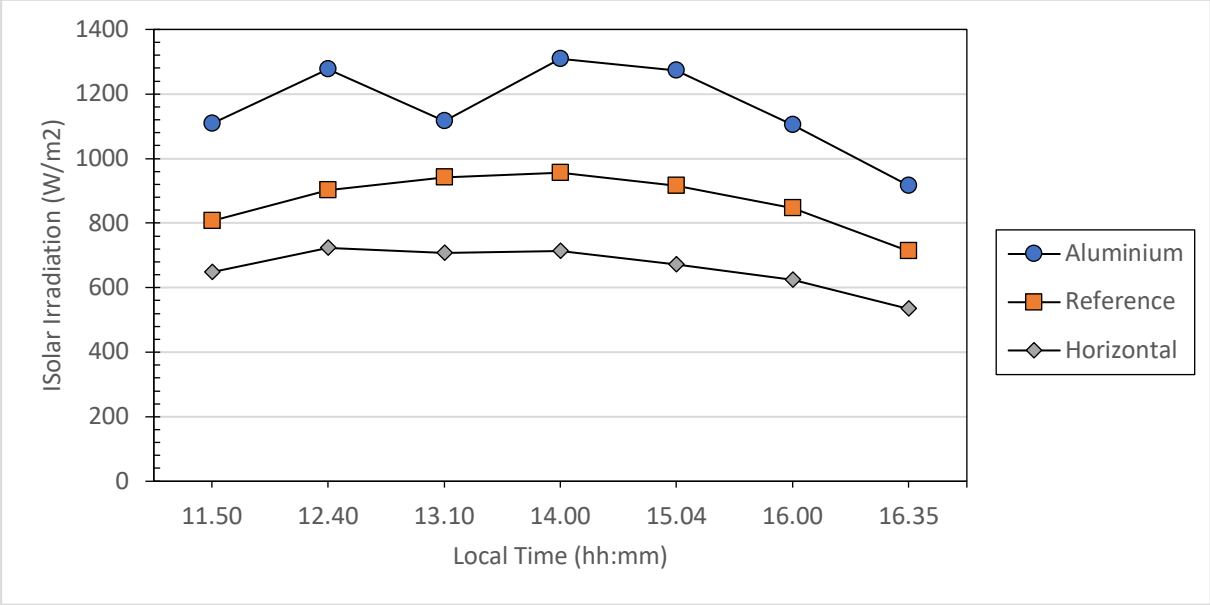

Figure 67. Solar irradiance on various solar panels and the horizontal plane during the aluminum test (Viljami Kukkola).

The electrical measurements are shown in Figures 68–72. The maximum output of the solar panels is demonstrated in Figure 68. Aluminum increases the maximum power of the panel by approximately 18-63 W, which is nearly twice the amount of the RST sheet. Figures 69 and 70 show the voltage and the maximum current power. The open-circuit voltage is shown in Figure 71, while the closed-circuit current is displayed in Figure 72. The shadow's effect on the reflector at 13:10 is also clearly visible in these measurements.

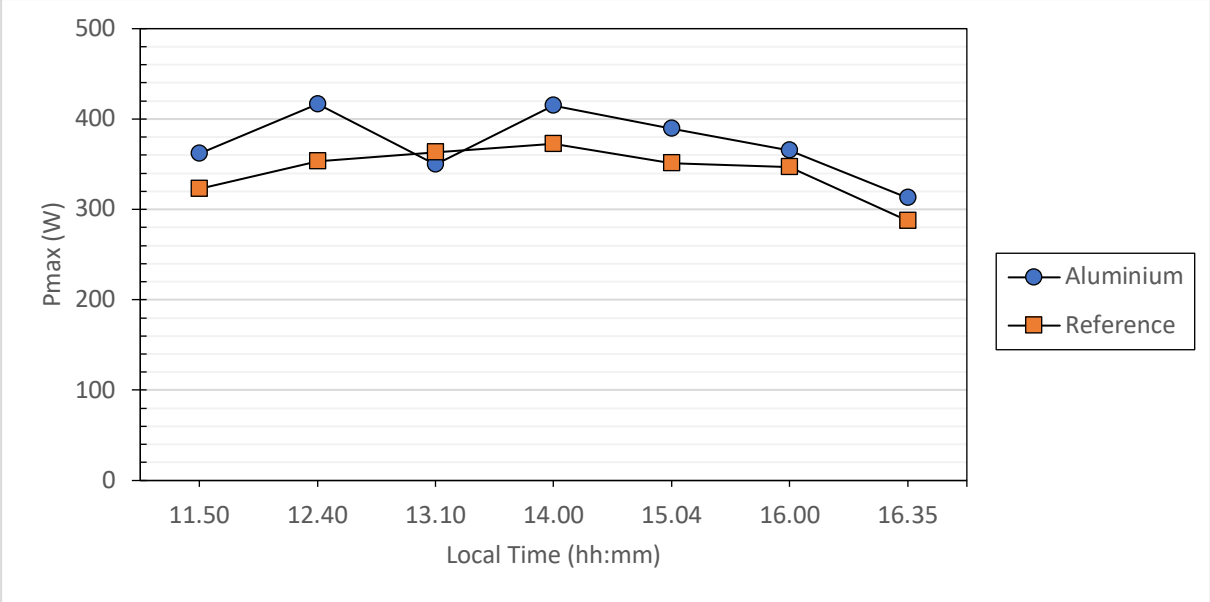

Figure 68. Maximum power output of solar panels during the aluminum test (Viljami Kukkola).

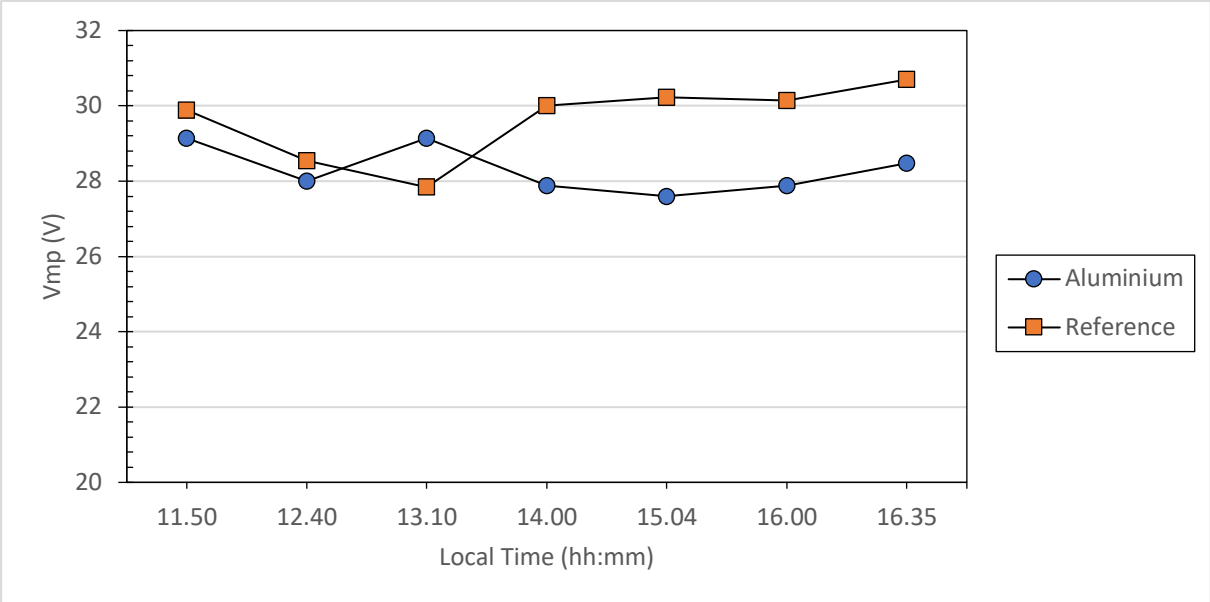

Figure 69. Voltage at maximum power during the aluminum test (Viljami Kukkola).

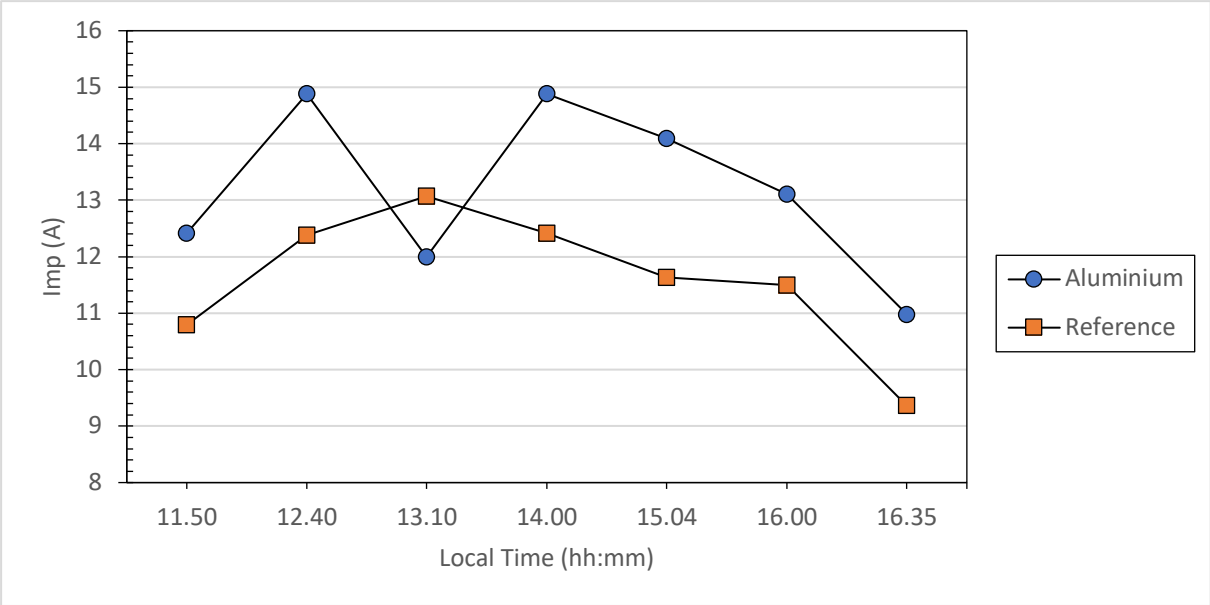

Figure 70. Electric current at maximum power during the aluminum test (Viljami Kukkola).

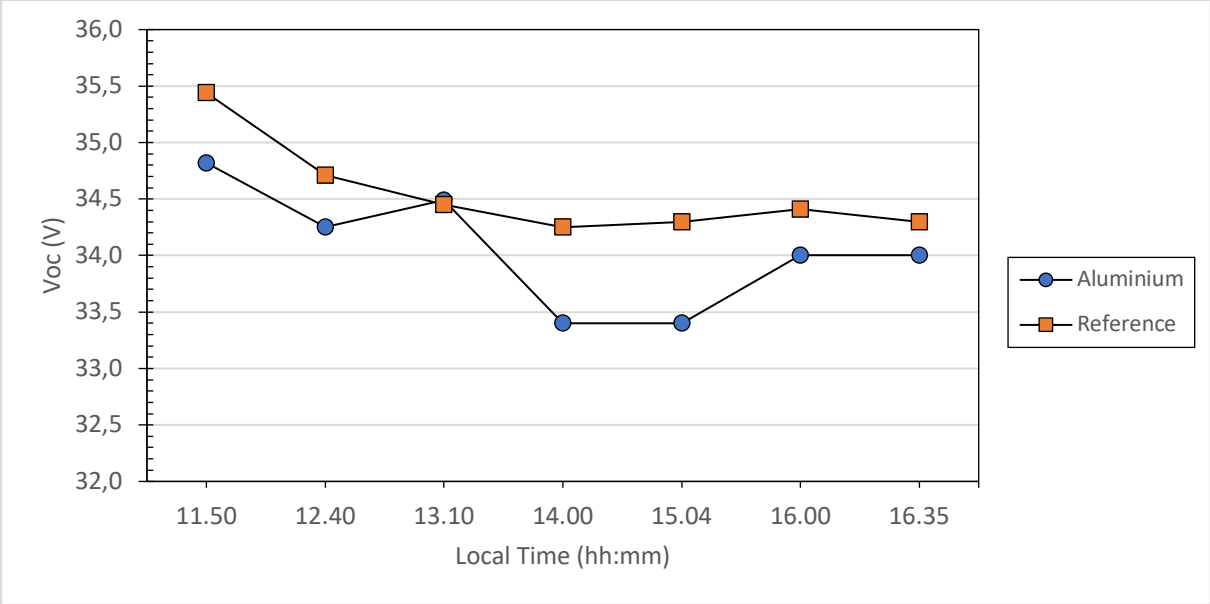

Figure 71. Open-circuit voltage during the aluminum test (Viljami Kukkola).

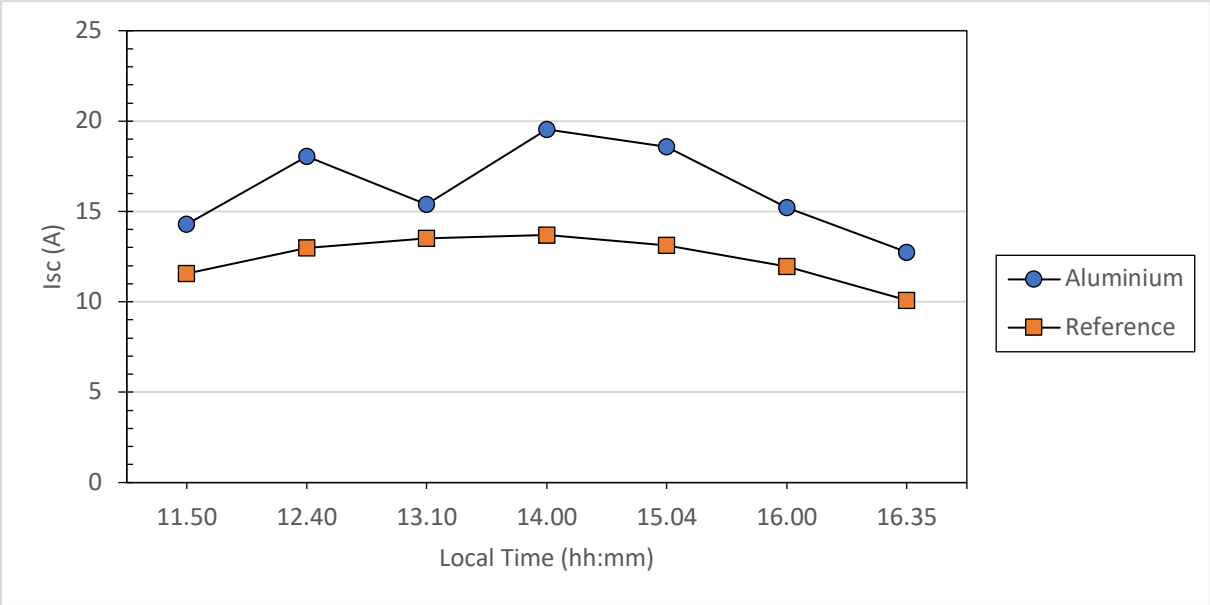

Figure 72. Short-circuit electrical current during the aluminum test (Viljami Kukkola).

3.4 Roof Reflector Design

FinnFoam's main business is the manufacture of insulation materials, so the concept behind this work is to install both additional insulation and a solar panel on the roof. Chapter 3.4.1 explains how to install solar panels and a reflector on the roof. Due to their large size, this additional insulation would be intended for warehouses and factories' roofs. Installation on the roof is limited by its steepness, so the practical targets are flat roofs, which are easier and safer to work on.

The added insulation's triangular shape also allows the roof to serve as a reflector for the solar panels. The dimensions of the insulation block are calculated in Chapter 3.4.2. The effect of roof pitch on irradiance is explained in Chapter 3.4.3

3.4.1 Installation of PV panels on the rooftop

Solar panels are typically not installed at the optimal angle on roofs; instead, they are positioned to match the roof's slope. The exception is flat roofs, which usually have a pitch of 1:10 or less, meaning the angle is under 5.7 degrees. In these cases, specially designed mounting frames are used. These frames are generally installed at an angle of 10–30 degrees to account for factors such as wind, snow, and shadows cast by the panels. (Finelcomp 2025a)

Solar panels on a flat roof are installed using weights, so the roof structure does not need to be punctured or anchored, where the frame is fixed to the roof structure (Finelcomp 2025a). Larger commercial and office buildings often have flat roofs that, with good design, can

accommodate more panels in different directions, distributing electricity output throughout the day. Installations must follow local building regulations and weight limits. The roof's irregular shape and various obstacles present challenges for both design and installation. Barbón et al. (2022) developed an algorithm for installing solar panels on irregular roofs. The algorithm produced up to 28% more energy than a typical alignment, so good design can significantly improve solar panel output.

Solar panels are mounted on frames similar to those of ground-mounted solar panels, but the frames are attached directly to gable roofs. The installation method varies based on the roof material and angle. Several installation methods exist for metal sheet roofs, with clamp installation being the most common; in this method, an aluminum rail is secured to the roof seam with a clamp and bolts. For corrugated roofing, the installation is done using screws that attach the bracket to the roofing. On tiled roofs, special fixing hooks are employed, which are also screwed to the roof base. (Finelcomp 2025b) A 10 to 15 cm gap should be maintained to allow the solar panel to cool down and minimize potential freezing issues, particularly in northern regions (Gan 2009). Additionally, integrated solar panel systems, in which the roof is composed of solar panel units, are available.

In addition to screws and clamps, the frames for installing solar panels can also be glued to a flat sheet metal roof or corrugated sheeting. This method is particularly common in India and Southeast Asia. The adhesive used, such as acrylic adhesive, must be resistant to temperature and humidity fluctuations and strong enough to withstand wind forces. Using adhesive eliminates the need to drill a hole in the roof and speeds up rail installation. (Parker US, n.d.)

The initial structure of FinnFoam’s roof insulation includes an insulating piece to which the roof cladding is attached using a fire-resistant adhesive. Additionally, the roof cladding acts as a reflector. Solar panel brackets are either glued or screwed to the roof at the factory, reducing installation time for the solar panels. On a flat roof, the insulation pieces are arranged in rows to allow for solar panel installation in rows, as illustrated in Figure 73.

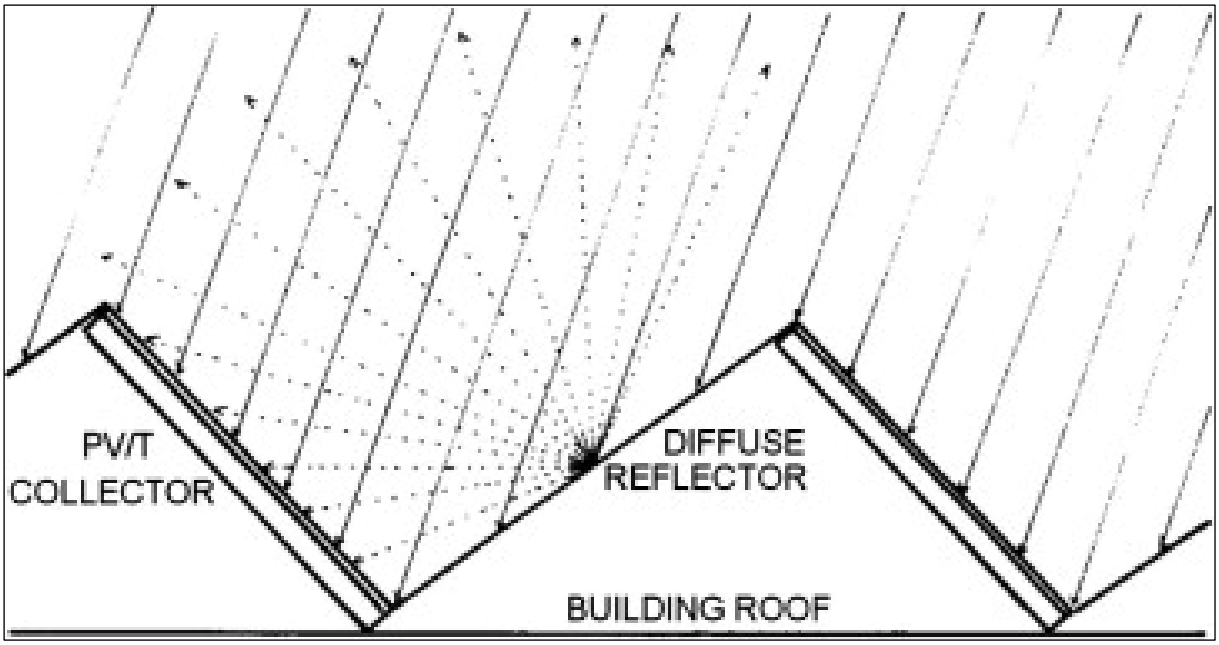

Figure 73. Example of reflector triangles on a flat roof (Tripanagnostopoulos et al. 2002).

3.4.2 Comparing reflective materials

Mirrors intended for reflective purposes usually comprise multiple layers of different materials, enabling the benefits of various materials, such as steel's durability, aluminum's reflectivity, and glass's transparency, to be utilized (García-Segura et al. 2016). For the FinnFoam product, the reflector is expected to offer good reflectivity, durability, and affordability, as it also serves as a roof. While mirrors and polymer-based reflectors cannot be used as the roof, stainless steel or aluminum, which can be coated or painted to enhance both reflectivity and durability, would be the optimal choice for this application.

FinnFoam’s roof reflector can be made from various metal sheets. In the experimental part of the work, a solar panel will be utilized to conduct a practical reflectivity test on different materials. Selecting the coating material is essential, and it’s crucial to consider the reflectivity of thermal radiation. The advantage of steel is that it typically reflects less thermal radiation than aluminum, making it the optimal substrate material for reflective coating. The reflector's performance in the wavelength range (400-1100 nm) for a silicon-based solar panel should be high, while low reflection of other radiation will help prevent an increase in the solar panel's temperature and consequently reduce its power output.

The reflectivity of standard materials and coatings is usually sourced from literature or manufacturers. There is a diverse array of steels with varying compositions. The reflectivity

of steel ranges from 0.5 to 0.8, although significant variations exist among steel alloys. The reflectivity of aluminium exceeds 0.85 at wavelengths up to 2000 nm. Aluminium is one of the best reflectors, and it is also relatively cheap, but it must be protected from the elements with a coating like PVD. Steels can be coated and painted to improve service life and corrosion resistance. The paint should be as reflective and glossy as possible while ensuring good reflectivity.

The selection of metal, coating, and potential paint should be made in collaboration with the manufacturer, who has the necessary expertise and testing equipment to determine the appropriate material and coating.

3.4.3 Dimensions of the insulation block

The insulation is produced as a rectangular block, which is then cut into wedge-shaped pieces. Two wedges can be cut and glued from a single edge, ensuring that no material is wasted. Figure 74 illustrates a simple example of various dimensions and angles of insulation. The wedge height is consistently 1.2 m, and the length is either 4 or 6 m, which can be halved to 2 or 3 m, depending on the mold size. The examples in this thesis are calculated for a 4-meter block. The width of the wedge is 1 meter, but the pieces can be glued together if necessary.

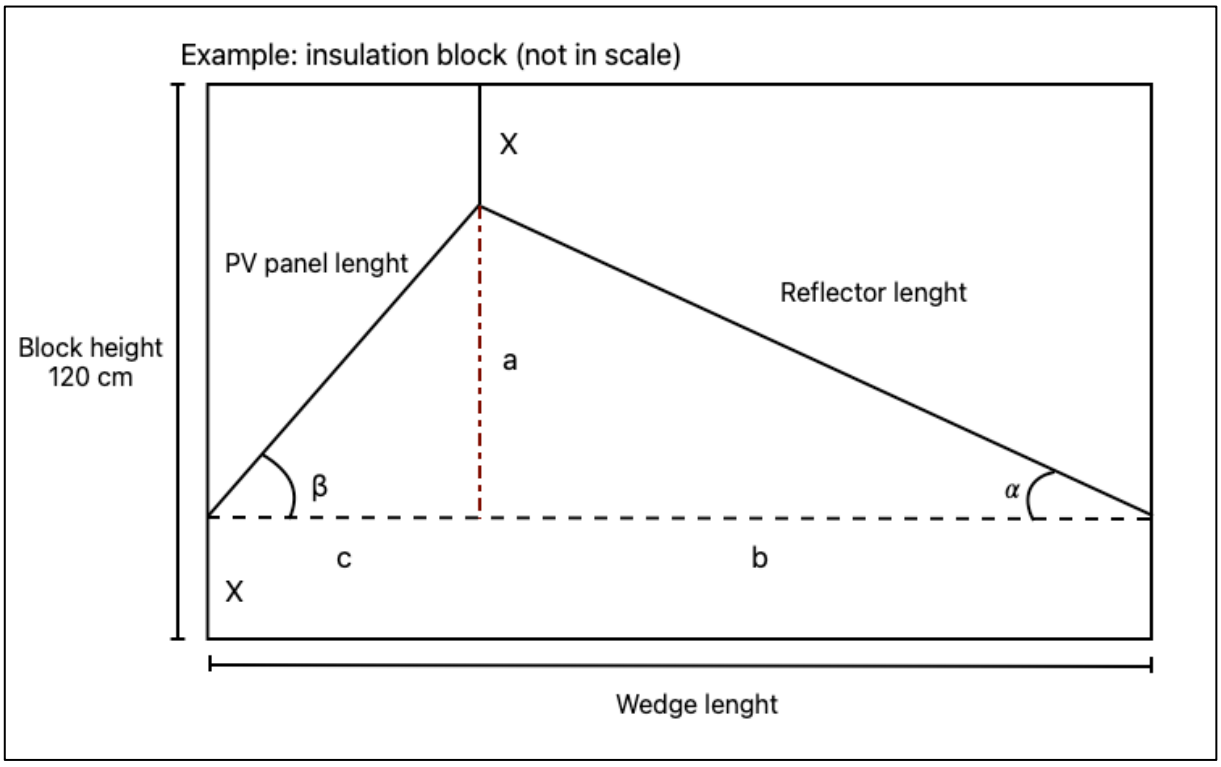

Figure 74. Example dimensions of an insulation block (Viljami Kukkola)

The dimensions of the wedge pieces can be easily calculated using trigonometry, for example, in Excel using formulas 49-54. Given that the height and length of the wedge are known, the length of the solar panel is set to 1.2 m; however, this length can vary depending on the solar panel used, and the angle can be chosen based on the optimal angle for the solar panel. From these parameters, the other dimensions, such as the reflector surface length, thickness, and angle, are calculated.

$$Wedge\ height, a\ (m) = \sin\beta \times PV\ panel\ lenght \tag{49}$$

$$Adjacent\ side\ of\ PV\ tilt\ angle, c\ (m) = a \div \tan\beta \tag{50}$$

$$Adjacent\ side\ of\ reflector\ angle, b\ (m) = Wedge\ lenght - c \tag{51}$$

$$Reflector\ lenght\ (m) = \sqrt{a^2 + b^2} \tag{52}$$

$$Reflector\ tilt\ angle, \alpha\ (°) = \sin^{-1}\left(\frac{a}{reflector\ lenght}\right) \tag{53}$$

$$Insulation\ height, X\ (m) = \frac{(Wedge\ lenght - a)}{2} \tag{54}$$

The simulation model presented can also be used to estimate the impact of wedge length on additional irradiance. Wedge length affects the reflector length, which in turn influences the additional irradiance. Figure 75 illustrates the impact of wedge length. Lengths of 3 and 4 meters are optimal because the reflector is 2-3 times as long as the solar panel. The longest 6-meter wedge is detrimental during the summer due to the reflector's shading and the wedge's low impact on the overall system.

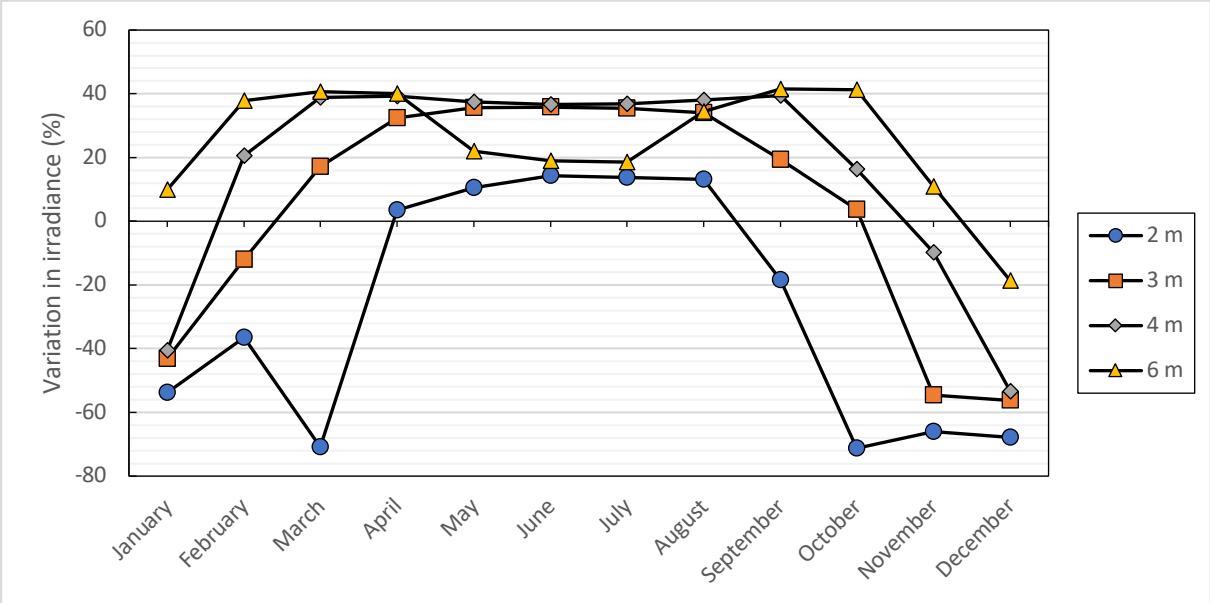

Figure 75. Effect of wedge length on irradiance in Helsinki with a 30° solar panel angle (Viljami Kukkola)

3.4.4 Examples of the insulation block

Figure 76 shows four example wedges at 30-60° solar panel angles, spaced at 10 ° intervals. The length of the solar panel is 1.2 meters (1200 mm). Other dimensions are determined by these, such as the reflector's angle and length, which are calculated using formulas 49–54.

The examples also demonstrate how the calculated insulation thickness affects its insulating properties. The panel's angle shifts by 30 degrees, from 30 to 60 degrees, while the reflector's angle changes by about 5.5 degrees, from 11.46 degrees to 17.0 degrees. The example side profiles in Figure 45 also show the corresponding insulation thickness, which ranges from 300 mm to 80 mm.

1. PV-panel 1200 mm, 30° and reflector 3021 mm, 11,46°

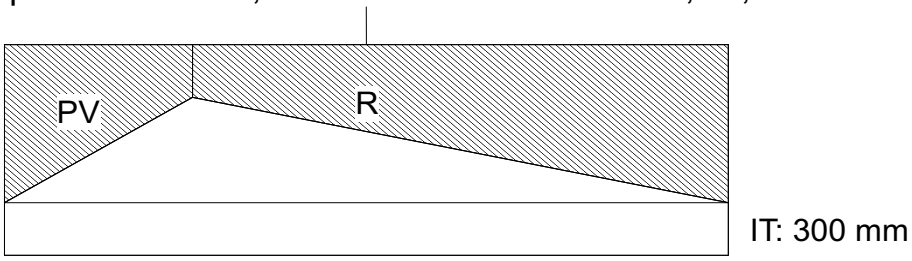

2. PV-panel 1200 mm, 40° and reflector 3176 mm, 14,06°

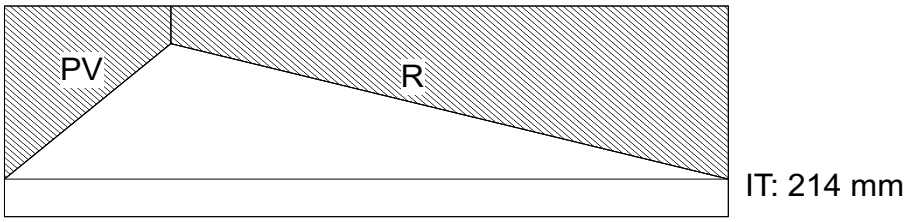

3. PV-panel 1200 mm, 50° and reflector 3357 mm, 15,89°

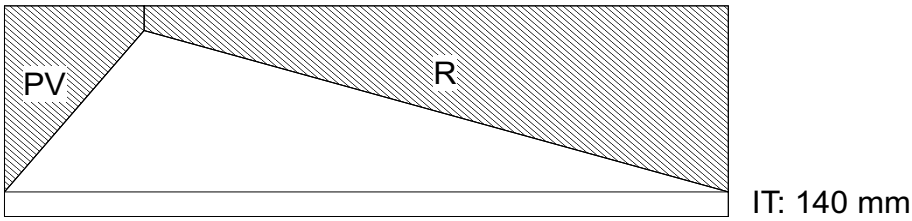

4. PV-panel 1200 mm, 60° and reflector 3555 mm, 17,0°

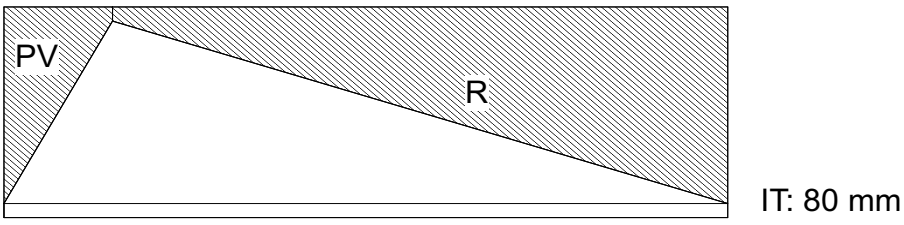

Mould dimensions (l x w x h): 4000 x 1000 x 1200
Unit of measurement: millimetre (mm)
Abbreviations:
PV - PV solarpanel
R - Reflector
IT - Insulation thickness
The dimensions of the images are in proportion to each other.

Figure 76. Four side profiles showing different block dimensions (Viljami Kukkola)

3.5 Results Evaluation

Figure 77 shows the average irradiance on PV panels with a reflector over a year, based on simulation results. Error bars are calculated using the standard error formula. The standard error, shown in Figure 77, is approximately 1 kW/m², and the standard deviation is 3–4 kW/m² due to Finland's seasonal variation in irradiation. The figure also illustrates the coastline's influence on total radiation intake, with Oulu receiving more average irradiation than Jyväskylä.

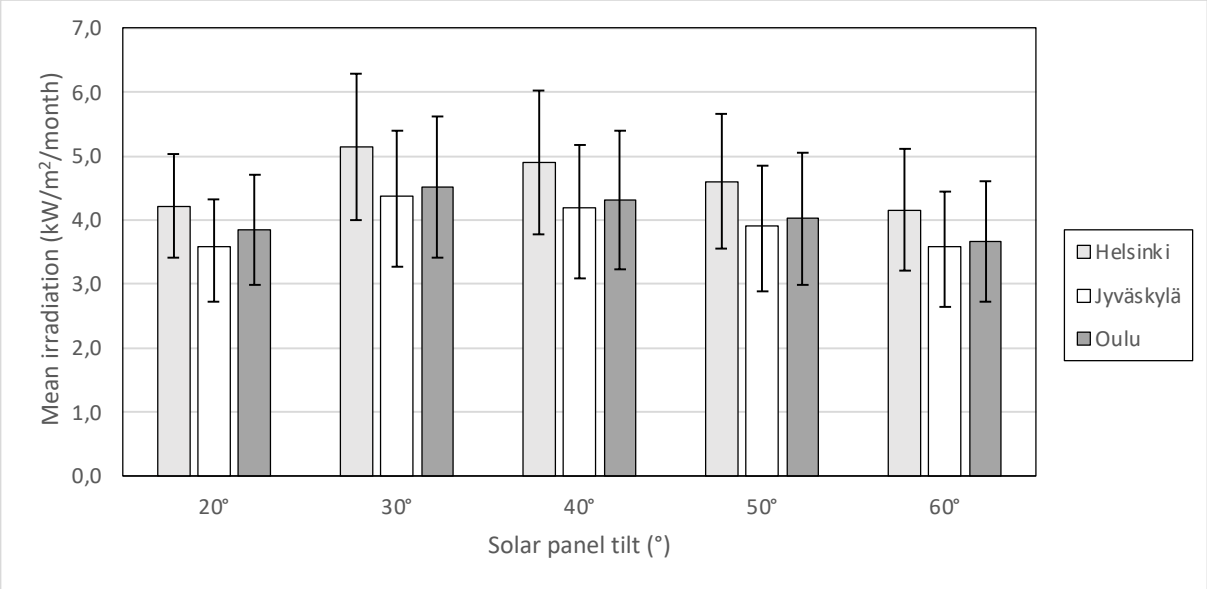

Figure 77. Average irradiation on PV panels with reflector over a year, based on simulation results (Viljami Kukkola)

Table 7 summarizes the average calculated effect of the reflector. Additionally, Table 7 includes the reflector angle, which depends on the solar panel angle. The additional irradiance provided by the reflector is nearly 36% for a solar panel positioned at a 30-degree angle. This comparison aligns well with the studies discussed in the theoretical section, which yielded varying results, typically ranging from 15% to 40%. The optimal angle for the solar panel is influenced by the roof's angle, as discussed in greater detail in Chapter 3.2.3.

Table 6. Reflector's effect on total annual irradiance with PV panel and reflector angles (Viljami Kukkola)

Location	20°, 8,13°	30°, 11,46°	40°, 14,06°	50°, 15,89°	60°, 17,0°
Helsinki	23,6 %	35,3 %	31,4 %	27,8 %	22,9 %
Jyväskylä	25,0 %	36,8 %	33,4 %	29,7 %,	25,8 %
Oulu	26,8 %	35,0 %	30,9 %	26,1 %	21,2 %

The ideal solar panel angle for flat roofs is around 40°, while for steeper roofs it can reach 50°. The differences between winter and summer are significant in Finland, with increases of up to 40% in spring and autumn. However, in winter, radiation can be reduced by half due to the reflector shading the solar panel.

The experimental tests were conducted in Southern Finland over three days. First, a comparison of reflectors was performed on a solar panel during mid-summer, and in August, full-day tests were carried out on aluminum and stainless steel sheets. Commercial equipment was used to measure electrical, temperature, and radiation levels.

Table 8 shows the average parameter results for reflector materials from outdoor tests. Irradiance and solar panel power output fluctuate significantly depending on the sun's position. Aluminum acts like a bright mirror, reflecting radiation nearly 50% more than the reference at noon. However, it also heats the solar panel much more than other materials.

Table 7. Mean parameters with different materials during outdoor testing and standard errors (Viljami Kukkola)

Parameters	Aluminium	Zinc-coated steel	White painted steel	RST	Reference
Irradiance (W/m2)	905 ± 148	779 ± 99	742 ± 91	788 ± 115	710 ± 61
Vmp (V)	29,1 ± 0,8	28,7 ± 0,7	29,3 ± 1,0	29,4 ± 0,6	29,8 ± 0,2
Imp (A)	11,0 ± 1,8	10,4 ± 1,5	10,3 ± 1,5	10,4 ± 1,5	9,8 ± 1,0
Pmax (W)	314,9 ± 44,8	294,5 ± 35,8	297,8 ± 35,4	301,2 ± 39,2	289,3 ± 33,0
Voc (V)	34,2 ± 0,2	34,2 ± 0,2	34,4 ± 0,2	34,4 ± 0,1	34,3 ± 0,1
Isc (A)	12,5 ± 2,1	11,2 ± 1,7	11,0 ± 1,5	11,5 ± 1,7	10,6 ± 1,5

The best improvement in solar panel yield was achieved with aluminum, which, because of its reflective properties, increased power by up to 19.9% and by an average of 7.9%. The second-best RST sheet consistently performed well throughout the day, boosting power by up to 8.2% and averaging 3.8%. The galvanized steel and white painted steel plates exhibited similar performance, reflecting radiation primarily at solar noon. The zinc treatment likely caused the scattering of reflected radiation at lower angles of incidence.

In additional tests, aluminum and RST were continuously monitored throughout the day. Aluminum performed very well, as expected, increasing panel yields by up to 17.9% and averaging 9.0%. The RST sheet improved panel yields by up to 10.6% and by an average of 6.4%. Table 9 summarises the average parameter measurements and standard errors for both

additional tests. The average panel power increased with aluminum by approximately 31 watts, compared to the RST's 21 watts. This was due to partial reflection from the solar panel and to more frequent measurements during the RST test.

Table 9. Average parameters with standard errors from RST sheet and aluminum tests (Viljami Kukkola)

Parameters	RST	Reference A	Aluminium	Reference B
Irradiance (W/m2)	1031 ± 48	904 ± 36	1158 ± 52	869 ± 33
Vmp (V)	28,6 ± 0,3	29,1 ± 0,3	28,3 ± 0,2	29,6 ± 0,4
Imp (A)	13,3 ± 0,6	12,3 ± 0,5	13,2 ± 0,6	11,6 ± 0,5
Pmax (W)	378 ± 15	357 ± 14	373 ± 14	342 ± 11
Voc (V)	34,4 ± 0,1	34,7 ± 0,1	34,1 ± 0,2	34,6 ± 0,2
Isc (A)	15,1 ± 0,7	13,2 ±0 ,5	16,3 ± 0,9	12,4 ± 0,5

The differences in the test results are significant, particularly for the RST panel, despite the follow-up tests not covering the entire solar panel and measurements being taken at slightly different times. Furthermore, there was roughly a 30-day gap between the tests. Another observation about the tests is their brevity; they lasted only one day. This measurement day was chosen because it was as bright and sunny as possible to assess the effect of reflection accurately. Most studies develop algorithms to quantify reflection and its impact on solar panels because practical tests typically last only a few days to a couple of weeks each season.

Aluminum is a good reflector material; however, its durability outdoors is poor without surface treatment. The tested stainless-steel sheet also lacked surface treatment, so a method other than galvanizing must be selected. Using paint is also feasible, provided the steel substrate's treatment does not compromise the metal's reflectivity. As mentioned in the theory section, the choice of reflector material is primarily influenced by its durability and the longevity of the reflection. The final selection of reflector material should only be made after conducting longer field tests with larger reflectors.

4 Conclusions

The goal of the master's thesis was to assess the use of a reflector to improve solar panel efficiency in Finland. FinnFoam's concept involves developing a product that combines a solar panel, a reflector, and an insulation material, aimed at increasing solar energy output and lowering heating costs in buildings. The theoretical section covers the technologies behind solar panels and the factors affecting their performance. Evaluating the use of reflectors and material options is essential to this work, as they greatly influence the product's overall feasibility. The selection of reflector material depends on its application, durability, and stability of reflectivity under Finnish weather conditions.

The main conclusions in this thesis are:

- The use of reflectors with solar panels has been studied worldwide; however, practical tests have mainly focused on latitudes between 20° and 40°.
- Aluminum is the best reflective material; however, it must be coated with a protective layer to endure outdoor conditions. Another option is steel, which can be painted with a reflective, glossy finish.
- Literature indicates that solar panel output can increase by 15–40% annually. However, practical tests revealed that the actual additional output was smaller, ranging from 10% to 30% annually.
- The extra energy output depends on the reflector's size, which influences the radiation directed at the panel and the shade it creates. More irradiation increases the temperature of the solar panel with a reflector, reducing the additional energy output and accelerating panel wear.
- According to the simulations conducted in the thesis, the maximum additional irradiation from the reflector is approximately 35–40% annually in Finland.
- In outdoor tests, additional irradiation reached a maximum of 46% and averaged 25% with an aluminum reflector of the same size as the panel on a summer day in southern Finland. The solar panel yield with the aluminum reflector increases by about 20% at noon in outdoor tests.

Preliminary tests and literature review have shown that boosting a solar panel's output with reflectors is very effective, depending on the location and material used for the reflector. The reflectors should be made of a reflective and durable material, as they also act as a roof for the FinnFoam product. A handheld tester can be used to assess the reflectivity of the chosen roofing materials.

The next research focus will be on determining the appropriate size of insulating wedges, ideally through outdoor tests where the wedges can act as reflectors. The mathematical analysis for calculating wedge dimensions is provided in Chapter 3.4.3, which helps in making the test wedges. The reflector's length should be two to three times that of a solar panel to maximize power output, based on several studies. Therefore, the wedge length should be around 3 or 4 meters.

The outdoor tests of the thesis showed that the reflector's size influences the panel's output. Due to uneven reflection, the additional output was less than 10%, even though the radiation increased to over 1000 W/m². A more comprehensive outdoor test should be conducted over a longer period to achieve better results, with measurement dates spread throughout the year, ideally in spring, summer, and fall.

When designing a larger solar panel system, it is essential to calculate the project's financial payback period and long-term return on investment. As noted in Chapter 2.6, this helps ensure the project's financial sustainability and successful implementation. The economic estimates for reflectors vary, but reflectors generally shorten the payback period for solar panels, as long as their costs are less than the additional revenue they generate and the cost of the solar panels used.

By combining a reflector, a solar panel, and extra insulation, FinnFoam develops a unique product suitable for larger roofs. In commercial settings, reflectors are rarely used in larger power plants, so introducing a new type of reflector product will be innovative, especially in the Finnish climate.

References

Abdelhady, Suzan. 2021. 'Performance and Cost Evaluation of Solar Dish Power Plant: Sensitivity Analysis of Levelized Cost of Electricity (LCOE) and Net Present Value (NPV)'. *Renewable Energy* 168 (May): 332–42. https://doi.org/10.1016/j.renene.2020.12.074.

Abed, Alaa N, Hazim H Hussain, and Naseer K Kasim. 2020. 'Efficiency and Performance Improvement Via Using Optical Reflectors of On-Grid CIGS PV Solar System'. *Karbala International Journal of Modern Science* 6 (1). https://doi.org/10.33640/2405-609X.1329.

Agarwal, Umesh, Narendra Singh Rathore, Naveen Jain, et al. 2023. 'Adaptable Pathway to Net Zero Carbon: A Case Study for Techno-Economic & Environmental Assessment of Rooftop Solar PV System'. *Energy Reports* 9 (December): 3482–92. https://doi.org/10.1016/j.egyr.2023.02.030.

Agrawal, Monika, Priyank Chhajed, and Amartya Chowdhury. 2022. 'Performance Analysis of Photovoltaic Module with Reflector: Optimizing Orientation with Different Tilt Scenarios'. *Renewable Energy* 186 (March): 10–25. https://doi.org/10.1016/j.renene.2021.12.149.

Agrawal, Monika, Avinash Kumar, and Amartya Chowdhury. 2021. 'A Detailed Simulation-Based Study on the Effect of Mirror Integration on PV Module(s) with Analysis of Different Wind Flow Scheme'. *Solar Energy* 222 (July): 129–44. https://doi.org/10.1016/j.solener.2021.05.028.

Agyekum, Ephraim Bonah, Seepana PraveenKumar, Naseer T. Alwan, Vladimir Ivanovich Velkin, Sergey E. Shcheklein, and Salam J. Yaqoob. 2021. 'Experimental Investigation of the Effect of a Combination of Active and Passive Cooling Mechanism on the Thermal Characteristics and Efficiency of Solar PV Module'. *Inventions* 6 (4): 63. https://doi.org/10.3390/inventions6040063.

Ahmed, Ramy, and Ghada Amer. 2021. 'Design of an Economic System for Improving the Performance of Three Types of PV Panels Using Solar Reflectors'. In *Proceedings of the 29th FRUCT Conference*, vol. 29. FRUCT Oy, May 14. https://doi.org/10.5281/zenodo.4770796.

Al-Ghussain, Loiy, Muhammed A. Hassan, and Ahmed Hamed. 2023. 'Modeling and Techno-Economic Optimization of Overhead Panels and Reflectors in near-Wall Mounted PV Systems'. *Solar Energy* 249 (January): 624–41. https://doi.org/10.1016/j.solener.2022.12.014.

Andrews, Rob W, Andrew Pollard, and Joshua Pearce. 2013. 'Photovoltaic System Performance Enhancement With Non-Tracking Planar Concentrators: Experimental Results and Bi-Directional Reflectance Function (BDRF) Based Modelling'. *IEEE 39th Photovoltaic Specialists Conference (PVSC)* (Tampa, United States), June. https://doi.org/10.1109/PVSC.2013.6744136.

Azaioud, Hakim, Arash Farnam, Jos Knockaert, Lieven Vandevelde, and Jan Desmet. 2024. 'Efficiency Optimisation and Converterless PV Integration by Applying a Dynamic Voltage on an LVDC Backbone'. *Applied Energy* 356 (February): 122416. https://doi.org/10.1016/j.apenergy.2023.122416.

Baccoli, Roberto, Andrea Frattolillo, Costantino Mastino, Sebastiano Curreli, and Emilio Ghiani. 2018. 'A Comprehensive Optimization Model for Flat Solar Collector Coupled with a Flat Booster Bottom Reflector Based on an Exact Finite Length Simulation Model'. *Energy Conversion and Management* 164 (May): 482–507. https://doi.org/10.1016/j.enconman.2018.02.091.

Baccoli, Roberto, Amit Kumar, Andrea Frattolillo, Costantino Mastino, Emilio Ghiani, and Gianluca Gatto. 2021. 'Enhancing Energy Production in a PV Collector – Reflector System Supervised by an Optimization Model: Experimental Analysis and Validation'. *Energy Conversion and Management* 229 (February): 113774. https://doi.org/10.1016/j.enconman.2020.113774.

Bader, Sebastian, Xinyu Ma, and Bengt Oelmann. 2019. 'One-Diode Photovoltaic Model Parameters at Indoor Illumination Levels – A Comparison'. *Solar Energy* 180 (March): 707–16. https://doi.org/10.1016/j.solener.2019.01.048.

Bamisile, Olusola, Caroline Acen, Dongsheng Cai, Qi Huang, and Iain Staffell. 2025. 'The Environmental Factors Affecting Solar Photovoltaic Output'. *Renewable and Sustainable Energy Reviews* 208 (February): 115073. https://doi.org/10.1016/j.rser.2024.115073.

Barbón, A., M. Ghodbane, L. Bayón, and Z. Said. 2022. 'A General Algorithm for the Optimization of Photovoltaic Modules Layout on Irregular Rooftop Shapes'. *Journal of Cleaner Production* 365 (September): 132774. https://doi.org/10.1016/j.jclepro.2022.132774.

Bell, Stephanie. 2001. *Measurement Good Practice Guide No. 11 (Issue 2)*.

Bellos, Evangelos. 2019. 'Progress in the Design and the Applications of Linear Fresnel Reflectors – A Critical Review'. *Thermal Science and Engineering Progress* 10 (May): 112–37. https://doi.org/10.1016/j.tsep.2019.01.014.

Bhandari, Khagendra P., Jennifer M. Collier, Randy J. Ellingson, and Defne S. Apul. 2015. 'Energy Payback Time (EPBT) and Energy Return on Energy Invested (EROI) of Solar Photovoltaic Systems: A Systematic Review and Meta-Analysis'. *Renewable and Sustainable Energy Reviews* 47 (July): 133–41. https://doi.org/10.1016/j.rser.2015.02.057.

Boulahia, Meskiana, Kahina Amal Djiar, and Miguel Amado. 2021. 'Combined Engineering—Statistical Method for Assessing Solar Photovoltaic Potential on Residential Rooftops: Case of Laghouat in Central Southern Algeria'. *Energies* 14 (6): 1626. https://doi.org/10.3390/en14061626.

Brogren, M. 2004. 'Analysis of the Effects of Outdoor and Accelerated Ageing on the Optical Properties of Reflector Materials for Solar Energy Applications'. *Solar Energy Materials and Solar Cells*, ahead of print, April 9. https://doi.org/10.1016/j.solmat.2004.02.011.

Chandler, David. 2011. 'Shining Brightly'. MIT News | Massachusetts Institute of Technology, October 26. https://news.mit.edu/2011/energy-scale-part3-1026.

Chandraprabu, V. 2019. 'Dataset of Solar Energy Potential Assessment for Adama City (Ethiopia)'. *Data in Brief* 24 (March): 103879. https://doi.org/10.1016/j.dib.2019.103879.

Choi, Jin S., Byeong G. Choi, Ji H. Kim, Seung-Tak Ryu, Chun T. Rim, and Yun-Su Kim. 2019. 'New Curved Reflectors for Significantly Enhanced Solar Power Generation in Four Seasons'. *Energies* 12 (23): 23. https://doi.org/10.3390/en12234602.

Dervishi, Sokol, and Ardeshir Mahdavi. 2011. *COMPARISON OF MODELS FOR THE DERIVATION OF DIFFUSE FRACTION OF GLOBAL IRRADIANCE DATA FOR VIENNA, AUSTRIA*.

Duffie, John A, and William A Beckman. 2013. *Solar Engineering of Thermal Processes*. 4. Edition. Wiley.

Durković, Vladan, and Željko Đurišić. 2021. 'Impact of a Horizontal Reflector on the Techno-Economic Characteristics of Large VPV Power Plants'. *Solar Energy* 220 (May): 650–59. https://doi.org/10.1016/j.solener.2021.03.069.

Dwivedi, Pushpendu, K. Sudhakar, Archana Soni, E Solomin, and I Kirpichnikova. 2020. 'Advanced Cooling Techniques of P.V. Modules: A State of Art'. *Case Studies in Thermal Engineering* 21 (October): 100674. https://doi.org/10.1016/j.csite.2020.100674.

ESMAP. 2020. *Global Photovoltaic Power Potential by Country*. https://documents1.worldbank.org/curated/en/466331592817725242/pdf/Global-Photovoltaic-Power-Potential-by-Country.pdf.

EU Comission. 2024. 'Photovoltaic Geographical Information System (PVGIS) - European Commission'. September 23. https://joint-research-centre.ec.europa.eu/photovoltaic-geographical-information-system-pvgis_en.

Fernández-Solas, Álvaro, Leonardo Micheli, Florencia Almonacid, and Eduardo F. Fernández. 2021. 'Optical Degradation Impact on the Spectral Performance of Photovoltaic Technology'. *Renewable and Sustainable Energy Reviews* 141 (May): 110782. https://doi.org/10.1016/j.rser.2021.110782.

Finelcomp. 2025a. 'Installation Manual for Solaclick Flat Roofs'.

Finelcomp. 2025b. 'Solarclick Solar Panel Mounting System'.

Fulcher, Jonathan. 2019. 'How Do Solar Cells Produce Electricity?' Lexology, July 9. https://www.lexology.com/library/detail.aspx?g=10aff4c1-37ba-4d43-a0ca-4154f5bd0473.

Gan, Guohui. 2009. 'Effect of Air Gap on the Performance of Building-Integrated Photovoltaics'. *Energy* 34 (7): 913–21. https://doi.org/10.1016/j.energy.2009.04.003.

García-Segura, A., A. Fernández-García, M.J. Ariza, F. Sutter, and L. Valenzuela. 2016. 'Durability Studies of Solar Reflectors: A Review'. *Renewable and Sustainable Energy Reviews* 62 (September): 453–67. https://doi.org/10.1016/j.rser.2016.04.060.

García-Segura, A., F. Sutter, L. Martínez-Arcos, et al. 2021. 'Degradation Types of Reflector Materials Used in Concentrating Solar Thermal Systems'. *Renewable and Sustainable Energy Reviews* 143 (June): 110879. https://doi.org/10.1016/j.rser.2021.110879.

Gautam, Vaishali, Shadihida Khatoon, and Faisal Mohd Jalil. 2024. *History of Solar PV System and Its Recent Development*. https://onlinelibrary.wiley.com/doi/chapter-epub/10.1002/9781394167678.ch1.

Gelegenis, John, Petros Axaopoulos, Stavros Misailidis, George Giannakidis, Maria Samarakou, and Bassilios Bonaros. 2015. *Feasibility for the Use of Flat Booster Reflectors in Various Photovoltaic Installations*. 5 (1).

Global Solar Atlas. n.d. 'Global Solar Atlas'. Accessed 3 April 2025. https://globalsolaratlas.info/download.

Gomaa, Mohamed R., Mujahed Al-Dhaifallah, Ali Alahmer, and Hegazy Rezk. 2020. 'Design, Modeling, and Experimental Investigation of Active Water Cooling Concentrating Photovoltaic System'. *Sustainability* 12 (13): 5392. https://doi.org/10.3390/su12135392.

Haegel, Nancy M., Pierre Verlinden, Marta Victoria, et al. 2023. 'Photovoltaics at Multi-Terawatt Scale: Waiting Is Not an Option'. *Science*, ahead of print, April 7. world. https://doi.org/10.1126/science.adf6957.

Hamed, Ahmed, Loiy Al-Ghussain, Muhammed A. Hassan, and Andres Annuk. 2022. 'Techno-Economic Analysis for Optimal Configurations of PV Systems with Back Reflectors'. *Energy Reports* 8 (November): 14979–96. https://doi.org/10.1016/j.egyr.2022.11.053.

Heimsath, Anna, and Peter Nitz. 2019. 'Scattering and Specular Reflection of Solar Reflector Materials – Measurements and Method to Determine Solar Weighted Specular Reflectance'. *Solar Energy Materials and Solar Cells* 203 (December): 110191. https://doi.org/10.1016/j.solmat.2019.110191.

Hermany. n.d. 'What Can Be Scanned Using a 3D Laser Scanner?' Hermary. Accessed 8 April 2025. https://hermary.com/learning/what-can-be-scanned/.

Heydarian, Minasadat, Maryamsadat Heydarian, Patrick Schygulla, et al. 2024. 'Recent Progress in Monolithic Two-Terminal Perovskite-Based Triple-Junction Solar Cells'. *Energy & Environmental Science* 17 (5): 1781–818. https://doi.org/10.1039/D3EE02822D.

Hirvonen, Janne, Genku Kayo, Sunliang Cao, Ala Hasan, and Kai Sirén. 2015. 'Renewable Energy Production Support Schemes for Residential-Scale Solar Photovoltaic Systems in Nordic Conditions'. *Energy Policy* 79 (April): 72–86. https://doi.org/10.1016/j.enpol.2015.01.014.

Honsberg, Chistiana, and Stuart Bowden. 2019a. 'Absorption Depth | PVEducation'. https://www.pveducation.org/pvcdrom/pn-junctions/absorption-depth.

Honsberg, Chistiana, and Stuart Bowden. 2019b. 'IV Curve | PVEducation'. https://www.pveducation.org/pvcdrom/solar-cell-operation/iv-curve.

Honsberg, Chistiana, and Stuart Bowden. 2019c. 'Solar Time | PVEducation'. https://www.pveducation.org/pvcdrom/properties-of-sunlight/solar-time.

Honsberg Cristiana and Bowden Stuart. 2019. 'Absorption of Light | PVEducation'. https://www.pveducation.org/pvcdrom/pn-junctions/absorption-of-light.

Honsbern, Cristiana, and Stuart Bowden. 2019. 'Light Generated Current | PVEducation'. https://www.pveducation.org/pvcdrom/solar-cell-operation/light-generated-current.

Hossain, Mohammad Jobayer, Mengdi Sun, and Kristopher O. Davis. 2024. 'Photon Management in Silicon Photovoltaic Cells: A Critical Review'. *Solar Energy Materials and Solar Cells* 267 (April): 112715. https://doi.org/10.1016/j.solmat.2024.112715.

IEA. 2023. *Renewables 2022*. https://www.iea.org/reports/renewables-2022.

IEA. n.d. '100 000 Roofs Solar Power Programme – Policies'. IEA. Accessed 31 March 2025. https://www.iea.org/policies/3476-100-000-roofs-solar-power-programme.

Ilmasto-opas. 2022. 'Rakennusten Lämmitys Kuluttaa Runsaasti Energiaa | Ilmasto-Opas'. October 7. https://www.ilmasto-opas.fi/artikkelit/rakennusten-lammitys-kuluttaa-runsaasti-energiaa.

Ilmatieteen Laitos. n.d.-a. '1991-2020 auringonpaiste- ja säteilytilastot - Ilmatieteen laitos'. Accessed 11 April 2025. https://www.ilmatieteenlaitos.fi/1991-2020-auringonpaiste-ja-sateilytilastot.

Ilmatieteen Laitos. n.d.-b. 'Vuositilastot - Ilmatieteen laitos'. Accessed 11 April 2025. https://www.ilmatieteenlaitos.fi/vuositilastot.

Isherwood, Patrick J. M. 2022. 'Reshaping the Module: The Path to Comprehensive Photovoltaic Panel Recycling'. *Sustainability* 14 (3): 1676. https://doi.org/10.3390/su14031676.

Iskandar, Handoko Rusiana, Een Taryana, and Yuda Bakti Zainal. 2023. 'Modelling and Analysis of Rooftop PV as an Energy Optimization of Flat Roof and Gable Roof Mounting System'. *SINERGI* 28 (1): 1–12. https://publikasi.mercubuana.ac.id/index.php/sinergi/article/view/19776.

Kabeel, A.E., Mohamed Abdelgaied, and Ravishankar Sathyamurthy. 2019. 'A Comprehensive Investigation of the Optimization Cooling Technique for Improving the Performance of PV Module with Reflectors under Egyptian Conditions'. *Solar Energy* 186 (July): 257–63. https://doi.org/10.1016/j.solener.2019.05.019.

Kallioğlu, Mehmet Ali, Aydın Durmuş, Hakan Karakaya, and Adem Yılmaz. 2019. 'Empirical Calculation of the Optimal Tilt Angle for Solar Collectors in Northern Hemisphere'. *Energy Sources, Part A: Recovery, Utilization, and Environmental Effects* 42 (11): 1335–58. https://doi.org/10.1080/15567036.2019.1663315.

Kalogirou, Soteris A. 2014. 'Photovoltaic Systems'. In *Solar Energy Engineering*. Elsevier. https://doi.org/10.1016/B978-0-12-397270-5.00009-1.

Kalyanam, Raghuram, and Sabine Hoffmann. 2020. 'A Novel Approach to Enhance the Generalization Capability of the Hourly Solar Diffuse Horizontal Irradiance Models on Diverse Climates'. *Energies* 13 (18): 4868. https://doi.org/10.3390/en13184868.

Kang, H. 2021. 'Crystalline Silicon vs. Amorphous Silicon: The Significance of Structural Differences in Photovoltaic Applications'. *IOP Conference Series: Earth and Environmental Science* 726 (1): 012001. https://doi.org/10.1088/1755-1315/726/1/012001.

Khan, Muhammad Saud, Makbul A. M. Ramli, Hatem Faiz Sindi, Taufal Hidayat, and Houssem R. E. H. Bouchekara. 2022. 'Estimation of Solar Radiation on a PV Panel Surface with an Optimal Tilt Angle Using Electric Charged Particles Optimization'. *Electronics* 11 (13): 13. https://doi.org/10.3390/electronics11132056.

Kim, Byung-ju, Ji-yong Lee, Kyung-hwan Kim, and Tak Hur. 2014. 'Evaluation of the Environmental Performance of Sc-Si and Mc-Si PV Systems in Korea'. *Solar Energy* 99 (January): 100–114. https://doi.org/10.1016/j.solener.2013.10.038.

Kim, Moon Keun, Khalid Osman Abdulkadir, Jiying Liu, et al. 2021. 'Optimal Design Strategy of a Solar Reflector Combining Photovoltaic Panels to Improve Electricity Output: A Case Study in Calgary, Canada'. *Sustainability* (Basel, Switzerland) 13 (11): 6115. https://doi.org/10.3390/su13116115.

Koppelaar, R.H.E.M. 2017. 'Solar-PV Energy Payback and Net Energy: Meta-Assessment of Study Quality, Reproducibility, and Results Harmonization'. *Renewable and Sustainable Energy Reviews* 72 (May): 1241–55. https://doi.org/10.1016/j.rser.2016.10.077.

Kostić, Lj.T., T.M. Pavlović, and Z.T. Pavlović. 2010. 'Optimal Design of Orientation of PV/T Collector with Reflectors'. *Applied Energy* 87 (10): 3023–29. https://doi.org/10.1016/j.apenergy.2010.02.015.

Lai, Chun Sing, and Malcolm D. McCulloch. 2017. 'Levelized Cost of Electricity for Solar Photovoltaic and Electrical Energy Storage'. *Applied Energy* 190 (March): 191–203. https://doi.org/10.1016/j.apenergy.2016.12.153.

Lewis, Mandy R., Silvana Ovaitt, Byron McDanold, Chris Deline, and Karin Hinzer. 2024. 'Artificial Ground Reflector Size and Position Effects on Energy Yield and Economics of Single-Axis-

Tracked Bifacial Photovoltaics'. *Progress in Photovoltaics: Research and Applications* 32 (10): 675–86. https://doi.org/10.1002/pip.3811.

Liang, Haoyue, and Fengqi You. 2023. 'Reshoring Silicon Photovoltaics Manufacturing Contributes to Decarbonization and Climate Change Mitigation'. *Nature Communications* 14 (1): 1274. https://doi.org/10.1038/s41467-023-36827-z.

LONGi. 2023. 'PV Panel Datasheet'.

Luis-Ruiz, Julio Manuel de, Benito Ramiro Salas-Menocal, Raúl Pereda-García, Rubén Pérez-Álvarez, Javier Sedano-Cibrián, and Carolina Ruiz-Fernández. 2024. 'Optimal Location of Solar Photovoltaic Plants Using Geographic Information Systems and Multi-Criteria Analysis'. *Sustainability* 16 (7): 7. https://doi.org/10.3390/su16072895.

Maatallah, Taher, Souheil El Alimi, and Sassi Ben Nassrallah. 2011. 'Performance Modeling and Investigation of Fixed, Single and Dual-Axis Tracking Photovoltaic Panel in Monastir City, Tunisia'. *Renewable and Sustainable Energy Reviews* 15 (8): 4053–66. https://doi.org/10.1016/j.rser.2011.07.037.

Maghami, Mohammad Reza, Hashim Hizam, Chandima Gomes, Mohd Amran Mohd Radzi, Sina Rezadad, and Shahrooz Hajighorbani. 2016. 'Power Loss Due to Soiling on Solar Panel: A Review'. *Renewable & Sustainable Energy Reviews* 59 (January): 1307–16. https://doi.org/10.1016/j.rser.2016.01.044.

Mäki, Elina, Eemeli Tsupari, and Jussi Ikäheimo. 2015. *The Role and Opportunities for Solar Energy in Finland and Europe*. https://doi.org/10.13140/RG.2.1.2764.0486.

Malik, Prashant, and Shyam Singh Chandel. 2020. 'Performance Enhancement of Multi-Crystalline Silicon Photovoltaic Modules Using Mirror Reflectors under Western Himalayan Climatic Conditions'. *Renewable Energy* 154 (July): 966–75. https://doi.org/10.1016/j.renene.2020.03.048.

Malwad, Dnyaneshwar, and Vinod Tungikar. 2021. 'Development and Performance Testing of Reflector Materials for Concentrated Solar Power: A Review'. *Materials Today: Proceedings*, 2nd International Conference on Manufacturing Material Science and Engineering, vol. 46 (January): 539–44. https://doi.org/10.1016/j.matpr.2020.10.744.

Manosroi, Woradej, Pitchaporn Prompattra, and Praw Kerngburee. 2020. 'Performance Improvement of Two-Axis Solar Tracking System by Using Flat-Mirror Reflectors'. *Energy Reports*, 2020 The 7th International Conference on Power and Energy Systems Engineering, vol. 6 (December): 9–14. https://doi.org/10.1016/j.egyr.2020.10.029.

Matsushima, Toshio, Tatsuyuki Setaka, and Seiichi Muroyama. 2003. 'Concentrating Solar Module with Horizontal Reflectors'. *Solar Energy Materials*.

Michael, Jee Joe, Iniyan S, and Ranko Goic. 2015. 'Flat Plate Solar Photovoltaic–Thermal (PV/T) Systems: A Reference Guide'. *Renewable and Sustainable Energy Reviews* 51 (November): 62–88. https://doi.org/10.1016/j.rser.2015.06.022.

Ministry of the Environment (FI). n.d.-a. 'Paris Climate Change Agreement'. Ministry of the Environment. Accessed 7 May 2025. https://ym.fi/paris-climate-change-agreement.

Ministry of the Environment (FI). n.d.-b. 'What Is the Green Transition?' Ministry of the Environment. Accessed 7 May 2025. https://ym.fi/what-is-the-green-transition.

Mokarram, Marzieh, Mohammad J. Mokarram, Mohammad R. Khosravi, Ali Saber, and Akbar Rahideh. 2020. 'Determination of the Optimal Location for Constructing Solar Photovoltaic Farms Based on Multi-Criteria Decision System and Dempster–Shafer Theory'. *Scientific Reports* 10 (1): 8200. https://doi.org/10.1038/s41598-020-65165-z.

Naghavi, M. S., A. Esmaeilzadeh, B. Singh, B. C. Ang, T. M. Yoon, and K. S. Ong. 2021. 'Experimental and Numerical Assessments of Underlying Natural Air Movement on PV Modules Temperature'. *Solar Energy* 216 (March): 610–22. https://doi.org/10.1016/j.solener.2021.01.007.

Nour, Christine Abdel, Anne Migan-Dubois, Jordi Badosa, Vincent Bourdin, Claude Marchand, and Tilda Akiki. 2020. 'Geometrical Optimization for a Photovoltaic Installation Equipped with Flat Reflectors Based on Plane of Array Estimations'. *EPJ Photovoltaics* 11: 1. https://doi.org/10.1051/epjpv/2019010.

NREL. n.d. 'PVWatts Calculator'. Accessed 3 April 2025. https://pvwatts.nrel.gov/index.php.

Odungat, Mohammed Mansoor, Sishaj Pulikottil Simon, Kevin Ark Kumar, Kinattingal Sundareswaran, Panugothu Srinivasarao Nayak, and Narayana Prasad Padhy. 2020. 'Estimation of System Efficiency and Utilisation Factor of a Mirror Integrated Solar PV System'. *IET Renewable Power Generation* 14 (10): 1677–87. https://doi.org/10.1049/iet-rpg.2019.0804.

OurWorld in Data. 2024. 'Solar (Photovoltaic) Panel Prices'. Our World in Data. https://ourworldindata.org/grapher/solar-pv-prices.

Parker US. n.d. 'Adhesives for Solar Panel Installation - Assembly & Protection Solutions Division | Parker US'. Parker Hannifin Corporation. Accessed 14 April 2025. https://www.parker.com/us/en/divisions/assembly-and-protection-solutions-division/industries/adhesives-for-solar-panel-installation.html.

Pavlović, Zoran T., and Ljiljana T. Kostić. 2015. 'Variation of Reflected Radiation from All Reflectors of a Flat Plate Solar Collector during a Year'. *Energy* 80 (February): 75–84. https://doi.org/10.1016/j.energy.2014.11.044.

PVGIS. n.d. 'PVGIS User Manual - European Commission'. Accessed 3 April 2025. https://joint-research-centre.ec.europa.eu/photovoltaic-geographical-information-system-pvgis/getting-started-pvgis/pvgis-user-manual_en.

Rajput, Pramod, Yogesh Kumar Singh, G.N. Tiwari, O.S. Sastry, Santosh Dubey, and Kailash Pandey. 2018. 'Life Cycle Assessment of the 3.2 kW Cadmium Telluride (CdTe) Photovoltaic System in Composite Climate of India'. *Solar Energy* 159 (January): 415–22. https://doi.org/10.1016/j.solener.2017.10.087.

Rönnelid, Mats, Björn Karlsson, Peter Krohn, and Johan Wennerberg. 2000. 'Booster Reflectors for PV Modules in Sweden'. *Progress in Photovoltaics: Research and Applications* 8 (3): 279–91. https://doi.org/10.1002/1099-159X(200005/06)8:3%253C279::AID-PIP316%253E3.0.CO;2-%2523.

Sandia National Laboratories. n.d. 'Shading, Soiling, and Reflection Losses'. PV Performance Modeling Collaborative (PVPMC). Accessed 2 April 2025. https://pvpmc.sandia.gov/modeling-guide/1-weather-design-inputs/shading-soiling-and-reflection-losses/.

Santiago, I., D. Trillo-Montero, I. M. Moreno-Garcia, V. Pallarés-López, and J. J. Luna-Rodríguez. 2018. 'Modeling of Photovoltaic Cell Temperature Losses: A Review and a Practice Case in South Spain'. *Renewable and Sustainable Energy Reviews* 90 (July): 70–89. https://doi.org/10.1016/j.rser.2018.03.054.

Seaward. n.d. 'Solar Survey 100/200R Series Datasheet'. https://www.seaward.com/gb/products/solar/irradiance-meters/396a914-solar-survey-200r/.

Setiawan, Eko Adhi, and Khairiah Dewi. 2013. 'Impact of Two Types Flat Reflector Materials on Solar Panel Characteristics'. *International Journal of Technology* 4 (2): 188. https://doi.org/10.14716/ijtech.v4i2.108.

Shanks, Katie, Senthilarasu Sundaram, and Tapas Mallick. 2016. 'Optics for Concentrating Photovoltaics: Trends, Limits and Opportunities for Materials and Design'. *Renewable and Sustainable Energy Reviews* 60 (July): 394–407. https://doi.org/10.1016/j.rser.2016.01.089.

Shekar, Vinay, Antonio Caló, and Eva Pongrácz. 2023. 'Experiences from Seasonal Arctic Solar Photovoltaics (PV) Generation- An Empirical Data Analysis from a Research Infrastructure in Northern Finland'. *Renewable Energy* 217 (November): 119162. https://doi.org/10.1016/j.renene.2023.119162.

SinoVoltaics. 2015. 'Solar Cell Production: From Silicon Wafer to Cell'. November 9. https://sinovoltaics.com/solar-basics/solar-cell-production-from-silicon-wafer-to-cell/.

Skoplaki, E., and J.A. Palyvos. 2009. 'On the Temperature Dependence of Photovoltaic Module Electrical Performance: A Review of Efficiency/Power Correlations'. *Solar Energy* 83 (5): 614–24. https://doi.org/10.1016/j.solener.2008.10.008.

Sultan, Sakhr M., M. Z. Abdullah, C. P. Tso, et al. 2024. 'An Economic Feasibility Assessment of Implementing Photovoltaic Module Reflectors under Malaysian Meteorological Conditions'. *Scientific Reports* 14 (1): 3349. https://doi.org/10.1038/s41598-024-54031-x.

SunWize. n.d. 'Testing PV Modules'. *SunWize | Power Independence*. Accessed 4 August 2025. https://www.sunwize.com/tech-notes/testing-pv-modules/.

Tabasi, Sanaz, Hossein Yousefi, Younes Noorollahi, and Mohamad Aramesh. 2019. 'A Detailed Investigation and Performance Optimization of a Photovoltaic Panel Integrated with a Reflecting Mirror'. *Applied Thermal Engineering* 160 (September): 114074. https://doi.org/10.1016/j.applthermaleng.2019.114074.

Tan, Dongli, Yao Wu, Zhiqing Zhang, Yue Jiao, Lingchao Zeng, and Yujun Meng. 2023. 'Assessing the Life Cycle Sustainability of Solar Energy Production Systems: A Toolkit Review in the Context of Ensuring Environmental Performance Improvements'. *Sustainability* 15 (15): 15. https://doi.org/10.3390/su151511724.

Tripanagnostopoulos, Y., Th. Nousia, M. Souliotis, and P. Yianoulis. 2002. 'Hybrid Photovoltaic/Thermal Solar Systems'. *Solar Energy* 72 (3): 217–34. https://doi.org/10.1016/S0038-092X(01)00096-2.

U. S. Department of Energy. 2022. 'Concentrating Solar-Thermal Power'. Energy.Gov, September 21. https://www.energy.gov/eere/solar/concentrating-solar-thermal-power.

U. S. Department of Energy. n.d. 'Solar Photovoltaic Manufacturing Basics'. Energy.Gov. Accessed 31 March 2025. https://www.energy.gov/eere/solar/solar-photovoltaic-manufacturing-basics.

Vartiainen, Eero, Christian Breyer, David Moser, et al. 2024. 'Attractiveness of Photovoltaic Prosumerism in the European Electricity Market'. *Solar RRL* 8 (1): 2300576. https://doi.org/10.1002/solr.202300576.

Vasel, Ahmad, and Frantzis Iakovidis. 2017. 'The Effect of Wind Direction on the Performance of Solar PV Plants'. *Energy Conversion and Management* 153 (December): 455–61. https://doi.org/10.1016/j.enconman.2017.09.077.

Venkatachalam, Chandraprabu, Samuel G/mariam, and Gedlu Solomon. 2019. 'Dataset of Solar Energy Potential Assessment for Adama City (Ethiopia)'. *Data in Brief* 24 (June): 103879. https://doi.org/10.1016/j.dib.2019.103879.

Verma, Preeti, Afroz Alam, Adil Sarwar, et al. 2021. 'Meta-Heuristic Optimization Techniques Used for Maximum Power Point Tracking in Solar PV System'. *Electronics* 10 (October): 2419. https://doi.org/10.3390/electronics10192419.

Wijesuriya, D.T.P., K.D.S.H. Wickramathilaka, L.S. Wijesinghe, D.M. Vithana, and H.Y. Ranjit Perera. 2017. 'Reduction of Solar PV Payback Period Using Optimally Placed Reflectors'. *Energy Procedia* 134 (October): 480–89. https://doi.org/10.1016/j.egypro.2017.09.606.

Wirth, Harry, Weiß, Karl-Anders, and Weismeier Cornelia. 2016. *Photovoltaic Modules*. De Gruyter.

Woodhouse, Michael, Alan Goodrich, and Ted James. 2011. *Solar PV Manufacturing Cost Analysis: U.S. Competitiveness in a Global Industry (Presentation): NREL (National Renewable Energy Laboratory)*. https://research-hub.nrel.gov/en/publications/solar-pv-manufacturing-cost-analysis-us-competitiveness-in-a-glob.

Yadav, Priya, and S. S. Chandel. 2014. 'Comparative Analysis of Diffused Solar Radiation Models for Optimum Tilt Angle Determination for Indian Locations'. *Applied Solar Energy* 50 (1): 53–59. https://doi.org/10.3103/S0003701X14010137.

Zainali, Sebastian, Johan Lindahl, Johan Lindén, and Bengt Stridh. 2023. 'LCOE Distribution of PV for Single-Family Dwellings in Sweden'. *Energy Reports* 10 (November): 1951–67. https://doi.org/10.1016/j.egyr.2023.08.042.

Zanatta, A.R. 2022. 'The Shockley–Queisser Limit and the Conversion Efficiency of Silicon-Based Solar Cells'. *Results in Optics* 9 (December): 100320. https://doi.org/10.1016/j.rio.2022.100320.

Appendices

Appendix 1 Example pictures of test reflectors: galvanized, aluminum, white and stainless steel

Picture 1. Galvanized steel sheet

Picture 2. Aluminium sheet

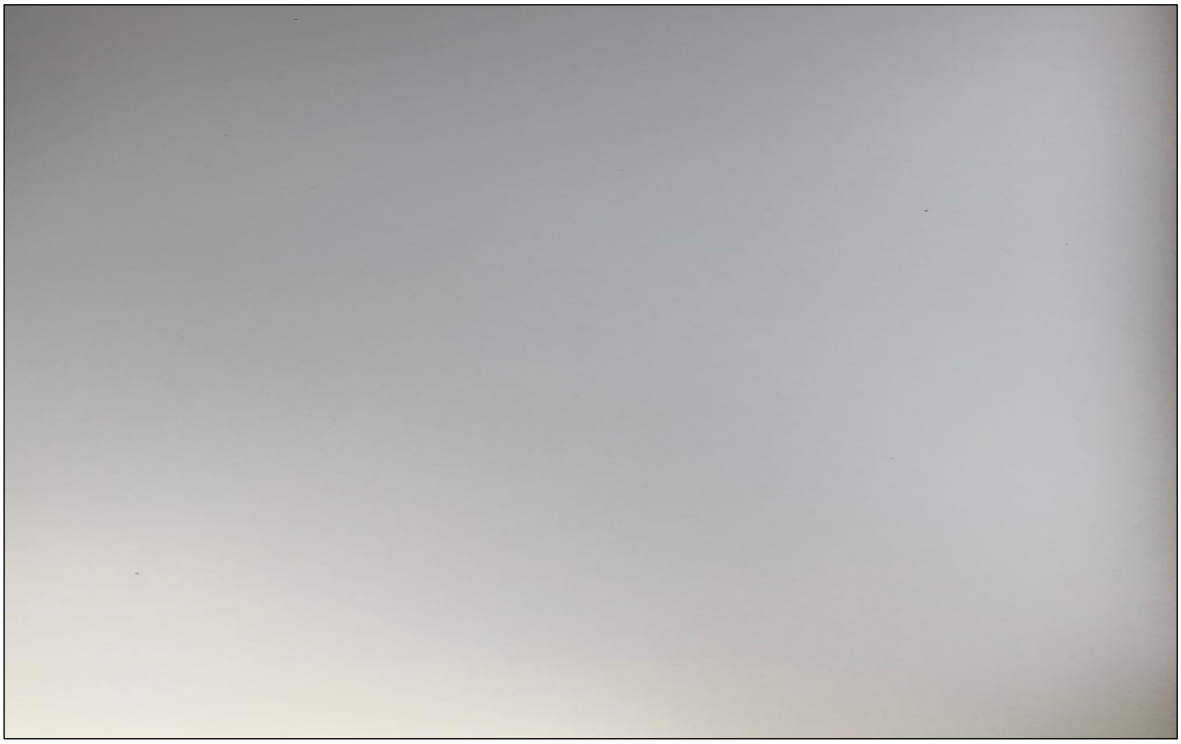

Picture 3. White steel sheet

Picture 4. Stainless steel sheet